Studies on
Rare Earth Separation Using Chemical Vapor Transport

（化学気相輸送法による希土類元素の分離に関する研究）

1996

Kuniaki Murase

Department of Applied Chemistry
Faculty of Engineering
Osaka University

Preface

The work of this thesis has been carried out under the guidance of Professor Dr. Gin-ya Adachi at Department of Applied Chemistry, Faculty of Engineering, Osaka University.

The object of this thesis is to present and develop a new simple dry process for rare earth separation and recycling using a chemical vapor transport reaction mediated by rare earth chloride vapor complexes with aluminium or alkali metal chlorides.

The author wishes that the knowledge obtained in this work provide useful suggestion and information for further development and establishment of the all-dry technique for rare earth separation and that the process stimulates still more utilization of rare earth–based materials in the 21 century.

Kuniaki Murase

Department of Applied Chemistry
Faculty of Engineering
Osaka University
Yamadaoka 2-1, Suita, Osaka 565
Japan

January 1996

Contents

General Introduction

In recent years, various kinds of new materials, in which rare earth elements play a key role, have been increasingly developed in the corresponding research fields. Some intermetallic compounds, such as $SmCo_5$, Sm_2Co_{17}, $Nd_2Fe_{14}B$, and $Sm_2Fe_{17}N_x$, have been well investigated for high performance permanent magnet materials, some of which have been already produced industrially for uses in portable motors and so on. Hydrogen storage alloys of RNi_5 (R = rare earths) type have come into use as cathode materials for a nickel-metal hydride secondary battery as a substitute for Ni-Cd battery, since cadmium is harmful to the environment. Phosphors for lamps or color displays are also important materials which contains rare earth elements as activator and matrix. Naturally enough, this development of the application of rare earth elements has led to an increase in their demand.

Since the first separation of rare earth elements in 19th century using a fractional crystallization or precipitation method, various wet precesses have been developed and widely employed for their mutual separation. At present, purified rare earths for commercial use are produced almost exclusively by means of a solvent extraction and ion-exchange chromatography, and the methods have been well investigated and established. However, these are also wet processes which always require a series of complicated treatments. First of all, raw materials containing rare earths have to be decomposed and dissolved. And after separation process, still more steps are necessary to obtain rare earth oxides: concentration of solution, precipitation and filtering off the rare earth components, drying and calcination of the precipitate. Furthermore, halogenation of the oxides is necessary to produce rare earth metals by means of metallothermic or electrolytic reduction. Since these complicated precesses result in high production costs of rare earths, new techniques other than the wet precesses have to be developed in order to lower the cost.

Meanwhile, a number of metal halides form halogen-bridged vapor complexes with other volatile metal halides called complex formers [1–7]. Typical halides which are known as the complex formers are aluminium, iron, and alkali-metal (A) halides. Vapor complexes of rare earth halides (RX_3) with these complex formers have also been investigated for many systems; the formation schemes are expressed as

$$RX_3(s, l) + n/2\ Al_2Cl_6(g) = RAl_nX_{3+3n}(g) \quad (n = 1-4), \qquad (1)$$

and

$$RX_3(s, l) + AX(s, l) = ARX_4(g). \quad (2)$$

In general, the volatility of metal halides is appreciably enhanced by this reversible formation of the vapor complexes. For example, the volatility enhancements, namely the factors of increase in the volatility due to the complexation in the presence of 1 atm of complex former $Al_2Cl_6(g)$, have been calculated as 10^{13} for $NdCl_3$ and 10^{11} for $HoCl_3$ at 600 K [4b]. Therefore, rare earth vapor complexes have been studied in terms of various application possibilities directed toward luminescent and laser materials. Some vapor complexes composed of rare earth and alkali metal iodides have already been applied to high performance metal halide lamps [1].

It is noteworthy that the vapor complexation with some complex formers renders it possible to transport chemically the nonvolatile rare earth chloride. Vapor complexes of the RCl_3-$AlCl_3$ systems have been tried as carrier species for chemical transport reactions to prepare anhydrous chlorides on a laboratory scale [8, 9]. The transport phenomenon mediated by the RCl_3-$AlCl_3$ complex has also been applied to some separation techniques. One of them is a gas-solid chromatograph, which Zvarova and Zvara applied to the mutual separation of mixed rare earth radiotracers [10].

Particularly, Adachi *et al* are also recently reported briefly that the mutual separation of some rare earth pairs can be conducted by a chemical vapor transport through a reactor with a temperature gradient [11]. Since the separation precess using chemical vapor transport phenomenon is based on difference in the temperature dependence of formation-decomposition equilibrium of each vapor complex, it is all-dry precess free from the above-mentioned complicated treatments characteristics of the wet precesses.

The present work deals with development of the rare earths separation process using the chemical vapor transport (CVT) phenomenon mediated by vapor complexes.

Chapters 1 and 2 describe the rare earth separation experiments using the CVT process mediated by vapor complexes of the RCl_3-$AlCl_3$ and RCl_3-ACl systems (A = alkali metals), respectively. Here, quasi-binary ($PrCl_3$-$ErCl_3$, $PrCl_3$-$SmCl_3$, and $PrCl_3$-$NdCl_3$) or quasi-ternary ($PrCl_3$-$GdCl_3$-$ErCl_3$) rare earth chloride model mixtures were used as raw materials, and the resulting separation efficiency is discussed in terms of the transport condition and mechanism.

In **Chapter 2**, the separation of mixed praseodymium and neodymium oxides was also studied by means of the CVT process. In order to use rare earth oxide directly as raw material for the CVT reaction, some potassium salts were adopted as a precursor of potassium chloride. The results

were discussed in terms of the reaction condition and, further, a simulation of the transport phenomena was carried out by a calculation based on known thermodynamic data.

Chapter 3 deals with the CVT reactions using rare earth crude oxides and concentrates as raw materials as the ultimate case. In order to chlorinate, monazite, one of the rare earth concentrates, carbon tetrachloride was tried in addition to chlorine gas, and the chlorination kinetics are argued.

As well as the rare earth separation process from their ores and concentrates, recycling from industrial wastes is also an important process for the supply of rare earths. **Chapter 4** describes the recovery process of rare earths from scraps of some rare earth-based intermetallic materials Sm_2Co_{17}, $Nd_2Fe_{14}B$, and $LaNi_5$ by means of the CVT technique using $AlCl_3$ as the complex former. In addition, the recovery of some rare metals other than rare earths form a fly-ash of bitumen-in-water emulsion is also proposed.

In the work described in **Chapters 5 and 6**, some fundamental properties of the vapor complexes themselves and related molten mixtures were investigated. **Chapter 5** describes the measurement of vapor pressures of the gaseous species over the $NdCl_3$-KCl equimolar melt at high temperatures by means of Knudsen-effusion mass spectrometry. Qualitative observation of the vapor over the $ErCl_3$-KCl quasi-binary and $NdCl_3$-$ErCl_3$-KCl quasi-ternary melts was also carried out using the method. **Chapter 6** gives the result of Raman spectroscopic investigation of the structure of the $NdCl_3$-$AlCl_3$ and $GdCl_3$-$AlCl_3$ liquids (melts) and glasses. The structures of $RAl_3Cl_{12}(g)$ vapor complexes are, further, discussed in terms of a similarity in coordination number of R^{3+} ion.

List of Publications

[1] Mutual Separation Characteristics for Lanthanoid Elements *via* Gas Phase Complex with Alkaline Chlorides

Gin-ya Adachi, Kuniaki Murase, Kiyoshi Shinozaki, and Ken-ichi Machida

Chemistry Letters, **1992**, 511–514.

[2] Mutual Separation Characteristics and Mechanism for Lanthanoid Elements *via* Gas Phase Complexes with Alkaline Metal and/or Aluminium Chloride

Kuniaki Murase, Kiyoshi Shinozaki, Ken-ichi Machida, and Gin-ya Adachi

Bulletin of the Chemical Society of Japan, **65**, 2724–2728 (1992).

[3] Recovery of Rare Metals from the Sludge of Samarium-Cobalt Magnetic Alloy by a Chemical Vapor Transporting Method

Kuniaki Murase, Ken-ichi Machida, and Gin-ya Adachi

Chemistry Letters, **1992**, 1555–1558.

[4] Rare Earth Separation Using a Chemical Vapour Transport Process Mediated by Vapour Complexes of the $LnCl_3$-$AlCl_3$ System

Kuniaki Murase, Kiyoshi Shinozaki, Yoshiyuki Hirashima, Ken-ichi Machida, and Gin-ya Adachi

Journal of Alloys and Compounds, **198**, 31–38 (1993).

[5] Vapor Phase Extraction and Mutual Separation of Rare Earths from Monazite Using Chemical Vapor Transport Mediated by Vapor Complexes

Kuniaki Murase, Ken-ichi Machida, and Gin-ya Adachi

Chemistry Letters, **1994**, 1297–1300.

[6] Recovery of Nickel and Vanadium from a Fly Ash of Bitumen-in-Water Emulsion by Chemical Vapor Transport

Kuniaki Murase, Ken-ichi Nishikawa, Ken-ichi Machida, and Gin-ya Adachi

Chemistry Letters, **1994**, 1845–1848.

[7] Raman Spectra of Liquids and Glasses in the RCl_3-$AlCl_3$ (R = Nd, Gd) Systems
Kuniaki Murase, Gin-ya Adachi, Georgia D. Zissi, Soghomon Boghosian, and George N. Papatheodorou
Journal of Non-Crystalline Solids, **180**, 88–90 (1994).

[8] Recovery of Rare Metals from Scrap of Rare Earth Intermetallic Material by Chemical Vapour Transport
Kuniaki Murase, Ken-ichi Machida, and Gin-ya Adachi
Journal of Alloys and Compounds, **217**, 218–225 (1995).

[9] Vapor Phase Extraction and Separation of Rare Earths Using Chemical Vapor Transport Mediated by Vapor Complexes
Kuniaki Murase, Ken-ichi Machida, and Gin-ya Adachi
Journal of Rare Earths (Special Issue), Proceeding of the 3rd International Conference on Rare Earth Development and Application, Vol. 1, p. 12–15 (1995).

[10] Mutual Separation of Mixed Praseodymium and Neodymium Oxides *via* Metal Halide Gaseous Complexes
Kuniaki Murase, Teruaki Fukami, Ken-ichi Machida, and Gin-ya Adachi
Industrial and Engineering Chemistry Research, **34**, 3963–3969 (1995).

[11] Extraction and Mutual Separation of Rare Earths from Concentrates and Crude Oxides Using Chemical Vapor Transport
Kuniaki Murase, Tetsuya Ozaki, Ken-ichi Machida, and Gin-ya Adachi
Journal of Alloys and Compounds, (1996) in press.

[12] Mass Spectrometric Investigation of the Vapor over the $LnCl_3$-KCl Equimolar Melt (Ln = Nd, Er) at High Temperatures
Kuniaki Murase, Gin-ya Adachi, Masashi Hashimoto, and Hiroshi Kudo
Bulletin of the Chemical Society of Japan, (1996) in press.

[13] Chlorination of Monazite Using Carbon Tetrachloride as a Rare Earth and Thorium Separation Processes

Kuniaki Murase, Tetsuya Ozaki, Ken-ichi Machida, and Gin-ya Adachi

Transaction of the Institution of Mining and Metallurgy, Section C, (1996) in press.

List of Supplementary Publication

[1] Plasma Nitriding Characteristics of $Sm_2Fe_{17}N_x$

Ken-ichi Machida, Eiji Yamamoto, Kuniaki Murase, Gin-ya Adachi, Masahiro Taniguchi, and Ken-ichi Tanaka

Chemistry Letters, **1992**, 1243–1246.

Chapter 1

Mutual Separation of Mixed Rare Earth Chlorides Using Chemical Vapor Transport Mediated by Vapor Complexes of the RCl_3-$AlCl_3$ (R = rare earths) System

1.1. Introduction

It is well known that a number of metal chlorides form halogen-bridged vapor complexes with other volatile metal chlorides (complex formers) [1a, 2–7]. The most typical complex former is aluminium chloride, and vapor complexes of the RCl_3-$AlCl_3$ system have also been investigated. Vapor complexes of four different compositions, *i.e.* $RAlCl_6$, RAl_2Cl_9, RAl_3Cl_{12}, and RAl_4Cl_{15}, were known to form in the RCl_3-$AlCl_3$ system, and abundance of each complex depends on the temperature and the vapor pressure of aluminium chloride vapor, Al_2Cl_6 [12].

Since the first observation of RAl_nCl_{3+3n} vapor complex in the $NdCl_3$-$AlCl_3$ system by Gruen and Øye in 1967 [13], the vapor complexes have been studied in terms of various application possibilities (see General Introduction). Among them, Zvarova and Zvara applied the complexes to the mutual separation of mixed rare earth chlorides by means of a gas-solid chromatographic method [10]. However, the method deals only with amounts at the radiotracer level and, therefore, is not suitable for large-scale production of separated rare earths. On the contrary, Adachi *et al* have recently reported briefly that the mutual separation of a rare earth pair can be successfully conducted by a chemical vapor transport (CVT) process along a well-controlled temperature gradient using $AlCl_3$ as a vapor complex former [11]. The CVT technique is based on the difference in the temperature dependencies of the formation-decomposition equilibria for the vapor complex RAl_nCl_{3+3n} and is fit for separation of rare earths on a large industrial scale, unlike the gas-solid chromatography.

In the work described in this chapter the mutual separation characteristics were studied for mixtures of rare earth chlorides in the $PrCl_3$-$ErCl_3$, $PrCl_3$-$SmCl_3$, and $PrCl_3$-$NdCl_3$ quasi-binary systems and the $PrCl_3$-$GdCl_3$-$ErCl_3$ quasi-ternary system by the CVT process using aluminium chloride as the complex former. The resulting separation efficiency is discussed in terms of the transport conditions and mechanism.

1.2. Experimental Details

1.2.1. Materials

Hydrous rare earth chlorides were prepared by dissolving the corresponding oxides (purity, 99.9%) in a small excess of hydrochloric acid. The hydrous chlorides produced were further purified by repeating the recrystallization from a solution of deionized water. The hydration numbers of the hydrous salts were estimated by chelate titration with a standard solution of ethylenediaminetetraacetic acid (EDTA) to the yellow end point of a xylenol orange indicator at a pH value of 5.1–5.3 using hexamethylenetetramine (98.0%) as buffer.

Anhydrous rare earth chlorides were prepared by reaction of the corresponding oxides with a large excess of ammonium chloride (99.0%). The oxide and the NH_4Cl were mixed in an agate mortar for 30 min. The mixture was loaded in a mullite boat, introduced into an electric furnace and allowed to react for 2 or 3 h up to 250–350 °C in a stream of N_2 gas dried by passage through a P_2O_5 column. Finally, the residual NH_4Cl was removed by sublimation at 400 °C.

The aluminium chloride (98%) used as complex former and the active carbon powder were reagent grade and used without any further purification.

1.2.2. Apparatus

Figure 1.1 shows the apparatus employed for the CVT reaction. The apparatus comprises two tubular electric furnaces, A (length, 180 mm) and B (length, 500 mm). These furnaces are made from a kanthal-wound mullite tube (inner diameter, 35 mm) and ceramic wool. Furnace A was used to generate the gas phase Al_2Cl_6. The heating element in furnace B was divided into several separate heating zones, with every zone controlled independently by a thermoregulator so as to produce various temperature gradients along the quartz tube reactor (inner diameter, 25 mm; length, *ca* 100 cm). On setting the temperature gradient, the temperature of every zone was roughly set first on the thermoregulators and, then, the real temperatures along the central axis of the tube reactor were measured with a thermocouple inserted from the right-hand end in order to adjust the gradient precisely to the desired temperature. In order to avoid reaction of the Al_2Cl_6 vapor with the fused silica tube [26] *via*

$$2\ Al_2Cl_6(g) + 3\ SiO_2(s) = 2\ Al_2O_3(s) + 3\ SiCl_4(g), \qquad (1.1)$$

12 or 13 pieces of alumina tubing (outer diameter, 21 mm; inner diameter, 16 mm; length, 30 mm) were put side by side along the inner wall of the reactor. The sample transported by the vapor

complex along the temperature gradient was collected by recovering these alumina tubes.

1.2.3. Procedure

Supply of Aluminium Chloride. For the generation of gaseous Al_2Cl_6, two types of method

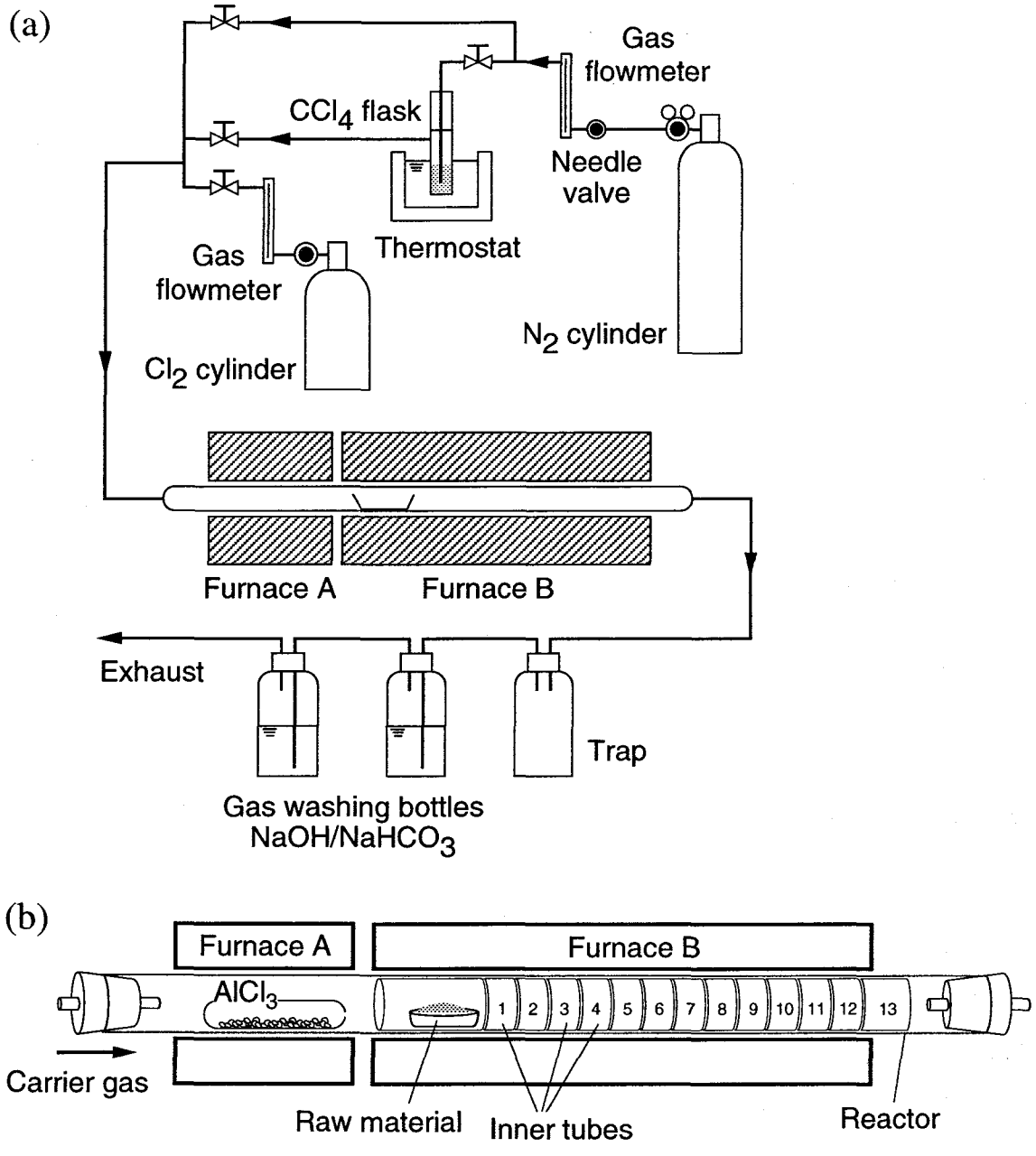

Figure 1.1. (a) Apparatus for chemical vapor transport reaction and (b) assembly of electric furnaces. Unit for generation of carbon tetrachloride vapor was employed only for studies in Sections 3.2.2 and 3.3.2. Furnace A was operated when complex former $AlCl_3$ was used. Numbers in furnace B denote fraction number (*FN*) of separation.

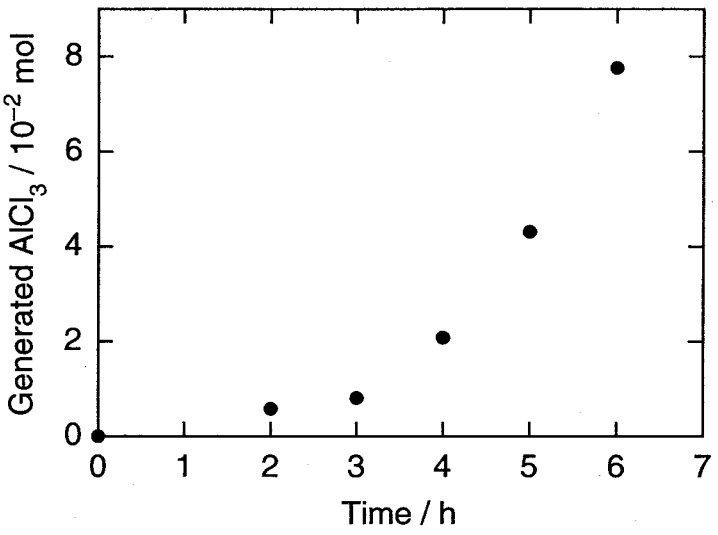

Figure 1.2. Change in total generated $AlCl_3$ vapor with procedure I (see text).

were used. In one method (procedure I), 8.0×10^{-2} mol of solid $AlCl_3$ was sealed in a glass ampule (inner diameter, 14 mm; length, *ca* 10 cm) with a small hole of diameter about 0.3 mm so as to control the evaporation rate of $AlCl_3$. The ampule of $AlCl_3$ was then introduced into the middle of furnace A. The charged amount of $AlCl_3$ was not more than 8.0×10^{-2} mol (*ca* 10 g) in order to avoid clogging of the reactor tube with $AlCl_3$ deposits, which accumulated at the outlet of furnace B through the operation of the CVT reaction (mentioned below). The operation time of furnace A, *i.e.* the reaction time for CVT, was generally 6 h unless noted otherwise. In the course of the CVT reaction, furnace A was heated over the temperature range from 80 to 200 °C at a rate of 20 °C h^{-1}, because sublimation of $AlCl_3$ had been observed over this range on heating the ampule.

Figure 1.2 shows the total amount of $AlCl_3$ evaporated during the course of the CVT reaction when procedure I was employed. The rate of $AlCl_3$ supply to the CVT reaction varied greatly. Therefore, when necessary, another method (procedure II) of $AlCl_3$ supply was employed in order to keep the evaporation rate constant. In this method the $AlCl_3$ material for the CVT reaction was divided into several portions in advance and introduced into furnace A from the left-hand end of the reactor tube at regular time intervals.

Chemical Vapor Transport. A raw mixture of rare earth chlorides RCl_3 and active carbon was weighed and put in an alumina boat (approximate length, 90 mm). The boat was placed in an alumina tube (outer diameter, 21 mm; inner diameter, 16 mm; length, 140 mm) and set at the upper

end of the temperature gradient in furnace B. The CVT reaction was performed in a stream of mixed N_2 and Cl_2 gases with flow rates of 40 and 6 cm^3 min^{-1}, respectively. The raw mixture was then heated to 1000 °C; further, furnace A was operated to generate gaseous Al_2Cl_6 according to the procedures described above. The rare earth chlorides were converted to the vapor complexes RAl_nCl_{3+3n} (n = 1–4) *via* reaction with Al_2Cl_6(g) as

$$RCl_3(s, l) + n/2\ Al_2Cl_6(g) = RAl_nCl_{3+3n}(g). \qquad (1.2)$$

These were driven with the carrier gas along the temperature gradient, decomposed according to the reverse process of eq. 1.2 and regenerated RCl_3 at a different position of the temperature gradient owing to the difference in their formation-decomposition equilibria.

The resulting deposits were collected by removing the alumina tubes. They were then dissolved individually in deionized water and the composition of rare earths was determined for each portion (fraction number) on a double-beam absorption spectrophotometer (Shimadzu UV-180), an X-ray fluorescent spectrometer (Rigaku System 3270A), and an inductively coupled argon plasma emission spectrophotometer (Nippon Jarrel-Ash ICAP-575 Mark-II). In the case of absorption spectroscopy the concentration of each rare earth element was determined from the peak intensity of the characteristic band: Pr^{3+}, 444.2 nm; Nd^{3+}, 794.0 nm; Sm^{3+}, 401.5 nm; Er^{3+}, 379.6 nm. For the X-ray fluorescence analysis $ZnCl_2$ was used as internal standard.

1.3. Results and Discussion

1.3.1. Necessity for Active Carbon

The gaseous complexation is known to take place only between anhydrous rare earth chlorides and the complex former, because, on heating, hydrous rare earth chlorides are generally self-hydrolyzed and give oxychlorides (ROCl) or oxides (R_2O_3) which are inert against the complexation with aluminium chloride. However, the anhydrous chlorides are very hygroscopic and thus are too difficult to handle under atmospheric conditions. Therefore hydrous rare earth chlorides were also tried as raw material.

It turned out that when $ErCl_3 \cdot nH_2O$ (2.0×10^{-3} mol) was used as raw material, about 75 mol% of initially loaded $ErCl_3$ was evaporated and chemically transported. This is because the resulting oxychlorides or oxides are re-chlorinated by the gaseous Al_2Cl_6 acting as a chlorinating agent [8, 9, 12a]. These reactions are expressed as

$$2\ R_2O_3(s) + 3\ Al_2Cl_6(g) \rightarrow 4\ RCl_3(s) + 6\ AlOCl(s) \qquad (1.3)$$

and

$$R_2O_3(s) + Al_2Cl_6(g) \rightarrow 2\,RCl_3(s) + Al_2O_3(s). \qquad (1.4)$$

It seemed, however, that the raw mixture of rare earth chlorides on the boat was covered with the inert AlOCl or Al_2O_3 layer generated by these reactions, whereby the reaction between RCl_3 and $AlCl_3$ is inhibited. Actually, after the CVT reaction of $ErCl_3 \cdot nH_2O$ a white residue insoluble in hydrochloric acid remained on the boat. In order to avoid the formation of AlOCl and Al_2O_3, active carbon powder was mixed with the $RCl_3 \cdot nH_2O$.

Figure 1.3 gives a plot of the total amount of transported $ErCl_3$ *vs* the atomic ratio (C/Er) of the raw material. The CVT reaction of $ErCl_3$ was promoted by an increase in the carbon content. However, the amount of transported $ErCl_3$ reached about 1.8×10^{-3} mol at C/Er = 2/1 and remained constant at molar ratios above 2/1. Although unreacted carbon remained in the boat after the CVT reaction, even at C/Er = 3/1 a large enough amount of rare earth chlorides for an effective mutual separation seems to have been transported. Thus a molar quantity of carbon twice as high as that of RCl_3 was mixed with the hydrous chlorides when hydrous RCl_3 were used as the raw material for further investigation of the mutual separation characteristics.

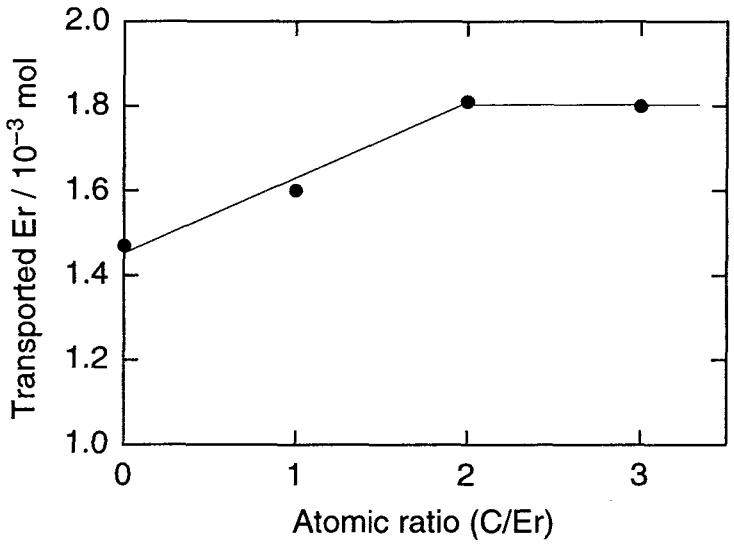

Figure 1.3. Effect of mole ratio (C/Er) on total amount of transported $ErCl_3$. Raw material was $ErCl_3 \cdot nH_2O$ (2.0×10^{-3} mol); complex former was $AlCl_3$ (8.0×10^{-3} mol); mixed N_2 and Cl_2 gases (N_2, 40 cm^3 min^{-1}; Cl_2, 6 cm^3 min^{-1}) was flowed as carrier; reaction time was 6 h (procedure I).

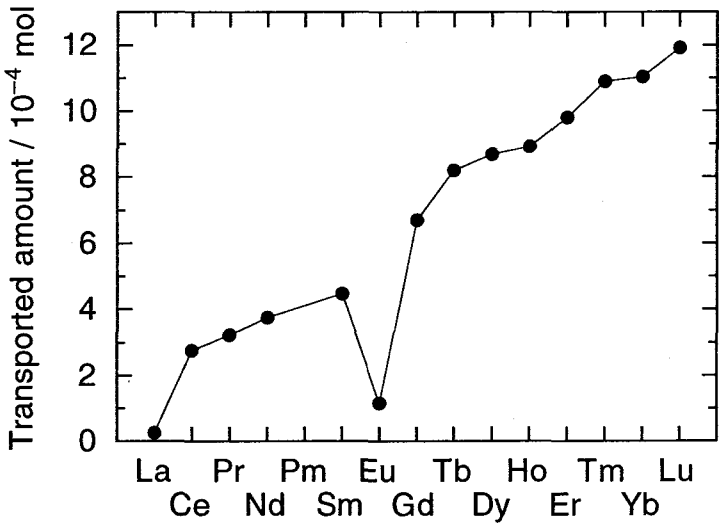

Figure 1.4. Variation in total transported amount for series of 14 lanthanoid elements. Raw material was RCl_3 (2.0×10^{-3} mol); complex former was $AlCl_3$ (2.7×10^{-3} mol); mixed N_2 and Cl_2 gases (N_2, 40 cm^3 min^{-1}; Cl_2, 6 cm^3 min^{-1}) was flowed as carrier; reaction time was 1 h (*procedure II*).

1.3.2. Chemical Vapor Transport of Pure RCl_3

A series of pure anhydrous RCl_3 (2.0×10^{-3} mol) samples were used as raw materials. The reaction time was 1 h for all runs and procedure II was employed for the gaseous Al_2Cl_6 supplied at constant rate. The total amount of transported RCl_3 increases with the increase in atomic number of the rare earth element (Fig. 1.4) and therefore the chlorides of heavier rare earths more easily form the corresponding vapor complexes and are more readily transported. This feature certainly suggests the possibility of mutual separation of rare earths using the fractional CVT reaction based on the difference in stability of the vapor complexes of the RCl_3-$AlCl_3$ systems.

However, the amount of transported $EuCl_3$ was exceptionally small (see Fig. 1.4), since the divalent chloride ($EuCl_2$) is more stable than the trivalent one ($EuCl_3$) at around 1000 °C [15], the complexation temperature employed in the present work. Hence, complexation between $EuCl_2$ and $AlCl_3$ hardly takes place.

Sørlie and Øye [16] have determined that the enthalpy of the reaction,

$$EuCl_2(s) + 3/2\ Al_2Cl_6(g) = EuAl_3Cl_{11}(g), \qquad (1.5)$$

is 70 kJ mol^{-1} (640–825 K). The enthalpy changes for the reactions,

$$RCl_3(s) + 3/2\ Al_2Cl_6(g) = RAl_3Cl_{12}(g), \qquad (1.6)$$

are generally less positive: $NdAl_3Cl_{12}$, 45.2 ± 1 kJ mol^{-1} (500–900 K) [14]; $SmAl_3Cl_{12}$, 28.1 ± 1 kJ mol^{-1} (600–800 K) [8]; $GdAl_3Cl_{12}$, 30.7 ± 4 kJ mol^{-1} [12b]; $HoAl_3Cl_{12}$, 11 kJ mol^{-1} (500–800 K) [17]; $TmAl_3Cl_{12}$, 27.7 ± 4 kJ mol^{-1} [12b]; $YbAl_3Cl_{12}$, 27.6 ± 4 kJ mol^{-1} [12a].

1.3.3. Chemical Vapor Transport of Quasi-Binary RCl_3 Mixtures

The $PrCl_3$-$ErCl_3$ System. An equimolar mixture of hydrous $PrCl_3$ and $ErCl_3$ (total 2.0×10^{-3} mol), *i.e.* a mixture of lighter and heavier rare earth chlorides, was used for the CVT reaction. In this CVT reaction gaseous Al_2Cl_6 was provided according to procedure I. Figure 1.5 shows the deposition profiles for the transported chlorides *vs* the fraction number (*FN*), together with the temperature gradients. Two types of temperature gradients were adopted: one was large (24 °C cm^{-1}) and almost linear and the other was smaller (13 °C cm^{-1}), mainly in the higher temperature region. With regard to $PrCl_3$ and $ErCl_3$, the difference observed between their deposition profiles was more or less independent of the temperature gradient: the peak position for $ErCl_3$ was shifted to the lower temperature side compared with that for $PrCl_3$. This indicates that the vapor com-

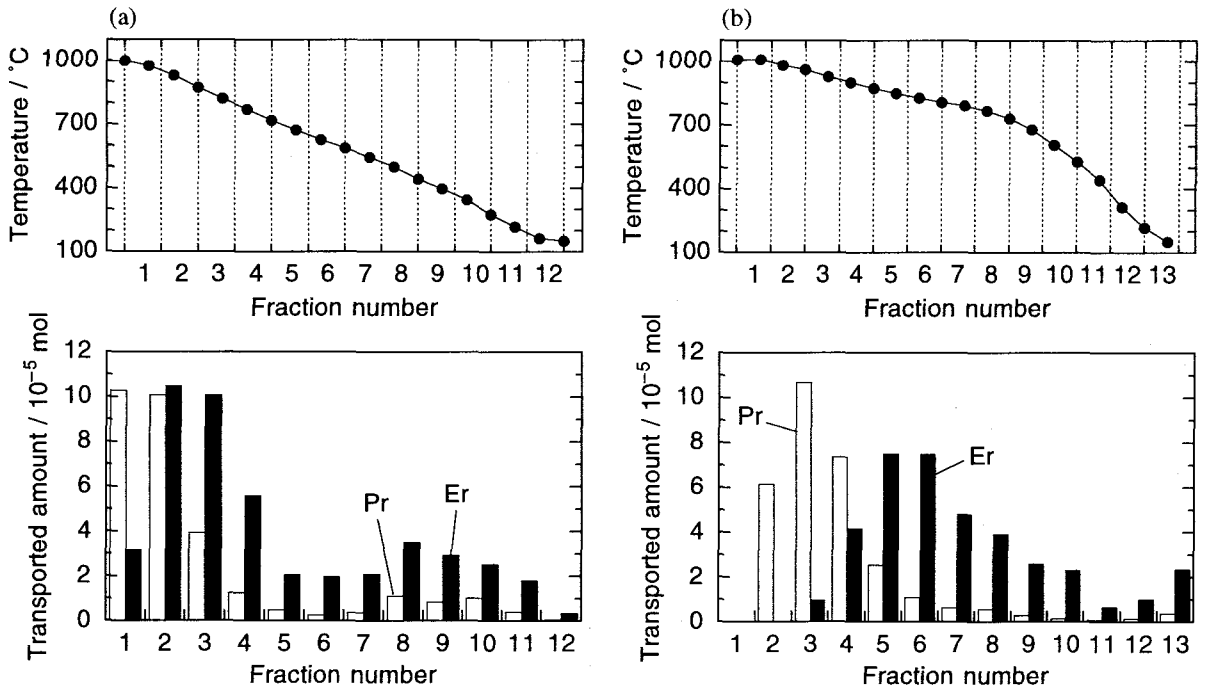

Figure 1.5. Temperature gradient and distribution profile of RCl_3: (a) linear gradient (24 °C cm^{-1}); (b) smaller gradient (13 °C cm^{-1}). Raw material was an equimolar mixture of $PrCl_3 \cdot nH_2O$ and $ErCl_3 \cdot nH_2O$ (2.0×10^{-3} mol); active carbon (C/R = 2/1) was mixed; complex former was $AlCl_3$ (8.0×10^{-3} mol); mixed N_2 and Cl_2 gases (N_2, 40 cm^3 min^{-1}; Cl_2, 6 cm^3 min^{-1}) was flowed as carrier; reaction time was 6 h (procedure I).

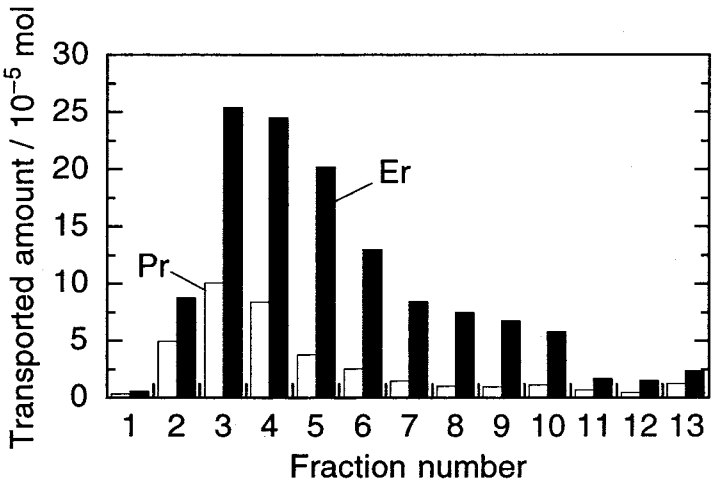

Figure 1.6. Distribution of $PrCl_3$ and $ErCl_3$ deposits under smaller temperature gradient. Raw material was $PrCl_3 \cdot nH_2O$ or $ErCl_3 \cdot nH_2O$ (each 2.0×10^{-3} mol); other reaction conditions were as in Fig. 1.5 (procedure I).

plexes in the $PrCl_3$-$AlCl_3$ system are less stable than those in the $ErCl_3$-$AlCl_3$ system, which is in agreement with the variation in the amounts of transported pure chlorides described above (Fig. 1.4). However, when the gradient with the smaller slope was used, both peak positions of the deposition profiles of $PrCl_3$ and $ErCl_3$ were much more separated from each other and therefore the resulting separation efficiency between the rare earths was improved. Separation factors between $PrCl_3$ and $ErCl_3$, defined as the value of the atomic ratio (Pr/Er) of the deposit divided by that of the raw mixture, were calculated for the fraction where $PrCl_3$ was most concentrated. The value increased from 3.25 ($FN = 1$ in Fig. 1.5(a)) to 10.8 ($FN = 3$ in Fig. 1.5(b)). Furthermore, under the gentler temperature gradient $PrCl_3$ was selectively deposited at $FN = 2$ and purified up to 100%. These results mean that the deposition rate of $ErCl_3$, *i.e.* the decomposition rate of the vapor complex $ErAl_nCl_{3+3n}$, is relatively depressed under the smaller temperature gradient. It is expected that precise control of the temperature gradient may realize good mutual separation and purification of rare earths using CVT phenomena.

Figure 1.6 shows the deposition profiles for the chlorides under the same CVT reaction condition with the smaller slope as in Fig. 1.5(b), where pure $PrCl_3$ (2.0×10^{-3} mol) or $ErCl_3$ (2.0×10^{-3} mol) was loaded as the raw material and the profiles were obtained from each run. They peaked at a common position ($FN = 3$), although the mixture of $PrCl_3$ and $ErCl_3$ gave independent peaks at $FN = 3$ and $FN = 5$ respectively (see Fig. 1.5(b)). This difference is explained as follows. When the pure chloride was loaded, the amount of $ErAl_nCl_{3+3n}$ complex ($w_{Er\text{-}Al\text{-}Cl}$) formed on the

Table 1.1. Comparison of total amounts and deposition maxima of transported chlorides

Raw material [a]	Temperature gradient [c]	Amount of RCl_3 deposit [d] (10^{-4} mol)	
		$PrCl_3$	$ErCl_3$
$PrCl_3$-$ErCl_3$ [b]	Linear	3.0 (1)	4.7 (2)
$PrCl_3$-$ErCl_3$ [b]	Smaller Slope	3.0 (3)	3.8 (5)
$PrCl_3$	Smaller Slope	3.7 (3)	—
$ErCl_3$	Smaller Slope	—	12.7 (3)

[a] The loaded amount of RCl_3 for all runs was 2.0×10^{-3} mol.

[b] Equimolar mixture of $PrCl_3$ and $ErCl_3$.

[c] See text.

[d] Fraction number of deposition maximum is designated in parentheses.

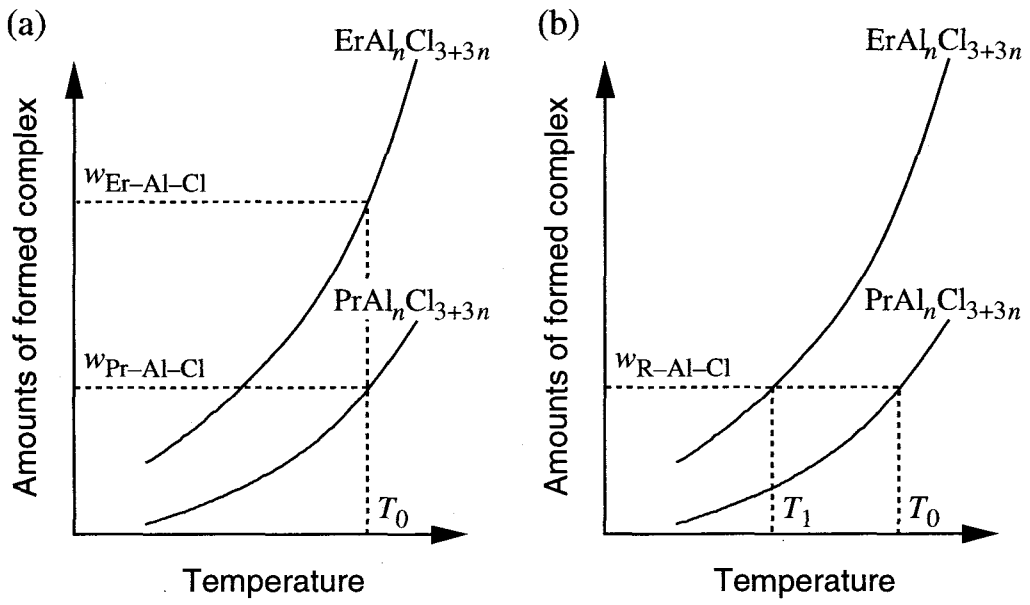

Figure 1.7. Schematic representation of relation between temperature and amounts of formed vapor complexes. Raw materials are (a) pure RCl_3 (R = Pr, Er) and (b) their equimolar mixture.

surface of the raw mixture in the boat was greater than that of $PrAl_nCl_{3+3n}$ ($w_{Pr\text{-}Al\text{-}Cl}$), since the former complex was more volatile (see Fig. 1.4) and readily formed.

Therefore the temperatures (T_0) at which the equilibria,

$$PrCl_3(s, l) + n/2\ Al_2Cl_6(g) = PrAl_nCl_{3+3n}(g) \quad (1.7)$$

and

$$ErCl_3(s, l) + n/2\ Al_2Cl_6(g) = ErAl_nCl_{3+3n}(g), \quad (1.8)$$

are attained and the chlorides begin to deposit are almost equal (see Fig. 1.7(a)). In contrast, an equimolar mixture of $PrCl_3$ and $ErCl_3$ provides almost equal amounts ($w_{R\text{-}Al\text{-}Cl}$) of $PrAl_nCl_{3+3n}$ and $ErAl_nCl_{3+3n}$ complexes, because the complexation reactions (eqs. 1.7 and 1.8) take place only on the surface of the raw mixture and thus the chances of complexation are nearly equal. This is reflected in the total amounts of transported chloride, which were not very different from each other, as shown in Table 1.1. Therefore the temperature for attaining the equilibrium of eq. 1.8 is lowered from T_0 to T_1 under the temperature gradient and the deposition peak maximum of $ErCl_3$ is shifted to the lower temperature side (see Fig. 1.7(b)). This is supported by the fact that the deposition profile of $PrCl_3$ in Fig. 1.5(b) is similar to that in Fig. 1.6 and, furthermore, that the profile of $ErCl_3$ in Fig. 1.5(b) is also similar to that in Fig. 1.6 at the lower temperature region ($FN = 6$–13).

The free $Al_2Cl_6(g)$ species reproduced by the reverse processes of eqs. 1.7 and 1.8 and unreacted Al_2Cl_6 were passed through both higher and lower temperature zones of furnace B and finally condensed at $FN = 12$ and 13 because of the relatively low sublimation temperature of $AlCl_3$ (below 200 °C). In other words, since both RCl_3 and $AlCl_3$ were obtained in pure forms in different deposition regions, $AlCl_3$ can be recovered and recycled for further CVT processing.

The $PrCl_3$-$SmCl_3$ System — Multiple CVT Reactions. The deposition profiles for an equimolar mixture (2.0×10^{-3} mol) of $PrCl_3$ and $SmCl_3$ are shown in Fig. 1.8. The transport conditions in this system were the same as those used in the $PrCl_3$-$ErCl_3$ system with the smaller temperature gradient. The deposition profile of $PrCl_3$ was maximized at $FN = 3$ while that of $SmCl_3$ appeared at $FN = 4$, so that the separation efficiency was decreased compared with that obtained in the $PrCl_3$-$ErCl_3$ system. This is because the difference in atomic number between Pr and Sm is smaller than that between Pr and Er. Hence the chemical properties, *e.g.* formation equilibria, of Pr- and Sm-containing vapor complexes are not very different from each other. Consequently, the mutual separation from such a system is not thoroughly achieved by only one CVT operation.

In order to separate mutually and purify these neighboring element pairs in the periodic table, it is necessary to repeat the CVT reaction several times, similarly to the solvent extraction process

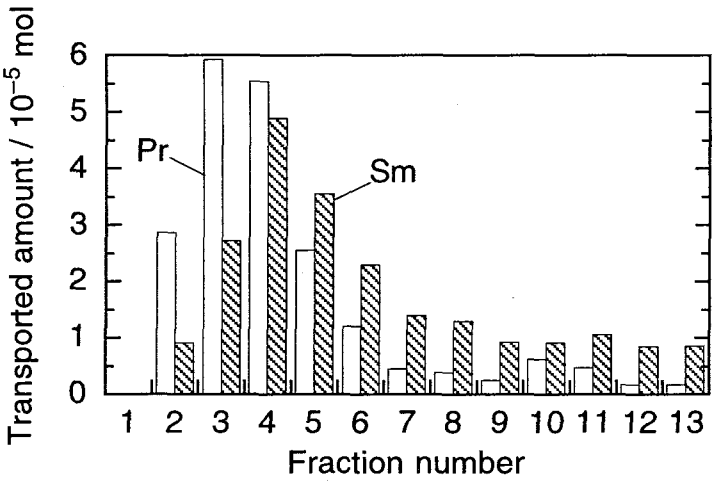

Figure 1.8. Distribution of $PrCl_3$ and $SmCl_3$ deposits under smaller temperature gradient. Raw material was an equimolar mixture of $PrCl_3 \cdot nH_2O$ and $SmCl_3 \cdot nH_2O$ (2.0×10^{-3} mol); other reaction conditions were as in Fig. 1.5 (procedure I).

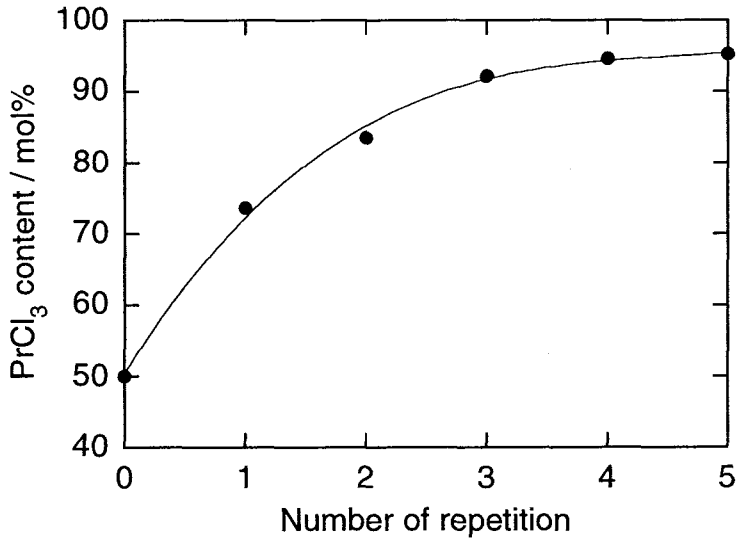

Figure 1.9. Variation in molar fraction of $PrCl_3$ per RCl_3 contents for multiple chemical vapor transport reactions in $PrCl_3$-$SmCl_3$ system.

which requires a number of mixer-settler stepwise operations. Multiple CVT reactions were applied to the mixture in the $PrCl_3$-$SmCl_3$ binary system. For an equimolar mixture of $PrCl_3$ and $SmCl_3$ the molar fraction of $PrCl_3$ (x_{Pr}) had a maximum of 73.6 mol% in the second portion (FN = 2), as shown in Fig. 1.8. Therefore a mixture (total 2.0×10^{-3} mol) close to this composition (x_{Pr} = 70 mol%) was chosen as the raw material for the second CVT reaction. In this second CVT reac-

tion $PrCl_3$ became more concentrated, up to 83.5 mol% at $FN = 2$. The composition of the raw mixture used for the third reaction was chosen accordingly as $x_{Pr} = 84$ mol%. Analogously, mixtures (2.0×10^{-3} mol) of $x_{Pr} = 90$ and 95 mol% were used for the fourth and fifth CVT reactions respectively.

Figure 1.9 shows the relationship between the number of CVT reactions and the molar fraction (x_{Pr}) of the portion where $PrCl_3$ was most concentrated. As a result, one can mutually separate even rare earth pairs with neighboring atomic numbers by means of multiple CVT reactions.

A separation factor between $PrCl_3$ and $SmCl_3$ was calculated for five runs of the multiple reactions in the same manner as described above. The average value was 2.29. On the assumption that the value (2.29) is unchanged under the same transport conditions, $PrCl_3$ with a purity of 99.9 mol% can be obtained after the ninth CVT reaction.

The $PrCl_3$-$NdCl_3$ System. By using $AlCl_3$ as the complex former, the mutual separation of neighboring element pairs such as the $PrCl_3$-$NdCl_3$ system was also possible if the CVT reaction was repeated. However, the CVT reactions using alkali metal chlorides as complex formers was more appropriate for this separation (see Chapter 2).

1.3.4. Chemical Vapor Transport of Quasi-Ternary RCl_3 Mixture

Mutual separation characteristics of a rare earth quasi-ternary system were examined using

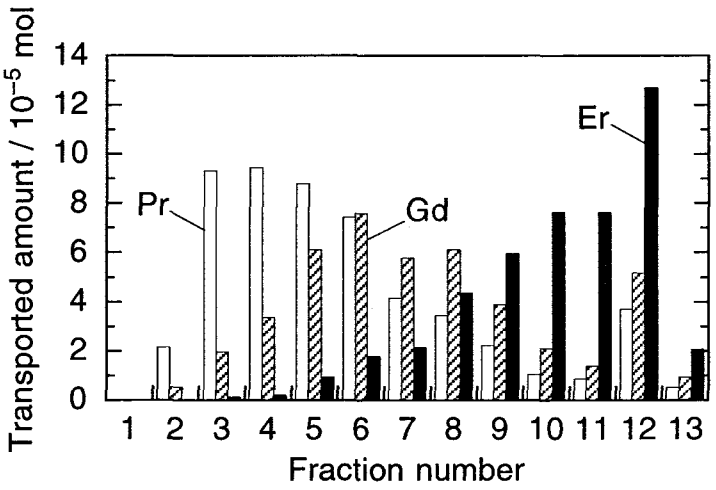

Figure 1.10. Distribution of $PrCl_3$, $GdCl_3$, and $ErCl_3$ deposits under smaller temperature gradient. Raw material was an equimolar mixture of $PrCl_3 \cdot nH_2O$, $GdCl_3 \cdot nH_2O$, and $ErCl_3 \cdot nH_2O$ (3.0×10^{-3} mol); complex former was $AlCl_3$ (11.8×10^{-3} mol); active carbon and carrier gas were as in Fig. 1.5; reaction time was 12 h (procedure II).

3.0×10^{-3} mol of a $PrCl_3$-$GdCl_3$-$ErCl_3$ equimolar mixture. Procedure II was employed to generate the gaseous Al_2Cl_6 and 4.9×10^{-4} mol of $AlCl_3$ was introduced into furnace A at intervals of 30 min for 12 h. The deposition profiles of the individual transported chlorides are shown in Fig. 1.10. Their deposition peak maxima are well separated, hence good mutual separation characteristics were observed. The deposition peaks observed on going from the higher to the lower temperature side are in accordance with the increasing atomic numbers of the elements. This agrees with the deposition peak positions observed for binary systems: the amount of the deposit of the lighter rare earth chlorides is greater than that of the heavier ones in the higher temperature fractions. The situation is reversed in the lower temperature fractions.

1.4. Conclusions

It turned out that the mutual separation of rare earths can be conducted effectively in a flow-type reactor using the chemical vapor transport process mediated by vapor complexes in the RCl_3-$AlCl_3$ system. A high separation efficiency was attained by precise control and optimization of the temperature gradient. Rare earths of almost 100% purity were obtained by multiple reactions. This method is suitable for the industrial mass production of rare earths of high purity. The rare earth chlorides obtained can be converted directly to rare earth metals, the demand for which is increasing year by year owing to applications in high performance intermetallic compounds.

Chapter 2

Mutual Separation of Mixed Praseodymium and Neodymium Using Chemical Vapor Transport Mediated by Rare Earth Chloride–Alkali Metal Chloride Vapor Complex

2.1. Introduction

In addition to vapor complex formation in the RCl_3-$AlCl_3$ (R = rare earths) system as

$$RCl_3(s, l) + n/2\ Al_2Cl_6(g) = RAl_nCl_{3+3n}(g), \quad (2.1)$$

rare earth chlorides are known to form another series of vapor complex with alkali metal chlorides (ACl) [1–7] according to the reaction,

$$RCl_3(s, l) + ACl(s, l) = ARCl_4(g). \quad (2.2)$$

Though the vapor complexes in the corresponding iodide systems, RI_3-AI, have been well studied in terms of luminescent materials for high-intensity discharge lamps [1], any application of the $ARCl_4$ complexes has not been reported until now.

In general, mutual separation of rare earth elements, particularly of neighboring element pairs in the periodic table, is quite difficult because of the similarity in their chemical properties. This chapter describes the mutual separation characteristics of a $PrCl_3$-$NdCl_3$ mixture, which is one of the neighboring rare earth pairs and the most difficult system for mutual separation, by means of the chemical vapor transport (CVT) reaction *via* vapor complexes with alkali metal chlorides. Furthermore, the transport reactions using mixed rare earth oxides were also attempted, since rare earth chlorides hitherto used for the raw material for the CVT reactions are difficult to handle due to high hygroscopicity. The resulting separation efficiency was discussed from the viewpoints of the chlorination and transport conditions and mechanism, and, further, a simulation of the transport phenomena was carried out by a calculation based on known thermodynamic data and empirical factors.

2.2. Experimental Details

2.2.1. Mutual Separation of Mixed Praseodymium and Neodymium Chlorides

Materials. Anhydrous rare earth chlorides, RCl_3 (R = Pr, Nd), were prepared by heating the corresponding oxides, Pr_6O_{11} and Nd_2O_3 (purity, 99.9%), with a large excess of NH_4Cl (99.0%) at 623 K for 2 h in a stream of the N_2 gas dried by passing through a P_2O_5 column; further, the residual NH_4Cl was removed by sublimation at 673 K. The resulting RCl_3 was identified by the powder X-ray diffraction pattern [18].

A series of chlorides, *i.e.* anhydrous $AlCl_3$ (98.0%), LiCl (99.0%), NaCl (99.9%), KCl (99.5%), RbCl (99.0%), and CsCl (99.0%), was used as complex formers without any pretreatment for the CVT reaction.

Operation. The apparatus employed for the CVT reaction is the same as described in Chapter 1. An equimolar mixed chloride of $PrCl_3$ and $NdCl_3$ was weighed and then put on an alumina boat (length, 90 mm). The boat was placed in an alumina tube (outer diameter, 21 mm; inner diameter, 16 mm; length, 140 mm) and set at the upper end of the temperature gradient. The complex former (ACl) was added directly to RCl_3. Since $AlCl_3$ is very volatile compared to ACl, it was charged into a glass ampule with a small orifice with a diameter of about 0.5 mm. The ampule was then loaded into furnace A (length, 180 mm) and mildly heated in order to control its evaporation rate.

The CVT reaction was performed in a stream of mixed N_2 and Cl_2 gases with flow rates of 30 and 5 $cm^3\ min^{-1}$, respectively. By operating furnace B, the desired temperature gradient was attained. The raw material of RCl_3, or its mixture with ACl, was heated to 1273 K. Further, if need be, furnace A was heated over the temperature range 353 to 473 K at a rate of 20 K h^{-1} in order to generate gas-phase aluminium chloride, Al_2Cl_6 (*cf* Procedure I in Chapter 1). The rare earth chlorides reacted with ACl or Al_2Cl_6 to form gas-phase complexes: $ARCl_4$ or RAl_nCl_{3+3n} (n = 1–4). The resulting complexes were driven with the carrier gas and decomposed along the temperature gradient according to the reverse process of eqs. 2.1 and 2.2 to regenerate RCl_3. The transport reaction lasted for 6 h.

The deposits were collected by removing the twelve pieces of alumina tubing; they were then dissolved individually in deionized water, and the compositions of $PrCl_3$ and $NdCl_3$ were determined for every portion from the peak intensity values of the visible absorption spectra at 444.2 nm for the Pr^{3+} ion and 794.0 nm for the Nd^{3+} ion. The content of ACl (except for LiCl) in each portion

was checked by means of an X-ray fluorescence analysis (Rigaku System 3270A) using $ZnCl_2$ as an internal standard.

2.2.2. Mutual Separation of Mixed Praseodymium and Neodymium Oxides

Materials. The equimolar mixture of praseodymium and neodymium oxides (total 6.0×10^{-3} mol) was used for the CVT reactions. In order to obtain a homogeneously mixed raw material, the mixed oxide was prepared from a corresponding aqueous solution of the mixed praseodymium and neodymium chlorides by precipitation with a saturated $(COONH_4)_2$ solution in pH = 2. The obtained $R_2(COO)_3$ was then filtered off, washed with deionized water, and calcined with a methane flame on a platinum crucible for 1 day to give the mixed oxide, R_2O_3. The oxide was analyzed on an X-ray fluorometer to make sure the composition was Pr/Nd = 1/1.

Potassium chloride (6.0×10^{-3} mol) equimolar with a R^{3+} ion in the R_2O_3 was used as the complex former (transporting agent) for the CVT reaction. As well as KCl, some potassium salts, K_2CO_3, K_2SO_4, KNO_3, KF, and $KAl(SO_4)_2$, were also used as a precursor of the complex former, KCl, in order to avoid a deviation of the composition of the raw melt where a mole ratio R/K of 1/1 is desirable as mentioned below. These potassium salts were reagent grade (> 99.0%) and used without any further purification except for $KAl(SO_4)_2$ which was prepared from a corresponding hydrate by heating at 423 K.

A powdery active carbon (*ca* 0.5 g) as a deoxidant was also mixed with the raw material without any pretreatment.

Operation. The instrumentation to obtain a temperature gradient for CVT reaction has been described in detail in Chapter 1. A raw mixture of the mixed oxide, potassium salt, and active carbon was put in a mullite boat (length, 90 mm). The boat was then placed in a quartz inner tube (outer diameter, 22 mm; inner diameter, 19 mm; length, 140 mm) and loaded in a quartz reactor tube with a stream of N_2 (30 cm^3 min^{-1}) and Cl_2 (5 cm^3 min^{-1}) gases. Upon heating by electric furnace up to 1273 K, the rare earth mixed oxide and potassium salt were chlorinated by Cl_2 to RCl_3 and KCl. These reactions are expressed as follows:

$$R_2O_3(s) + 3\ Cl_2(g) + 3\ C(s) \rightarrow 2\ RCl_3(s, l) + 3\ CO(g), \qquad (2.3)$$

$$K_2CO_3(s) + Cl_2(g) + 2\ C(s) \rightarrow 2\ KCl(s, l) + 3\ CO(g), \qquad (2.4)$$

and

$$K_2SO_4(s) + Cl_2(g) + 2\ C(s) \rightarrow 2\ KCl(s, l) + SO_2(g) + 2\ CO(g). \qquad (2.5)$$

The mixture was finally heated at 1273 K, and the resulting RCl_3 and KCl were converted to the vapor complexes *via* reaction as

$$RCl_3(s, l) + KCl(s, l) = KRCl_4(g). \quad (2.6)$$

The complexes, $KPrCl_4(g)$ and $KNdCl_4(g)$, were driven with the N_2–Cl_2 gas stream in the reactor along a temperature gradient and decomposed according to the reverse process of eq. 2.6, and rare earth chlorides were regenerated. After the CVT reaction lasted for 6–82 h, the resulting deposits along the temperature gradient were collected from the inner tubes. The deposits in the inner tubes and the residual mixture on the boat were dissolved individually in dilute hydrochloric acid to determine the composition of Pr, Nd, and K for each inner tube (*FN* = fraction number) on an X-ray fluorometer (Rigaku System 3270A).

2.3. Results and Discussion

2.3.1. Mutual Separation of Mixed Praseodymium and Neodymium Chlorides

(1) Effect of Alkali Metal Chloride as a Complex Former

Three metal chlorides ($AlCl_3$, NaCl, and KCl) were used as complex formers. Figure 2.1 shows a series of deposition profiles for the CVT reaction over the divided twelve portions, numbered as fraction numbers (*FN*), together with the temperature gradient. The charged amounts of RCl_3, $AlCl_3$, and ACl were as follows: RCl_3, 1.65×10^{-3}; $AlCl_3$, 7.5×10^{-2}; ACl, 1.65×10^{-3} mol.

For $AlCl_3$ (see Fig. 2.1(b)), the deposition profile of $PrCl_3$ was almost same as that of $NdCl_3$, peaking at $FN = 4$. This means that the formation and decomposition conditions of vapor complexes $PrAl_nCl_{3+3n}$ and $NdAl_nCl_{3+3n}$ are closely similar to each other. Under this condition tailing up to the end of the temperature gradient ($FN = 12$) and the second small peak at $FN = 9$ were also observed on their profiles. The latter is probably due to a steep decline in the temperature gradient.

The deposition profiles of RCl_3 observed for the CVT reactions upon using NaCl and KCl were greatly sharpened, and their gravity centers were shifted to the higher-temperature side compared with the case of $AlCl_3$. This means that the temperature region for the formation of vapor complex $ARCl_4$ is higher than that for RAl_nCl_{3+3n}. Furthermore, some differences between the deposition profiles for $PrCl_3$ and $NdCl_3$ were emphasized by using them as complex formers. Generally, the amount of the lighter rare earth chloride is larger than that of the heavier one at higher temperature fractions, while the situation is inverted at the lower-temperature side. This tendency was more or less observed in each case of $AlCl_3$, NaCl, and KCl. Particularly, when KCl was used,

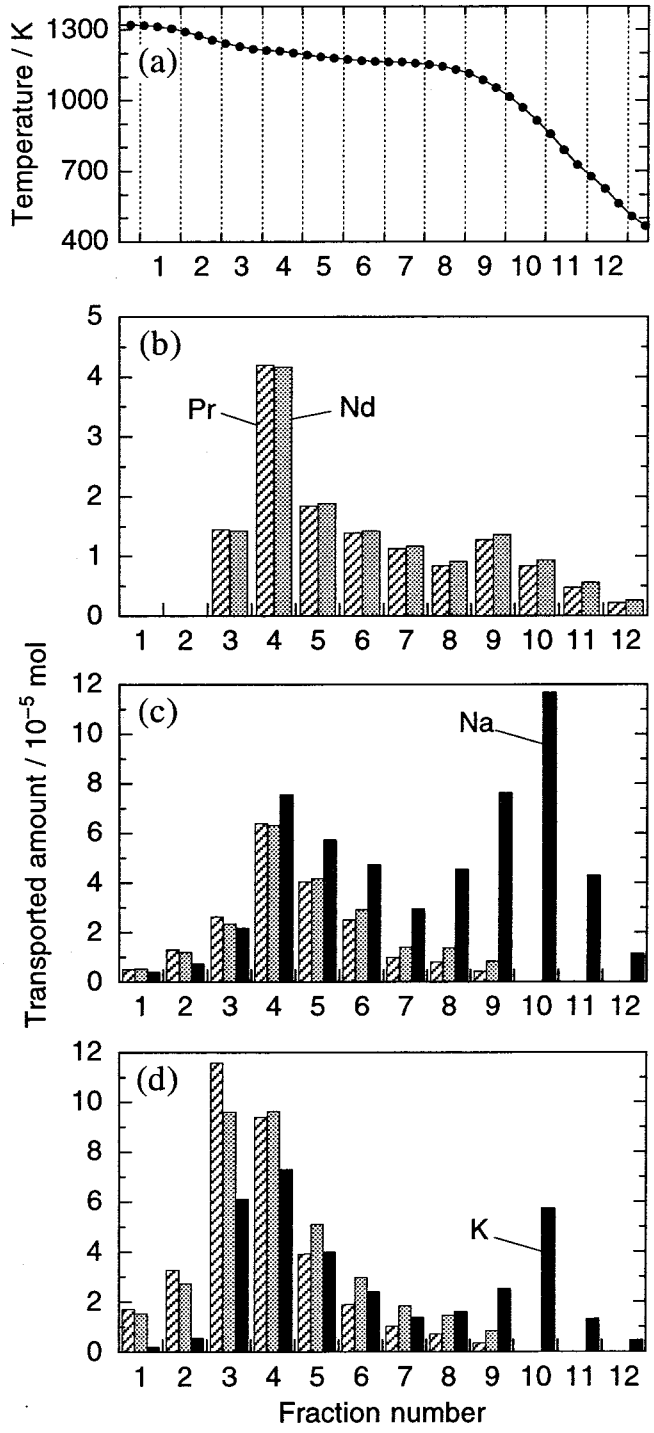

Figure 2.1. (a) Temperature gradient and (b–d) distribution of RCl_3 and ACl deposits. Raw material was an equimolar mixture of $PrCl_3$ and $NdCl_3$ (1.65×10^{-3} mol); complex formers were (b) $AlCl_3$ (7.5×10^{-2} mol), (c) NaCl (1.65×10^{-3} mol), and (d) KCl (1.65×10^{-3} mol); mixed N_2 and Cl_2 gases (N_2, 30 cm^3 min^{-1}; Cl_2, 5 cm^3 min^{-1}) was flowed as carrier; reaction time was 6 h.

Table 2.1. Separation factors and recovery for the chemical vapor transport using various complex formers

Complex former	Separation factor [a]		Recovery (%)
	$\beta_{Pr/Nd}$	$\beta_{Nd/Pr}$	
$AlCl_3$	1.00	1.07	17
NaCl	1.04	1.21	25
KCl	1.07	1.33	42
LiCl and $AlCl_3$	1.04	1.16	19
NaCl and $AlCl_3$	1.08	1.20	33
KCl and $AlCl_3$	1.07	1.20	40
RbCl and $AlCl_3$	1.08	1.24	26
CsCl and $AlCl_3$	1.11	1.19	38

[a] See text.

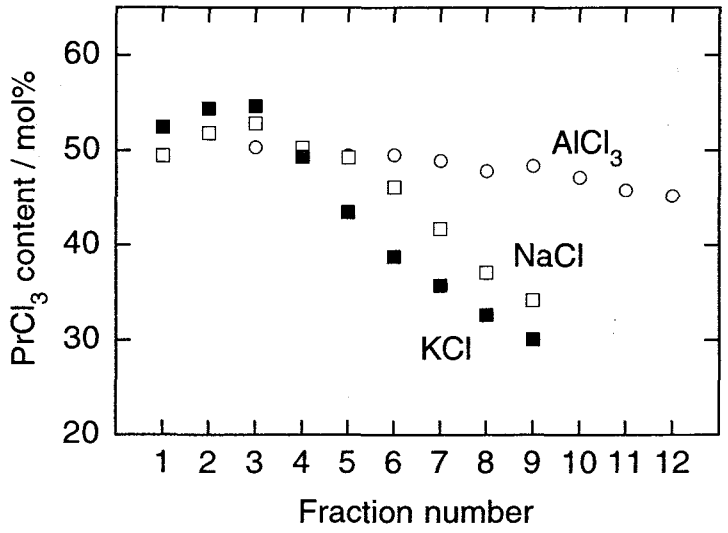

Figure 2.2. Molar fraction of $PrCl_3$ per RCl_3 contents for deposits shown in Fig. 2.1. Complex formers were $AlCl_3$, NaCl, and KCl.

$PrCl_3$ peaked at $FN = 3$, while $NdCl_3$ peaked at $FN = 4$.

The total amount of the RCl_3 deposited, that is, the recovery of RCl_3, was low (17%) when $AlCl_3$ was employed as the complex former. However, by using ACl in place of $AlCl_3$, the recovery was improved: NaCl, 25%; KCl, 42% (see Table 2.1). This indicates that the formation of vapor complex RAl_nCl_{3+3n} is limited and, hence, is too slow to equilibrate [14], since in this case complexation takes place only on the surface of the RCl_3 melt, compared with the bulk reaction in

the melt of RCl_3 and ACl.

Figure 2.2 shows the molar fraction profiles of $PrCl_3$ for deposits transported by $AlCl_3$, NaCl, and KCl. Transport with $AlCl_3$ gave a flat relation against *FN*, and the separation efficiency between $PrCl_3$ and $NdCl_3$ was very poor. The molar fraction value of $PrCl_3$ slightly decreased with an increase in *FN*. The above-mentioned tendency, that the deposition profile of RCl_3 schematically shifts to the lower temperature side with an increase in the atomic number of R, was also observed under this condition. This feature is in accord with the previous results obtained regarding the $PrCl_3$-$ErCl_3$, $PrCl_3$-$SmCl_3$, and $PrCl_3$-$GdCl_3$-$ErCl_3$ systems (see Chapter 1).

On the other hand, the use of ACl as a complex former makes the molar fraction profiles sharpen and allows an improved separation efficiency. The molar-fraction profiles of $PrCl_3$ were maximized at around $FN = 3$ and steeply declined with an increase in *FN* compared with the values for $AlCl_3$ (see Fig. 2.2). This results in a selective concentration of $PrCl_3$ or $NdCl_3$ onto every fraction along the temperature gradient, and realizes mutual separation between $PrCl_3$ and $NdCl_3$ in high efficiency.

The difference in sharpness of the molar-fraction curves for NaCl and KCl indicates that the formation equilibria of $KPrCl_4$ and $KNdCl_4$ cause an apparent difference from each other compared with that of $NaPrCl_4$ and $NaNdCl_4$; further, deposition is more selective when using KCl. Novikov *et al* have determined that though the formation enthalpies and entropies of these complexes are equal to each other ($\Delta H^\circ_{1350K} = 59.3 \pm 4$ kcal mol^{-1}; $\Delta S^\circ_{1350K} = 32.3 \pm 3$ e.u. (e.u. = cal $^\circ C^{-1}$)), the compositions of the vapor complexes over 50 mol% melt of the RCl_3-KCl system (R = Pr, Nd) are quite different at 1273 K: $KPrCl_4$, 13.0 mol%; $KNdCl_4$, 23.0 mol% [19a]. Unfortunately, thermodynamic data with respect to the sodium-containing complex have been obtained only for $NaNdCl_4$ [19b]. Therefore, one can not argue for a difference between the formation conditions of $NaPrCl_4$ and $NaNdCl_4$ as well as the reason for the improved separation efficiency (NaCl < KCl) from the viewpoint of thermodynamics.

In order to compare the separation efficiency for each complex former, the value separation factor β was evaluated. The β values at the high- and low-temperature sides, where each amount of RCl_3 deposited is equal to half the total (*i.e.* $N_{HPr} + N_{HNd} = N_{LPr} + N_{LNd}$), are defined as

$$\beta_{Pr/Nd} = \frac{N_{HPr}/N_{HNd}}{N_{0Pr}/N_{0Nd}} = N_{HPr}/N_{HNd} \qquad (2.7)$$

and

$$\beta_{Nd/Pr} = \frac{N_{LNd}/N_{LPr}}{N_{0Nd}/N_{0Pr}} = N_{LNd}/N_{LPr}. \qquad (2.8)$$

Here, N_{HR} and N_{LR} (R = Pr, Nd) are the molar quantities of the deposits transported to high- and low-temperature sides, respectively, and N_{0Pr} and N_{0Nd} are Pr- and Nd-contents of the initially loaded raw mixture. In this work, N_{0Pr} and N_{0Nd} are equal to each other and, hence, the β values can be simply expressed as the right-hand sides of the equations.

The obtained separation factors are summarized in Table 2.1 together with the recoveries. The $\beta_{Pr/Nd}$ and $\beta_{Nd/Pr}$ values show a tendency to increase in the order $AlCl_3 < NaCl < KCl$, as well as the recoveries. In general, the $\beta_{Pr/Nd}$ value is smaller than the $\beta_{Nd/Pr}$, since the vapor complex comprising $NdCl_3$, $NdAl_nCl_{3+3n}$ and $ANdCl_4$, are easy to form, compared with those of $PrCl_3$. $NdCl_3$ thus tends to be transported more than $PrCl_3$. If the amounts of $PrCl_3$ and $NdCl_3$ deposits were similar to each other, the two above-mentioned β values should be equal. It is noteworthy that the $\beta_{Nd/Pr}$ value for KCl (1.33) is not inferior to those of the complexing agents for conventional solvent extractions, *e.g.*, 1.38 for bis(2-methylhexyl)phosphoric acid (D2EHPA) [20a] and 1.50 for tributyl phosphate (TBP) [20b].

When $AlCl_3$ was used as the complex former, the $AlCl_3$ residue reproduced by the reverse process of eq. 2.1 was passed through the lower temperature region and condensed at the right-hand end of furnace B, due to the relatively low sublimation temperature of $AlCl_3$ (below 473 K). Consequently, the RCl_3 deposits transported by $AlCl_3$ are obtained in pure form without any contamination of the used complex former. In other words, it is possible that complex former $AlCl_3$ can be recovered and recycled for further processing. In contrast, the volatility of ACl is low in the temperature region studied in this work; these are widely spread over furnace B, showing two deposition peaks at $FN = 4$ and $FN = 10$. The peak at $FN = 4$ is assigned to the ACl deposit related to the CVT reaction, since it almost coincides with the deposition peak position of RCl_3. The peak at $FN = 10$ seems to be responsible for the residue which results from the free ACl vapor after migrating *via* the gas phase, since the deposition profile of the ACl usually has a single peak at $FN = 6$ in furnace B when only ACl is loaded. As a result, the RCl_3 deposits transported by ACl contain a significant amount of ACl as an impurity and, thus, they need to be removed from the RCl_3 deposits.

(2) Simultaneous Use of ACl (A = alkali metal) and $AlCl_3$

To remove the ACl residue from the RCl_3 deposit, both ACl and $AlCl_3$ were simultaneously used as complex formers. That is to say, 1.65×10^{-3} mol of ACl (A = Li, Na, K, Rb, and Cs) was mixed with an equimolar amount of raw RCl_3 (Pr/Nd = 1/1); furthermore, gaseous Al_2Cl_6 (total 7.5×10^{-2} mol) was introduced from furnaces A to B as a second complex former.

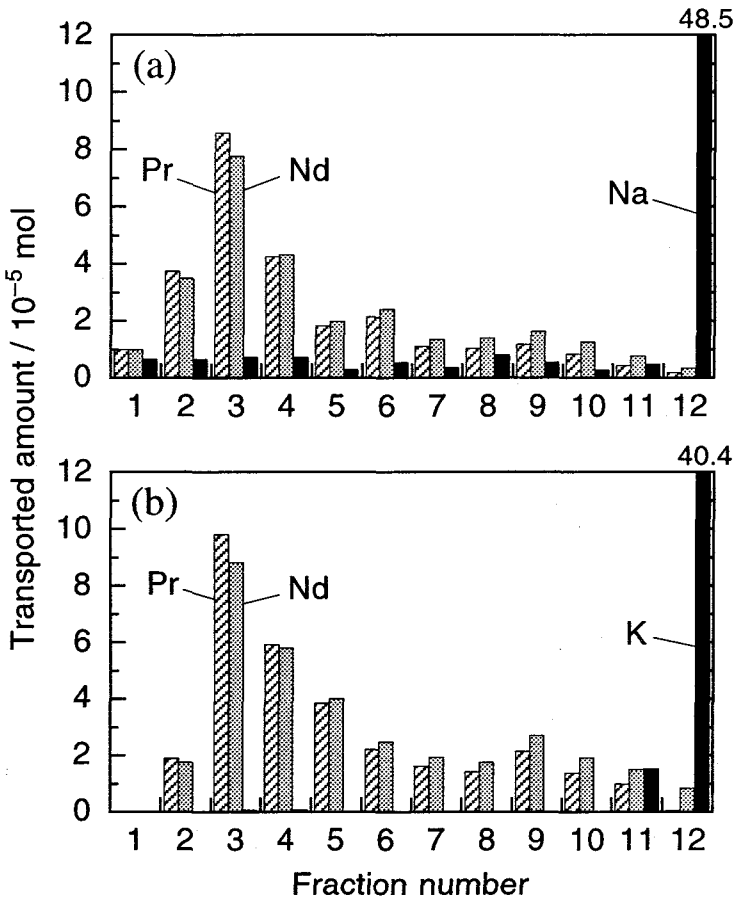

Figure 2.3. Distribution of RCl_3 and ACl deposits under simultaneous uses of two complex formers: (a) NaCl (1.65×10^{-3} mol) and $AlCl_3$ (7.5×10^{-2} mol); (b) KCl (1.65×10^{-3} mol) and $AlCl_3$ (7.5×10^{-2} mol). Carrier gas and reaction time were as in Fig. 2.1.

Figure 2.3 shows the deposition profiles for RCl_3 and ACl. The profile of ACl was remarkably changed upon the addition of $AlCl_3$. The greatest amount of ACl was carried to fraction FN= 12 and, hence, the transported RCl_3 scarcely contained any ACl residue as an impurity. Furthermore, the separation factors and recoveries of RCl_3 (see Table 2.1) were maintained at similar levels to that obtained for the transport reaction where only ACl was used as a complex former . It has been found that complexation between ACl and $AlCl_3$ [21],

$$ACl(s) + 1/2\ Al_2Cl_6(g) = AAlCl_4(g), \qquad (2.9)$$

takes place. It is concluded that any ACl residue codeposited according to the reverse process of eq. 2.2 is removed by the regeneration of much more volatile complexes. *i.e.*, $NaAlCl_4$ and $KAlCl_4$.

All of the alkali metal chlorides had a positive effect on the separation factor. Among them,

RbCl gave the best result under the condition of simultaneously using ACl with $AlCl_3$ as the complex formers. However, KCl may be better from the viewpoint of economical efficiency.

(3) Amount Dependence of ACl

The CVT reaction was carried out by using a variable amount of ACl. In order to compare the RCl_3 contents of the transported deposits, the amount of RCl_3 (Pr/Nd = 1/1) initially loaded was kept constant at 1.65×10^{-3} mol. The chloride (NaCl) was mixed at two amounts: 5.50×10^{-4} mol (Na/R = 1/3) and 4.95×10^{-3} mol (Na/R = 3/1). As the second complex former, a total of 7.5×10^{-2} mol of $AlCl_3$ was also used.

The amounts RCl_3 in the deposits transported for a series of runs are summarized in Table 2.2, together with the separation factors and recoveries. As mentioned above, each $\beta_{Nd/Pr}$ value is generally larger than the corresponding $\beta_{Pr/Nd}$ value, due to the difference in the complexation rates between RCl_3 and the complex formers. The highest $\beta_{Nd/Pr}$ value and recoveries were 1.20 and 33% upon the addition of 1.65×10^{-3} mol of NaCl (Na/R = 1/1). The fact that those values are maximized when the raw mixture comprises an equimolar composition of NaCl and RCl_3 explains the increase in the amounts of RCl_3 deposits transported, since RCl_3 and ACl are known to form 1:1 vapor complexes, such as $NaPrCl_4$ and $NaNdCl_4$ [7a, 19]. Moreover, the result that the β values varied in a similar manner as the yield indicates that NaCl plays a key role in the CVT reaction for RCl_3, even when $AlCl_3$ and NaCl are simultaneously used as complex formers.

Table 2.2. Separation factors, amounts, and recoveries of the RCl_3[a] deposits transported with various amounts of NaCl

NaCl (10^{-3} mol)	Separation factor[a]		Amounts of RCl_3 deposit (10^{-4} mol)	Recovery (%)
	$\beta_{Pr/Nd}$	$\beta_{Nd/Pr}$		
0	1.00	1.07	2.79	17
0.55	1.04	1.17	4.11	25
1.65	1.08	1.20	5.40	33
4.95	1.08	1.18	4.97	30

[a] The loaded amount of RCl_3 for all runs was 1.65×10^{-3} mol.

2.3.2. Mutual Separation of Mixed Praseodymium and Neodymium Oxides

(1) CVT Reaction Using Various Potassium Salts as a Precursor of KCl

In the previous study (see Section 2.3.1), where an equimolar mixture of anhydrous chlorides, RCl_3 (1.65×10^{-3} mol; Pr/Nd = 1/1) and KCl (1.65×10^{-3} mol), was used as a starting material for the CVT reaction, 82% of initially loaded RCl_3 was transported after the reaction for 6 h; the yield was calculated as

$$\text{yield}/\% = 100\,(N_0 - N_B)/N_0 \qquad (2.10)$$

where N_0 and N_B are the molar quantity values of the total rare earth contents of raw material initially loaded and residue in the boat after the CVT reaction, respectively. However, in the present study where not RCl_3 but R_2O_3 was used as the starting materials, the direct addition of KCl to the mixed R_2O_3 resulted in a low yield of rare earths, 25%, even if the same reaction temperature and time were employed. In this case, a part of the KCl may have vaporized before the chlorination of R_2O_3 to RCl_3, and, as a result, the composition of the raw material deviates from the mole ratio R/K of 1/1. This mole ratio is of importance for the effective transport of RCl_3 *via* the vapor complex, $ARCl_4(g)$, since the vapor pressure of $ARCl_4(g)$ above a melt with this composition is the highest (see Section 2.3.1(3)). In order to avoid the deviation of composition, some potassium salts other than KCl were tried to use as a precursor for KCl. The potassium salt charged as the precursor of KCl was gradually chlorinated simultaneously with the mixed rare earth oxide, and, therefore, the mole ratio (R/K = 1/1) was expected to be kept during chlorination.

Table 2.3 summarizes the amounts of transported rare earth chlorides and the yield for five precursors, K_2CO_3, K_2SO_4, KNO_3, KF, and $KAl(SO_4)_2$, and also for KCl. Of all the five precursors tested, K_2CO_3, K_2SO_4, and KNO_3 improved the transportation efficiency, that is the yield, of RCl_3. Among them the yield obtained by using K_2CO_3 was the highest, and 55% of rare earths initially loaded was transported. On the other hand, KF and $KAl(SO_4)_2$ provided negative effects on the yield of RCl_3. As for the KF, the decrease in the yield can be explained from a thermodynamical [22] aspect that the chlorination of KF is takes place with difficulty. Even for the most plausible chlorination reaction of KF,

$$KF(l) + Cl_2(g) = KCl(l) + ClF(g), \qquad (2.11)$$

lies far to the left-hand side, $\Delta G_{11}(1300\ K) = +63$ kJ mol^{-1}, while both the eqs. 2.4 and 2.5 are leaned toward the right-hand side, $\Delta G_4(1300\ K) = -533$ kJ mol^{-1} and $\Delta G_5(1300\ K) = -603$ kJ mol^{-1}. On the contrary, the chlorination of $KAl(SO_4)_2$ took place easily, and, furthermore, the

Table 2.3. Transported amounts and yields of rare earths when various kinds of potassium salts were used as a precursor of KCl[a]

Pottasium salt	Transported amount (10^{-3} mol)		Yield (%)
	Pr	Nd	
K_2CO_3	1.57	1.72	55
K_2SO_4	1.03	1.22	37
KNO_3	0.93	1.01	32
KF	0.48	0.58	18
$KAl(SO_4)_2$	0.64	0.76	9.8
KCl	0.69	0.82	25
KCl[b]	0.67	0.69	82

[a] Raw material was R_2O_3 (6.0×10^{-3} mol; Pr/Nd = 1/1).
[b] Mixed anhydrous chloride (1.65×10^{-3} mol; Pr/Nd = 1/1) was used as the raw material.

chlorination of $KAl(SO_4)_2$ gives KCl and $AlCl_3$ at the same time, both of which function as the complex formers against RCl_3. Therefore, the amount of RCl_3 using $KAl(SO_4)_2$ was expected to be increased compared with that for K_2SO_4. However, the yield for $KAl(SO_4)_2$ was almost on the same level with that when KCl was directly used. This can be interpreted as the generation of a more stable vapor species $KAlCl_4(g)$ from KCl and $AlCl_3$ [21]. Hence, the effective amount of KCl for the vapor complexation with RCl_3 was reduced.

Consequently, the use of some potassium salts as a precursor of KCl renders the effective CVT reaction of rare earth oxides possible, and K_2CO_3 is the most appropriate from a viewpoint of the transport efficiency. Equations 2.4 and 2.5 shows that CO gas generates during the process. Though the CO generation seems disadvantageous, it is usual for a high-temperature chlorination process and oxidation processes of CO to CO_2 have been established.

(2) CVT Reaction Using Stepwise Temperature Gradients

Introduction of Stepwise Temperature Gradients. The vapor complex $KNdCl_4(g)$ is more stable than $KPrCl_4(g)$, and the $KPrCl_4(g)$ tends to decompose at higher temperatures than $KNdCl_4(g)$ (see Section 2.3.1). Therefore, Pr- and Nd-rich deposits are obtained from high- and low-temperature fractions in the temperature gradients, respectively. In the present section temperature gradi-

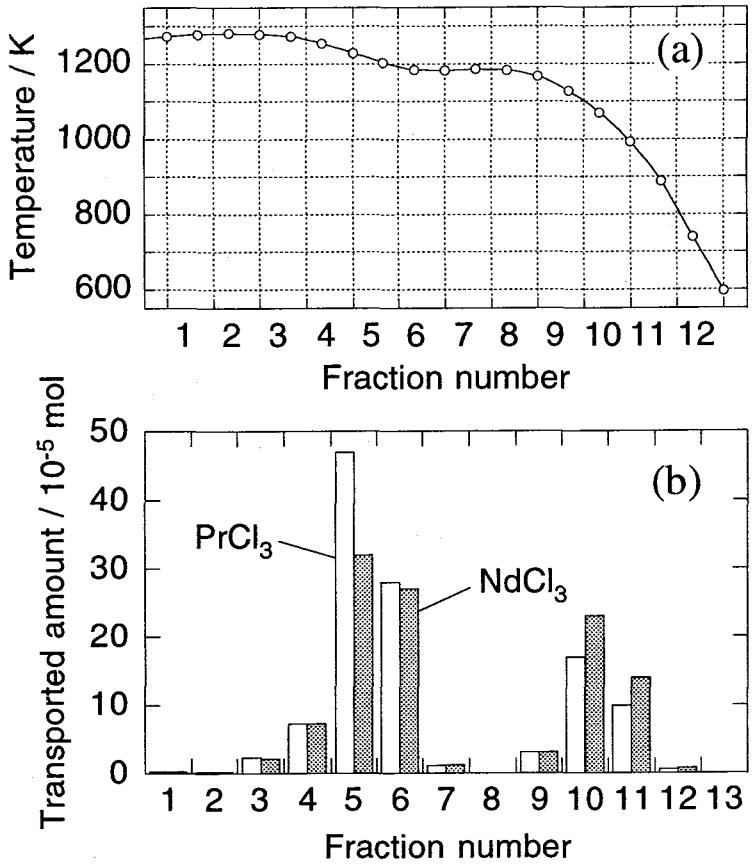

Figure 2.4. Typical profile of (a) a stepwise temperature gradient with a plateau zone maintained at T_{const} = 1183 K and (b) distribution of $PrCl_3$ and $NdCl_3$ deposits. Raw material was equimolar mixed praseodymium and neodymium oxide (6.0×10^{-3} mol); complex former was K_2CO_3 (3.0×10^{-3} mol) as a precursor of KCl; active carbon powder (0.5 g) was added to raw material as deoxidant; mixed N_2 and Cl_2 gases (N_2, 30 cm^3 min^{-1}; Cl_2 5 cm^3 min^{-1}) was flowed as carrier; reaction time was 82 h.

ents with a plateau zone (see Fig. 2.4(a)) with a temperature of T_{const} — stepwise temperature gradients — were employed. Figure 2.4(b) shows the amount of rare earths condensed over 13 fractions when a typical stepwise gradient with the constant temperature of 1183 K was employed. Here, K_2CO_3 was added to the R_2O_3 raw mixture as a precursor for KCl. At the fraction number of 8 (FN = 8), which corresponds to the constant temperature zone, no deposition took place and, hence, the Pr- and Nd-rich deposits were separately obtained from high-temperature fractions (FN = 3–7; $T > T_{const}$) and low-temperature fractions (FN = 9–13; $T < T_{const}$), respectively. In other words, the Pr- and Nd-rich fractions, that is the high- and low-temperature fractions, became clear by the use of the stepwise temperature gradients. Analogously to eqs. 2.7 and 2.8, separation factors, $\beta_{Pr/Nd}$ and $\beta_{Nd/Pr}$, were defined as follows for the Pr- and Nd-rich portions, respectively:

$$\beta_{Pr/Nd} = (1/r_H)/(1/r_0) = r_0/r_H \quad (2.12)$$

and

$$\beta_{Nd/Pr} = r_L/r_0 \quad (2.13)$$

where r_H, r_L, and r_0 are Nd/Pr mole ratios for the deposits of the high- and low-temperature fractions and the raw material, respectively. In the present work r_0 was kept at 1.00 for all runs. For the deposition profile of Fig. 2.4(b), for example, $\beta_{Pr/Nd}$ and $\beta_{Nd/Pr}$ were calculated as 1.19 and 1.25.

Since the transported RCl_3 was condensed not only on the surface of the inner tubes (see the apparatus in Fig. 1.1) but also on the inner wall of the quartz reactor tube, all RCl_3 deposits along the temperature gradient were unable to be recovered. We can recover the deposits only on the inner tubes. Thus, total amounts of RCl_3 detected from the inner tubes are always less than real transported amounts of RCl_3, which are expressed as $N_0 - N_B$ in eq. 2.10. On the other hand, the separation factors are invariant values whether the deposits are recovered thoroughly or not. In the following sections, the real transported amounts of $PrCl_3$ and $NdCl_3$ at the high- and low-temperature regions, N_{HPr}, N_{HNd}, N_{LPr}, and N_{LNd}, were calculated on the basis of the separation factors, $\beta_{Pr/Nd}$ and $\beta_{Nd/Pr}$, as

$$N_{HPr} = N_{0Pr} - N_{LPr}, \quad (2.14)$$

$$N_{HNd} = N_{0Nd} - N_{LNd}, \quad (2.15)$$

$$N_{LPr} = \frac{\beta_{Pr/Nd}N_{Nd} - r_0N_{Pr}}{r_0(\beta_{Pr/Nd}\beta_{Nd/Pr} - 1)}, \quad (2.16)$$

and

$$N_{LNd} = \frac{\beta_{Nd/Pr}(\beta_{Pr/Nd}N_{Nd} - r_0N_{Pr})}{\beta_{Pr/Nd}\beta_{Nd/Pr} - 1}, \quad (2.17)$$

where N_{0Pr} and N_{0Nd} are the molar quantities of Pr^{3+} and Nd^{3+} ions in the initially loaded mixed oxide, R_2O_3 ($N_0 = N_{0Pr} + N_{0Nd}$), and N_{Pr} and N_{Nd} are the total transported amounts of $PrCl_3$ and $NdCl_3$ ($N_0 - N_B = N_{Pr} + N_{Nd}$), respectively.

Effects of the Constant Temperatures, T_{const}, on Separation Efficiency. The CVT reactions using the stepwise temperature gradients with various constant temperature, T_{const}, were carried out. The reaction temperature was kept at 1273 K, and the reaction time was altered from 48 to 82 h. Figure 2.5 shows the relationship between the T_{const} and the separation factors ($\beta_{Nd/Pr}$ and

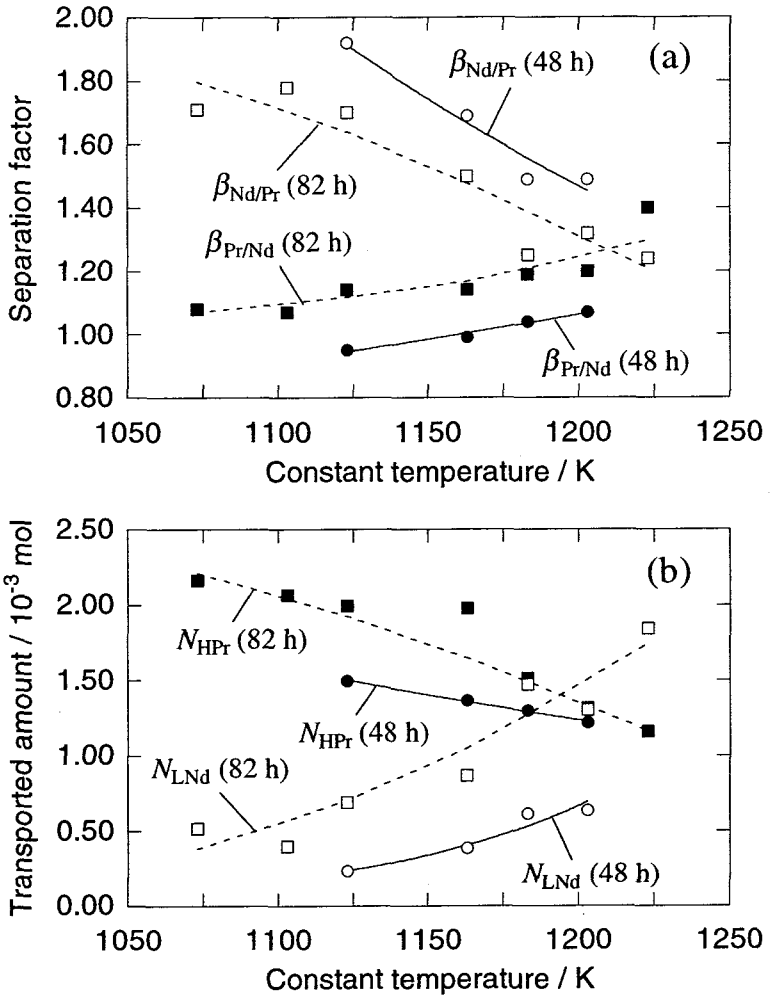

Figure 2.5. Relationship between constant temperature of stepwise temperature gradient (T_{const}) and separation characteristics: (a) separation factors for Pr-rich portion ($\beta_{Pr/Nd}$) and Nd-rich portion ($\beta_{Nd/Pr}$); (b) the transported amounts of $PrCl_3$ at Pr-rich portion (N_{HPr}) and of $NdCl_3$ at Nd-rich portion (N_{LNd}). Reaction times were 48 and 82 h.

$\beta_{Pr/Nd}$) and the transported amounts (N_{HPr} and N_{LNd}) when reacted for 48 and 82 h. As T_{const} is increased, $\beta_{Pr/Nd}$ increases and $\beta_{Nd/Pr}$ decreases (Fig. 2.5(a)), whereas N_{HPr} decreases and N_{LNd} increases. In other words, the CVT reaction using a temperature gradient with low T_{const} gives a high purity $NdCl_3$ whose yield is, however, very low and *vice versa*. These are explained as follows. Since the $KNdCl_4(g)$ complex is more stable than $KPrCl_4(g)$ (see Section 2.3.1), the temperature for the region where $NdCl_3$ deposits is lower than that for $PrCl_3$, as represented schematically in Fig. 2.6. If the constant temperature is relatively low ($T_{const} = T_a$, see Fig. 2.6(a)), then $\beta_{Nd/Pr}$ value becomes large since most of the deposit at a $T < T_a$ region is $NdCl_3$, while the amount of $NdCl_3$ deposit at this region, N_{LNd}, is small. On the contrary, if the constant temperature is high

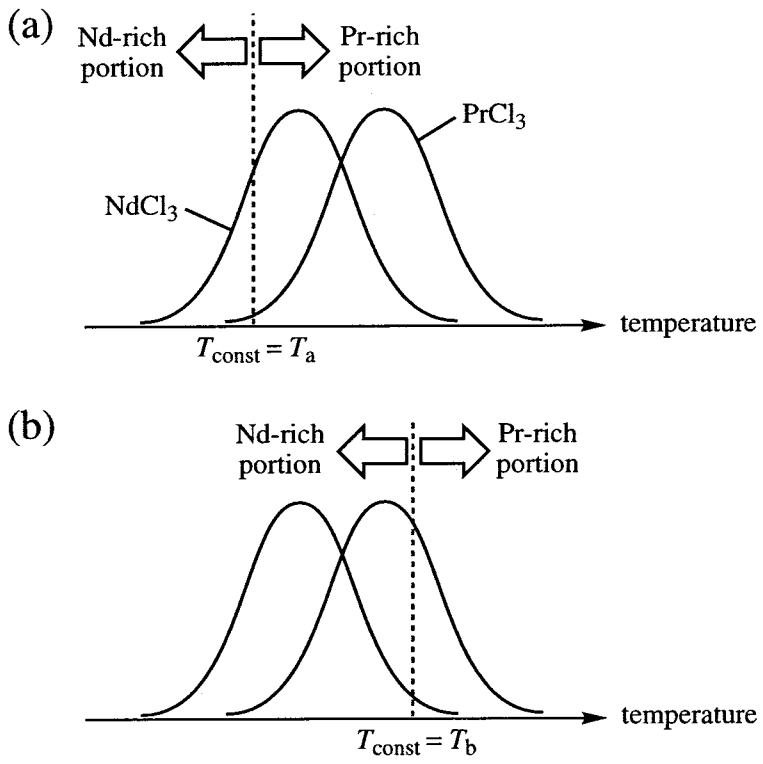

Figure 2.6. Schematic representation of distribution of $PrCl_3$ and $NdCl_3$ deposits as a function of temperature and definition of Pr-rich and Nd-rich portions when constant temperature of stepwise temperature gradient (T_{const}) is relatively (a) low and (b) high.

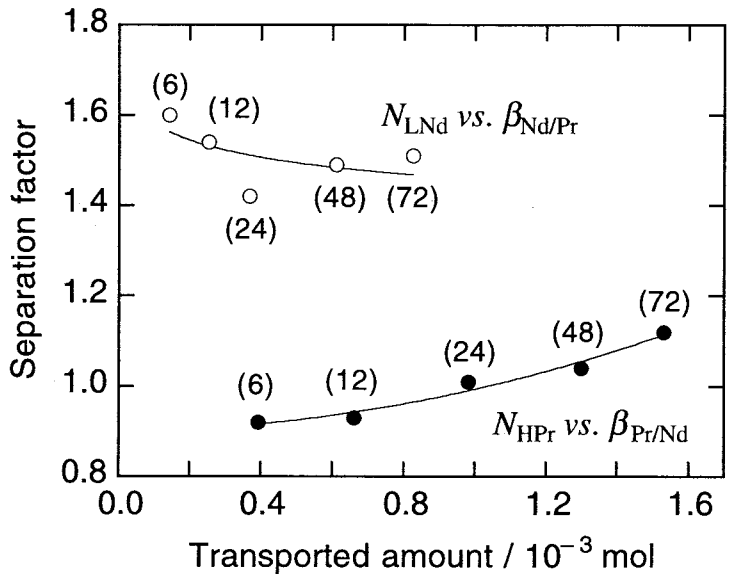

Figure 2.7. Relationship between transported amount of $PrCl_3$ at Pr-rich portion (N_{HPr}) and separation factor ($\beta_{Pr/Nd}$), and between that of $NdCl_3$ at Nd-rich portion (N_{LNd}) and separation factor ($\beta_{Nd/Pr}$) when reacted using a temperature gradient with a plateau zone maintained at T_{const} = 1183 K. Reaction times are designated in parentheses.

($T_{const} = T_b$, see Fig. 2.6(b)), $\beta_{Nd/Pr}$ becomes small, whereas N_{LNd} increases.

Consequently, it is difficult to raise the separation efficiency and the yield at the same time. One should select an appropriate T_{const} value according to the situations such as composition of the raw material and demand on the market.

Effects of the Reaction time on Separation Efficiency. Figure 2.5 shows that separation factor $\beta_{Nd/Pr}$ for 48 hour's reaction is better than that for 82 hour's. Figure 2.7 depicts the relationship between transported amounts (N_{HPr} and N_{LNd}) and separation factors ($\beta_{Pr/Nd}$ and $\beta_{Pr/Nd}$) when reacted using a stepwise temperature gradient with a plateau zone maintained at T_{const} = 1183 K. Separation factor $\beta_{Nd/Pr}$ decreased with increase in transported amount N_{LNd}, or with the elapse of reaction time. On the contrary, separation factor $\beta_{Pr/Nd}$ was less than 1.00 when reacted for 6–12 h; this means that the transported amount of $NdCl_3$ is larger than that of $PrCl_3$ even at the high-temperature region: $N_{HNd} > N_{HPr}$. For the reactions longer than 24 h separation factor $\beta_{Pr/Nd}$ increased beyond 1.00. These phenomena were explained as follows.

In the CVT reactions studied in this thesis, mutual separation of $PrCl_3$ and $NdCl_3$ is governed by two factors: (i) selectivity in generation of vapor complexes from raw mixture and (ii) selectivity in decomposition of vapor complexes by temperature gradient. According to the relationship between the total transported amounts (N_{Pr} and N_{Nd}) and the reaction time (see Fig. 2.8), the rate of

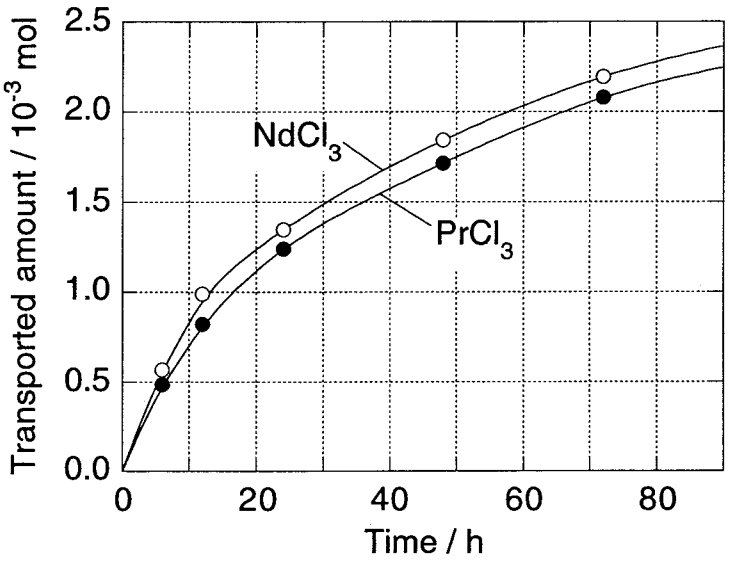

Figure 2.8. Total transported amounts of $PrCl_3$ (N_{Pr}) and $NdCl_3$ (N_{Nd}) as a function of reaction time when reacted at 1273 K. Other reaction conditions were as in Fig. 2.4.

$KNdCl_4(g)$ generation is larger than that of $KPrCl_4(g)$ at the early stage of the CVT reaction (t = 0–12 h), owing to the difference in stability of these complexes. Therefore, the transported amount of $NdCl_3$ was larger both at high- and low-temperature regions. On the contrary, the N_{Pr} and N_{Nd} *vs* t curves become parallel at $t > 20$ h, suggesting that the generating rates become almost equal and, as a result, the selectivity (i) decreased. This leads to the decrease in $\beta_{Nd/Pr}$ and increase in $\beta_{Pr/Nd}$.

(3) Simulation of the CVT Reaction

Since the CVT reaction takes place at high temperatures, the reaction mechanism is too complicated to be described as a simple reaction route. Therefore, it seems difficult to predict theoretically the separation efficiency based on some existing thermodynamic data. Furthermore, characteristics of this system, where the CVT reaction goes under thermodynamically nonequilibrium conditions due to a flow-type reactor, also make the theoretical interpretation of the reaction difficult. On the contrary, the fact that no deposition of RCl_3 was observed at around the constant-temperature region (see Fig. 2.4(b)) suggests that the gas phase in the constant-temperature region is apparently in an "equilibrium" condition. Hence, the transported amounts at the low-temperature portion, N_{LPr} and N_{LNd}, represent this "quasi equilibrium" composition of the gas phase at the constant temperature, T_{const}. In this section, on the basis of empirical vapor pressures calculated by changing the constant temperature and the reaction time, an estimate of the separation efficiency has been attempted.

First, the relationship between the total transported amounts, N_{Pr} and N_{Nd}, and the reaction time during the CVT reaction at 1273 K was obtained both for $PrCl_3$ and $NdCl_3$ (see Fig. 2.8). Partial vapor pressures of $KPrCl_4(g)$ and $KNdCl_4(g)$ above the raw mixture after the elapse of time t can be determined from the slope of the N_{Pr} and N_{Nd} *vs* t curves and the equation of state for an ideal gas. Though the N_{Pr} and N_{Nd} values increase with the time, the rate of increase gradually decreases as the time passes, indicating that the amounts of generating vapor complexes were changing through the CVT reaction. From the analysis of the residue on the boat, it turned out that this change of the vapor pressure is due to the deviation of composition of the melt, where the K/R ratio gradually decreases during the reaction, since KCl(g) vaporizes simultaneously with $KRCl_4(g)$ (see Chapter 5).

Empirical vapor pressures of the vapor complexes were, then, calculated for $KPrCl_4(g)$ and $KNdCl_4(g)$ according to the following procedures:

(a) Saturated vapor pressures of $KRCl_4(g)$ ($P_{KPrCl_4}(T)$ and $P_{KNdCl_4}(T)$) at a temperature T were calculated from the vapor pressures of $RCl_3(g)$ [23] and KCl(g) [24] by assuming the equilibrium

constants, $K_{Pr}(T)$ and $K_{Nd}(T)$, of the equation

$$KRCl_4(g) = KCl(g) + RCl_3(g), \quad (R = Pr, Nd) \tag{2.18}$$

whose enthalpy and entropy changes have been reported [12]: $\Delta H_{18} = 247$ kJ mol^{-1} and $\Delta S_{18} = 136$ J mol^{-1} K^{-1} for both Pr and Nd. Furthermore, empirical factors, $f_{Pr}(T)$ and $f_{Nd}(T)$, were introduced to evaluate apparent equilibrium constants, $f_{Pr}(T)K_{Pr}(T)$ and $f_{Nd}(T)K_{Nd}(T)$, *i.e.*

$$f_R(T)K_R(T) = \frac{P_{RCl_3}(T)P_{KCl}(T)}{P_{KRCl_4,\,app}(T)}. \quad (R = Pr, Nd) \tag{2.19}$$

The vapor pressures of RCl_3, $P_{RCl_3}(T)$, and KCl, $P_{KCl}(T)$, represented in atmospheres, were given as

$$\log P_{KCl}(T) = -10710\,T^{-1} - 3.0 \log T + 16.03, \tag{2.20}$$

$$\log P_{PrCl_3}(T) = -13810\,T^{-1} + 7.563, \tag{2.21}$$

and

$$\log P_{NdCl_3}(T) = -12930\,T^{-1} + 7.089. \tag{2.22}$$

(b) The reaction period was divided into short time intervals, Δt_i ($i = 1, 2, 3, \ldots$), and the amounts of generated vapor complexes, $\Delta N_{i,KRCl_4}$ (R = Pr, Nd), during each Δt_i were obtained from Fig. 2.8. For the sake of convenience, the N_{Pr} and N_{Nd} *vs* t curves (Fig. 2.8) were approximated by some adequate polynomial functions though there is no theoretical background. The amounts, $\Delta N_{i,KRCl_4}$, were then converted to vapor pressures, $P_{i,KRCl_4}$ (R = Pr, Nd), at the temperature of T_{const} using the relation

$$P_{i,\,KRCl_4} = \frac{\Delta N_{i,\,KRCl_4} R T_{const}}{S v \Delta t_i}, \quad (R = Pr, Nd;\ i = 1, 2, 3, \ldots) \tag{2.23}$$

where S, v, and R are the cross section of the reactor, the velocity of the N_2–Cl_2 current, and the ideal gas constant, respectively.

(c) If $P_{KPrCl_4,app}(T_{const}) \geq P_{i,KPrCl_4}$, then all of the $KPrCl_4(g)$ complex was considered to deposit at the low-temperature region below T_{const}, and if $P_{KPrCl_4,app}(T_{const}) < P_{i,KPrCl_4}$, then the complexes corresponding to the difference $P_{i,KPrCl_4} - P_{KPrCl_4,app}(T_{const})$ were assumed to deposit at the high-temperature region above T_{const}, and the rest $P_{KPrCl_4,app}(T_{const})$ was condensed to the lower-temperature region. For the $KNdCl_4(g)$ complex, a similar calculation was carried out.

(d) For each Δt_i the calculations (b)–(c) were done, and, then, a pair of calculated N_{HPr}, N_{HNd}, N_{LPr}, and N_{LNd} values was obtained as a summation over all i's.

Table 2.4. Empirical factors, $f_R(T)$, for apparent equilibrium constants of reaction $KRCl_4(g) = KCl(g) + RCl_3(g)$ and apparent vapor pressures of $KRCl_4(g)$, $P_{KRCl_4,app}(T)$, for the flow-type chemical vapor transport reaction (R = Pr and Nd)[a]

Reaction time (h)	T_{const}[b] (K)	$KPrCl_4(g)$		$KNdCl_4(g)$	
		$f_{Pr}(T_{const})$	$P_{KPrCl_4,app}(T_{const})$ (atm)	$f_{Nd}(T_{const})$	$P_{KNdCl_4,app}(T_{const})$ (atm)
48	1203	9.0	4.6×10^{-4}	11.0	6.8×10^{-4}
48	1183	7.4	4.0×10^{-4}	9.4	5.9×10^{-4}
48	1163	8.6	2.5×10^{-4}	9.8	4.2×10^{-4}
48	1123	9.4	1.1×10^{-4}	9.6	2.2×10^{-4}
82	1223	9.3	6.1×10^{-4}	9.9	1.0×10^{-3}
82	1203	8.2	5.1×10^{-4}	10.5	7.2×10^{-4}
82	1183	6.9	4.3×10^{-4}	9.7	5.8×10^{-4}
82	1163	9.4	2.3×10^{-4}	11.5	3.6×10^{-4}
82	1123	6.0	1.8×10^{-4}	6.9	3.1×10^{-4}
82	1103	6.9	1.1×10^{-4}	7.8	2.0×10^{-4}
82	1073	3.4	1.2×10^{-4}	4.2	2.1×10^{-4}

[a] Raw materials were R_2O_3 (6.0×10^{-3} mol), K_2CO_3 (3.0×10^{-3} mol), and an active carbon powder; a mixed N_2 (30 $cm^3\ min^{-1}$) and Cl_2 (5 $cm^3\ min^{-1}$) gases was passed through the reactor. Reaction temperature was 1273 K.

[b] Constant temperature in the stepwise temperature gradient; see the text.

(e) The calculations (b)–(d) were repeated by altering the $f_{Pr}(T)$ and $f_{Nd}(T)$ factors from 1 to larger values to fit the calculated N_{HPr}, N_{HNd}, N_{LPr}, and N_{LNd} with the experimental ones obtained from eqs. 2.14–2.17.

Table 2.4 summarizes the empirical factors together with the apparent vapor pressures, $P_{KRCl_4,app}(T)$, calculated from eq. 2.19. The empirical factors lie around 6–11, suggesting the apparent vapor pressures are lowered compared with the equilibrium vapor pressures, $P_{KRCl_4}(T)$, which are predicted from eqs. 2.18 and 2.20–2.22 ($P_{KRCl_4}(T) = P_{RCl_3}(T)P_{KCl}(T)/K_R(T)$). The factor $f_{Pr}(T)$ is generally larger than the correspondent $f_{Nd}(T)$ value. Several factors can be stipulated for the lowering of vapor pressures: (i) RCl_3 and KCl are thermally stabilized by forming the molten mixture and, therefore, the vapor pressures of $RCl_3(g)$ and KCl(g) are reduced compared to those expected from eqs. 2.20–2.22 (*cf* vapor pressures of $KNdCl_4(g)$, KCl(g), and $NdCl_3(g)$ over an equimolar $NdCl_3$-KCl melt; see Chapter 5); (ii) the vapor complexation usually has a slow reaction rate [14], resulting in an apparently low vapor pressure, since the CVT reaction takes place on a flow-type reactor where eq. 2.18 is not thoroughly thermodynamically equilibrated; (iii) there are

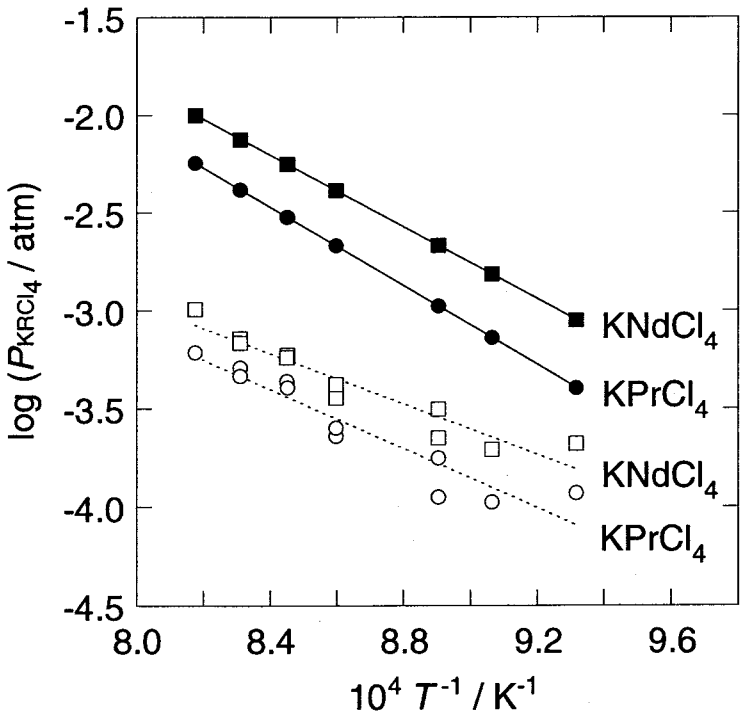

Figure 2.9. Vapor pressures of $KRCl_4$ complexes calculated from existing thermodynamic functions (solid line) and apparent vapor pressures of $KRCl_4$ observed in flow-type chemical vapor transport reaction (dashed line).

some interactions between Pr- and Nd-vapor species, though these are not taken into account in the above calculations. Although the extent of contribution of these factors is ambiguous, it is noteworthy that the apparent vapor pressures are more or less affected by equilibrium vapor pressures, $P_{KPrCl_4}(T)$ and $P_{KNdCl_4}(T)$, because the $\log P_{KRCl_4,app}(T)$ *vs* $1/T$ plots roughly show a linear relationship and the $P_{KNdCl_4,app}(T)$ is always larger than $P_{KPrCl_4,app}(T)$ in analogy with $P_{KRCl_4}(T)$ where $P_{KNdCl_4}(T)$ is also larger than $P_{KPrCl_4}(T)$.

Based on the apparent vapor pressures, the relationship between the transported amounts, N_{HPr} and N_{LNd}, and the separation factors, $\beta_{Pr/Nd}$ and $\beta_{Nd/Pr}$, was predicted for 48 and 82 h reaction. Here, the apparent vapor pressures were approximated as

$$\log P_{KPrCl_4,app}(T) = -7519\,T^{-1} + 29134 \qquad (2.24)$$

and

$$\log P_{KNdCl_4,app}(T) = -9537\,T^{-1} + 21850 \qquad (2.25)$$

by the least-squares method on the basis of the $\log P_{KRCl_4,app}$ *vs* $1/T$ plots given in Fig. 2.9. Together with the calculated relationship (Fig. 2.10) assuming reaction for 48 and 82 h, experimental

values for the same reaction time were plotted. When N_{LNd} is at a low level, the separation factor, $\beta_{Nd/Pr}$, is expected to reach around 1.8–1.9, which exceeds the factor for conventional solvent extraction ($\beta_{Nd/Pr}$ = 1.5) [20b] where tributyl phosphate (TBP) was used for an extractant and, actually, the factor of 1.7–1.9 was obtained.

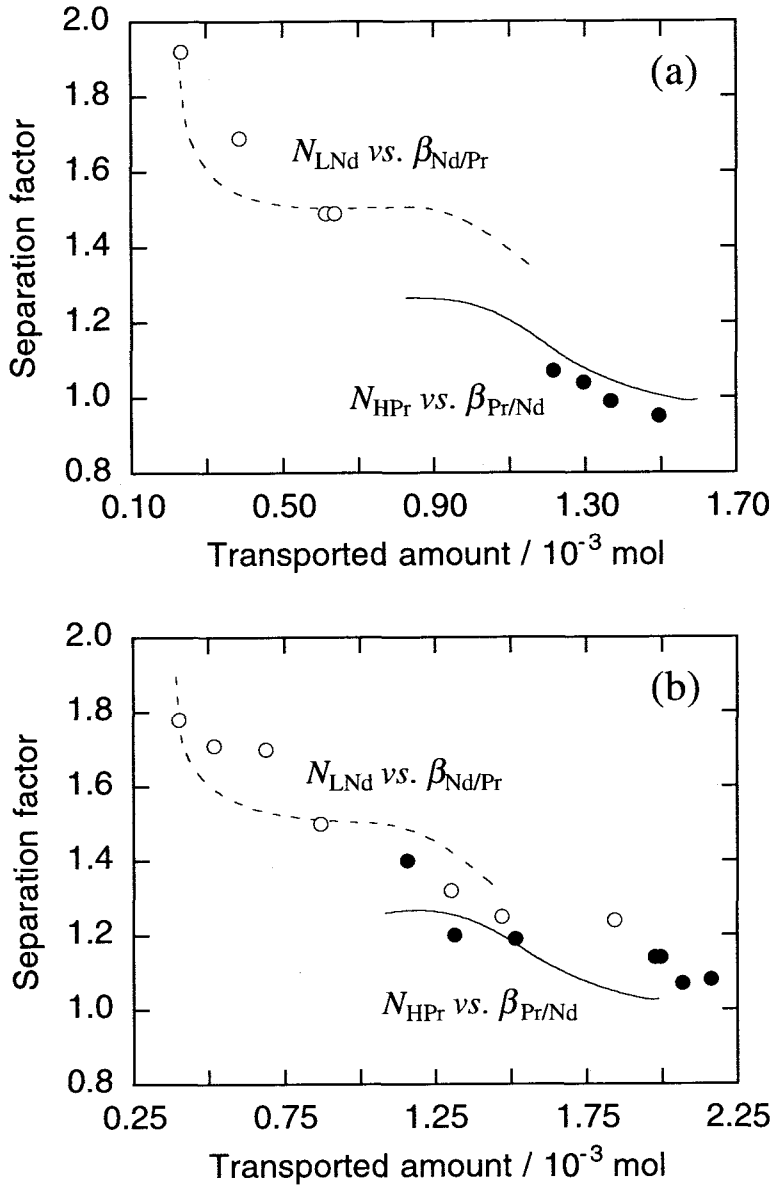

Figure 2.10. Relationship between transported amount of $PrCl_3$ at Pr-rich portion (N_{HPr}) and separation factor ($\beta_{Pr/Nd}$), and between that of $NdCl_3$ at Nd-rich portion (N_{LNd}) and separation factor ($\beta_{Nd/Pr}$) when reacted for (a) 48 and (b) 82 h. Solid and dashed lines are calculated and plots are experimentally observed values.

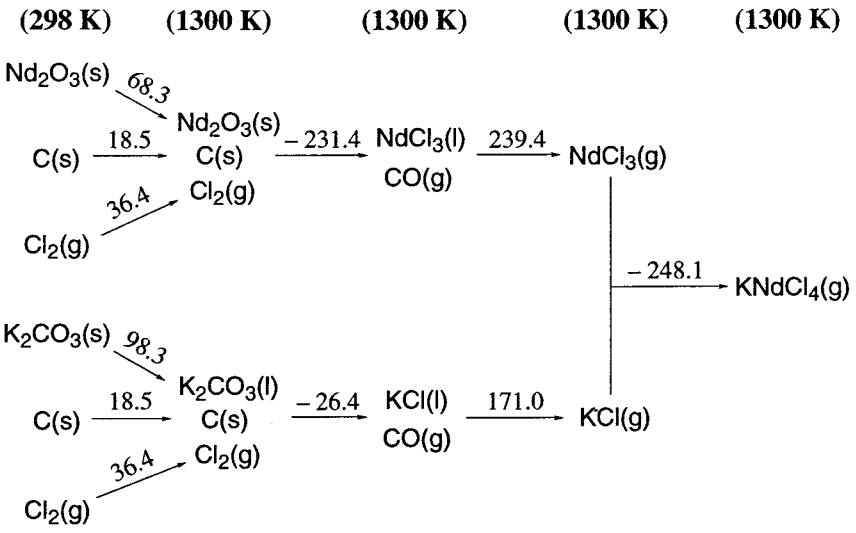

Figure 2.11. Change of enthalpy for each step for calculation of necessary heat of chemical vapor transport reaction represented in kJ mol^{-1} of Nd^{3+} or K^{+}, except for C(s) and Cl_2(g) which are in kJ mol^{-1}.

(4) Necessary Heat for the CVT Reaction

The chlorination and vapor complexation are so complicated that we cannot write down a simple reaction scheme as mentioned above. However, it is important to calculate the necessary energy for the CVT reaction for the sake of comparing the CVT process with the conventional wet methods. So, the necessary heat for formation of a vapor complex, $KNdCl_4$(g), was calculated by assuming some steps using existing thermodynamic functions [19a, 22, 25]. All starting materials, Nd_2O_3, K_2CO_3, C, and Cl_2, were supposed to be introduced into a reactor at room temperature (298 K) and heated up to 1300 K. Then, the Nd_2O_3 and K_2CO_3 are chlorinated, yielding $NdCl_3$, KCl, and CO gas, and the resulting $NdCl_3$ and KCl vaporize and subsequently form the vapor complex, $KNdCl_4$(g).

The enthalpy change for each step is summarized in Fig. 2.11. The heat necessary for the overall reaction

$$1/2\ Nd_2O_3(s) + 1/2\ K_2CO_3(s) + 5/2\ C(s) + 2\ Cl_2(g)\ [298\ K] \rightarrow KNdCl_4(g) + 3\ CO(g)\ [1300\ K] \qquad (2.26)$$

was calculated as 190.1 kJ mol^{-1} which corresponds to 1.12×10^6 kJ ton^{-1} of Nd_2O_3 treatment. For the formation of the $KPrCl_4$(g) complex, almost the same amount of heat is expected due to the similarity in chemical properties between Pr and Nd. Since the efficiency of the apparatus is less than 100%, a practical necessary heat for the CVT process is higher than the above calculated

value. However, the heat necessary for the CVT process can be reduced by combining the process with a conventional direct chlorination method for extracting rare earths from the ores (see Chapter 3), because the heating and chlorinating steps of Nd_2O_3

$$1/2\ Nd_2O_3(s) + 3/2\ C(s) + 3/2\ Cl_2(g)\ [298\ K] \rightarrow NdCl_3(l) + 3/2\ CO(g)\ [1300\ K] \qquad (2.27)$$

will be omitted in the combination process.

We cannot compare the necessary heat for the CVT process with that of other conventional wet methods. However, it is no doubt that the dry CVT process needs less energy than the wet methods, since the CVT process is quite simple whereas the wet ones always require a series of complicated treatments such as dissolution of raw material, precipitation of filtrates, and drying and calcination of precipitates.

2.4. Conclusions

The effective mutual separation of $PrCl_3$-$NdCl_3$ mixture was realized by the CVT method using alkali metal chlorides as complex formers. The separation factor evaluated in the system (RCl_3-KCl) is 1.33. It is comparable to the value observed by the conventional solvent-extraction method. Furthermore, the rare earth chlorides separated *via* the gas-phase complexes were obtained in pure form upon removing the codeposited alkali metal chloride by using aluminium chloride as the second complex former.

The mutual separation of mixed oxide was also conducted effectively using the CVT process, where K_2CO_3 was used as a precursor of the complex former, KCl. The separation characteristics of the complexes for the flow-type CVT reaction using the stepwise temperature gradients with various constant temperature zones strongly depended on the temperature of the plateau, T_{const}. When T_{const} is low, the amount of recovered $NdCl_3$ was small whereas the separation factor is high, and *vice versa*. By employing apparent vapor pressure curves of the complexes for the flow-type CVT reaction, this alternative feature of the recoveries was simulated.

2.5. Nomenclature

A = alkaline metals

CVT = chemical vapor transport

$f_{Pr}(T), f_{Nd}(T)$ = empirical factors for vapor pressures of $KPrCl_4(g)$ and $KNdCl_4(g)$

FN = fraction number for separation

ΔG_4, ΔG_5, ΔG_{11} = free energy changes of reactions 2.4, 2.5, and 2.11, kJ mol^{-1}

ΔH_{18} = enthalpy change of reaction 2.18, kJ mol^{-1}

$K_R(T)$ = equilibrium constant of reaction 2.18, atm

N_0 = amount of initially loaded rare earths (= $N_{0Pr} + N_{0Nd}$), mol

N_{0Pr}, N_{0Nd} = amounts of initially loaded praseodymium and neodymium oxides, mol

N_B = amount of residual rare earths on the boat, mol

N_{Pr}, N_{Nd} = total transported amounts of $PrCl_3$ (= $N_{HPr} + N_{LPr}$) and $NdCl_3$ (= $N_{HNd} + N_{LNd}$), mol

N_{HPr}, N_{HNd} = transported amounts of $PrCl_3$ and $NdCl_3$ at the high-temperature region, mol

N_{LPr}, N_{LNd} = transported amounts of $PrCl_3$ and $NdCl_3$ at the low-temperature region, mol

$\Delta N_{i,KRCl_4}$ = amount of generated $KRCl_4(g)$ vapor during Δt_i , mol

$P_{KCl}(T)$, $P_{PrCl_3}(T)$, $P_{NdCl_3}(T)$ = vapor pressures of KCl, $PrCl_3$, and $NdCl_3$, atm

$P_{KPrCl_4}(T)$, $P_{KNdCl_4}(T)$ = saturated vapor pressures of $KPrCl_4(g)$ and $KNdCl_4(g)$, atm

$P_{KPrCl_4,app}(T)$, $P_{KNdCl_4,app}(T)$ = apparent vapor pressures of $KPrCl_4(g)$ and $KNdCl_4(g)$, atm

$P_{i,KPrCl_4}$, $P_{i,KNdCl_4}$ = mean vapor pressures of $KPrCl_4(g)$ and $KNdCl_4(g)$ during Δt_i, atm

r_0, r_H, r_L = mole ratio (Nd/Pr) for the raw material (= N_{0Nd}/N_{0Pr}), for the deposit of the high-temperature region (= N_{HNd}/N_{HPr}), and for the deposit of the low-temperature region (= N_{LNd}/N_{LPr})

R = rare earths: praseodymium and/or neodymium

R = ideal gas constant

S = cross section of the reactor tube

ΔS_{18} = entropy change of reaction 2.18, J mol^{-1} K^{-1}

t = reaction time of CVT

Δt_i = time intervals for calculation of empirical vapor pressures

T = temperature, K

T_{const} = constant temperature of the stepwise temperature gradient, K

v = velocity of the N_2–Cl_2 current

$\beta_{Pr/Nd}$, $\beta_{Nd/Pr}$ = separation factor for Pr-rich and Nd-rich portions

Chapter 3

Vapor Phase Extraction and Mutual Separation of Rare Earths from Concentrates and Crude Oxides Using Chemical Vapor Transport

3.1. Introduction

The formation of halogen-bridged vapor complexes [1–7] renders it possible to transport chemically low-volatile metal halides, such as rare earth halides, through temperature gradients. In the previous chapters, the author reported on a promising dry rare earth separation technique using the chemical vapor transport (CVT) phenomenon as an alternative to the commercial wet process by which rare earths are currently produced. In the CVT process rare earth oxides can be directly used as a raw material by employing some potassium salts as a precursor of KCl, one of the typical vapor complex former (see Section 2.3.2(1)).

High temperature direct chlorination of ores using gaseous chlorinating agents such as Cl_2, HCl, CCl_4, and $SOCl_2$, has been widely used for metal extraction processes including rare earth extraction [26, 27]. Some rare earth ores contain thorium and uranium which are thoroughly extracted as gaseous chlorides in the course of the direct chlorination [27]. Rare earth chlorides are of importance for the processing of rare earth metals, the demand for which is increasing due to the development of various rare earth intermetallic materials.

This chapter describes a combination of the high-temperature direct chlorination and the CVT processes, in which the concentrates or crude oxides of rare earths were used directly as starting materials for the CVT process, and vapor phase extraction and separation characteristics of rare earths were discussed.

Throughout this work, chlorine gas was mainly used as a chlorinating agent, since it is the best in view of economy. On the other hand, carbon tetrachloride is, in many cases, able to chlorinate ores under milder conditions as compared with chlorine gas as recently reported on the chlorination of titanium ores [28]. Thus, chlorination characteristics using carbon tetrachloride were also examined with respect to monazite, one of the rare earth concentrate.

3.2. Experimental Details

3.2.1. Chlorination and Chemical Vapor Transport Reaction Using Chlorine Gas as a Chlorinating Agent

Materials. The concentrates of monazite and xenotime, which contain rare earths as the orthophosphates (RPO_4), were used as the starting materials for the chlorination and CVT reaction, as well as the crude oxides of rare earths (R_2O_3) which were prepared from bastnaesite, monazite, and ionic ore in Xun-wu, China. The oxides from bastnaesite and the ionic ore were supplied by Mitsubishi Kasei Corporation and Mitsui Mining & Smelting Co., Ltd., respectively, while the monazite oxide was prepared from monazite concentrate by acid decomposition in the following way. The monazite concentrate (10.00 g) was made to react with concentrated H_2SO_4 (15 cm^3) in an alumina crucible at 270 °C for 3 h, and the resulting metal sulfates were leached by deionized water. After filtering off the insoluble constituent, the pH value of the filtrate was adjusted using aqueous ammonia to 2.0 and saturated oxalic acid solution was added to precipitate rare earth components as oxalates. The rare earth oxalates were then sucked off and calcined in a platinum crucible, yielding the reddish brown mixed oxide. Table 3.1 summarizes the compositions of rare earth and non-rare earth elements in the concentrates and oxides, as determined by X-ray fluorescent analysis.

Two kinds of complex former, *i.e.* transporting agent, $AlCl_3$ and KCl, were tried; $AlCl_3$ was used only for the CVT reaction of the oxide from the ionic ore. Aluminium chloride (10.0 g) was sealed in a pyrex glass container with a small orifice (diameter, 0.5 mm) in order to generate the gaseous aluminium chloride $Al_2Cl_6(g)$ slowly during the CVT reaction (*cf* Procedure I described in Chapter 1). In contrast, in the case of KCl, K_2CO_3 was used as a precursor of KCl, being added directly to the rare earth raw materials in furnace B without using furnace A. The use of K_2CO_3 instead of KCl restrained the deviation in the R/K mole ratio of the raw mixture during the chlorination of rare earth components (see Section 2.3.2(1)).

Operation. The equipment used to obtain temperature gradients for the CVT reaction has been described in detail in Chapter 1. However, length of each inner tube (see Section 1.2.2) used for the CVT reaction of monazite is longer (60 mm) than those for other raw materials, since furnace B employed for monazite is longer (860 mm). When the complex former was KCl, the rare earth raw material, a small amount of active carbon as deoxidant, and K_2CO_3 were mixed and introduced into a carbon boat. The mixture was then placed in the quartz inner tube and loaded into

Table 3.1. Metal distribution in raw materials for chemical vapor transport reaction (wt%)

	Concentrates RPO_4		Oxides R_2O_3		
	Monazite	Xenotime	Monazite	Bastnaesite	Ionic ore
La_2O_3	15	0.67	22	32	28
CeO_2	27	1.9	39	43	3.6
Pr_6O_{11}	4.6	0.27	6.6	4.6	5.9
Nd_2O_3	10	1.3	14	12	24
Sm_2O_3		0.92			3.8
Eu_2O_3		*t*			*t*
Gd_2O_3		2.3			3.0
Tb_4O_7		0.55			0.38
Dy_2O_3		5.9			1.6
Ho_2O_3		0.92			
Er_2O_3		3.7			
Tm_2O_3		0.67			
Yb_2O_3		2.2			0.76
Lu_2O_3		*t*			*t*
Y_2O_3	0.52	39	0.62		8.6
MgO				0.28	
Al_2O_3	0.29	0.74			
SiO_2	1.8	1.5			
P_2O_5	19	18	0.17	0.33	
K_2O		0.17			
CaO	1.6	0.33	0.55	1.4	
TiO_2		9.8			
Cr_2O_3		0.34			
MnO		0.38			
Fe_2O_3	4.1	5.2			
SrO				3.5	
ZrO_2	4.4	0.44			
Nb_2O_5		0.14			
WO_3		0.12			
ThO_2	11	0.74	13		
U_3O_8	0.39	0.74			

the quartz reactor with a stream of N_2 (30 cm^3 min^{-1}). Once the desired temperature gradient had been attained by operating furnace B, a Cl_2 stream (5 cm^3 min^{-1}) was introduced into the reactor to chlorinate the mixture at 1000 °C, yielding RCl_3, KCl, and other metal chlorides. When $AlCl_3$ was the complex former, the container with solid $AlCl_3$ (10.0 g) was put into furnace A. Once the desired temperature gradient was attained by operating furnace B, the Cl_2 stream was introduced at the same flow rate as above and furnace A was heated over the temperature range from 80 to 200 °C in order to generate the gaseous aluminium chloride, $Al_2Cl_6(g)$, slowly during the reaction.

The concentrates (RPO_4) and the oxides (R_2O_3) were thoroughly chlorinated by the N_2–Cl_2 gas within 3 and 1 h at 1000 °C, respectively. The resulting RCl_3 was subsequently converted to the vapor complexes *via* reaction with KCl or $Al_2Cl_6(g)$,

$$RCl_3(s, l) + KCl(s, l) = KRCl_4(g) \qquad (3.1)$$

and

$$RCl_3(s, l) + n/2\ Al_2Cl_6(g) = RAl_nCl_{3+3n}(g) \quad (n = 1–4). \qquad (3.2)$$

The complexes were driven along a temperature gradient by the gas stream, cooled gradually, and allowed to decompose according to the reverse processes of eqs. 3.1 and 3.2, thus RCl_3 was regenerated. The chlorides of other metal elements, *e.g.* Th, U, Ca, Fe, and Zr, present in the raw materials, were also vaporized and transported *via* vapor complexes and/or simple halide molecules such as $ThCl_4(g)$ and $Fe_2Cl_6(g)$. The CVT reaction lasted for 30–82 h, after which the condensates along the temperature gradient were collected by removing the 13 pieces of alumina inner tubing from the reactor. These condensates and the residual mixture on the boat were then leached individually in dilute hydrochloric acid in order to determine the composition in each inner tube using an X-ray fluorescent spectrometer (Rigaku System 3270A) and an ICP-atomic emission spectrometer (Shimadzu ICPS-1000) using Zn^{2+} as internal standard substance.

3.2.2. Chlorination and Chemical Vapor Transport Reaction Using Carbon Tetrachloride as a Chlorinating Agent

A monazite concentrate (monazite sand) with particle diameter of 10^{-5}–10^{-4} m was used for this study without any pretreatment. Carbon tetrachloride was washed with a concentrated KOH aqueous solution and, then, with deionized water, dried with $CaCl_2$, and distilled in the presence of P_2O_5 before use.

The raw material, 2.925 g of the monazite sand containing 9.4×10^{-3} mol of R^{3+}, was put in

a carbon boat, which was then placed in the inner tube and loaded in a quartz reactor with a stream of N_2 (30 cm^3 min^{-1}). When the rare earth extraction *via* the vapor complex, $KRCl_4(g)$ or $RAl_nCl_{3+3n}(g)$, was investigated, K_2CO_3 or α-Al_2O_3 was used as a precursor of the complex former KCl or $AlCl_3$, respectively. The K_2CO_3 (0.648 g) containing 9.4×10^{-3} mol of K^+ equimolar with R^{3+} in the monazite was mixed directly with the monazite sand, while the α-Al_2O_3 (3.824 g) was put in another boat and heated in furnace A at 900 °C. After a desired temperature gradient was attained by operating furnace B, the chlorination was initiated by passing N_2 gas through a flask of CCl_4 (see Fig. 1.1). The K_2CO_3 or the α-Al_2O_3 was chlorinated by the CCl_4, yielding KCl(s, l) or $Al_2Cl_6(g)$. The CCl_4 flask was kept at a constant temperature during the reaction using a thermostat.

The monazite was chlorinated by the CCl_4 gas to form metal chlorides. Resulting volatile metal chlorides, such as $ThCl_4$ and UCl_4, were vaporized, driven along the temperature gradient with the gas stream, and condensed. Rare earth chlorides, which themselves have low volatility, were also vaporized in the presence of the complex former, KCl or $AlCl_3$, by formation of the vapor complex according to reactions 3.1 and 3.2. After the reaction, the condensates along the temperature gradient were collected by removing the 13 pieces of quartz inner tubing from the reactor. The condensates were then leached individually in dilute hydrochloric acid to determine the composition of metal elements for each inner tube with an X-ray fluorescent spectrometer (Rigaku System 3270A) and an ICP-atomic emission spectrometer (Shimadzu ICPS-1000) using Zn^{2+} as internal standard substance. The chlorination residue on the boat was leached with deionized water so as to remove residual chlorides and to separate them from unreacted monazite and active carbon by filtration. Then, the final residue was calcined in an alumina crucible to remove the active carbon and the unreacted monazite was weighed, while the filtrate was analyzed in the same way for the condensates. The partial pressure of CCl_4 was determined from the change in the weight of the CCl_4 flask and the total volume of the N_2 gas flow during the reaction.

3.3. Results and Discussion

3.3.1. Chlorination and Chemical Vapor Transport Reaction Using Chlorine Gas as a Chlorinating Agent

(1) Separation from Monazite

Extraction of Rare Earth Chlorides. The temperature gradient employed for the CVT reaction of monazite (both concentrate and crude oxide) is shown in Fig. 3.1(a), together with the

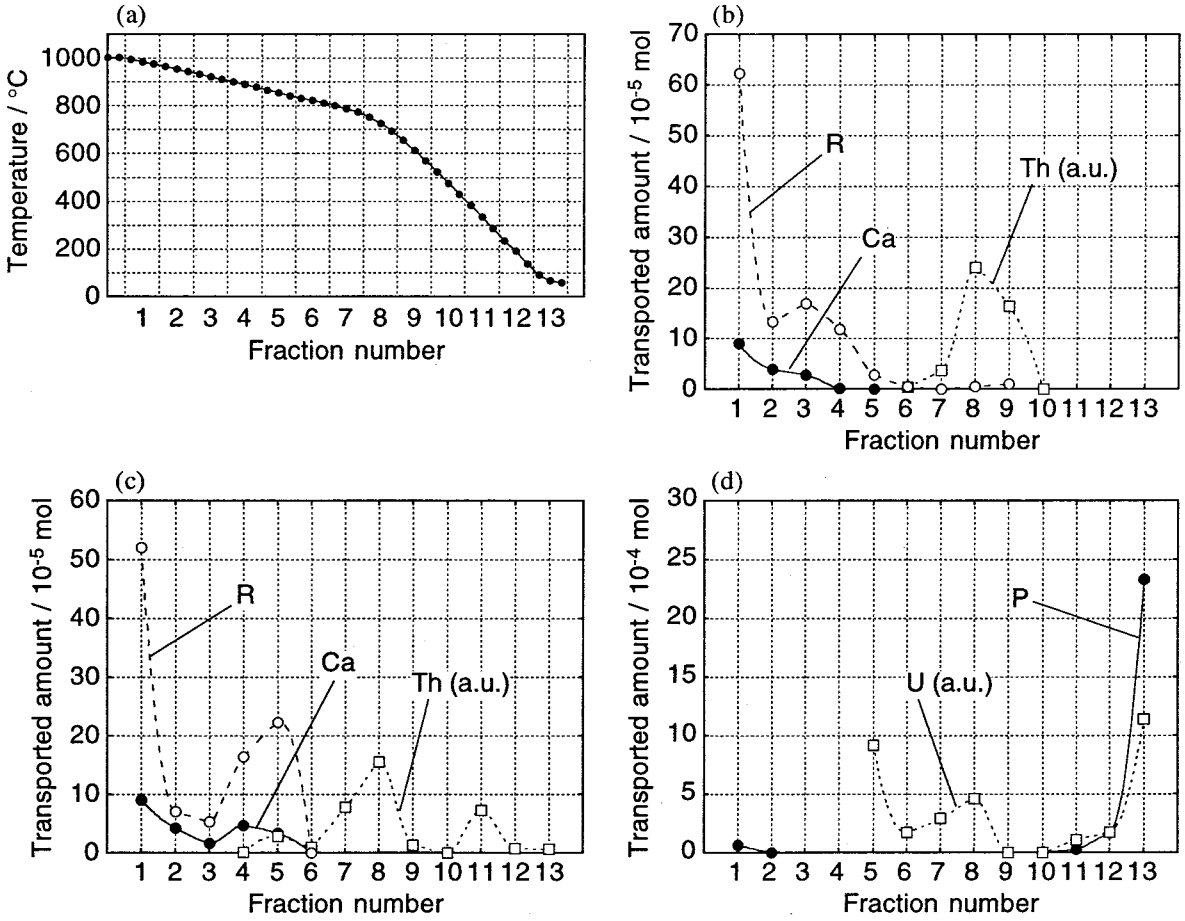

Figure 3.1. (a) Temperature gradient and (b–d) distribution of metal chloride deposits. Raw materials were (b) crude oxide and (c–d) concentrate of monazite; each contains 9.4×10^{-3} mol of rare earths. Complex former was KCl which was mixed as precursor K_2CO_3 (4.7×10^{-3} mol); active carbon powder was added to raw material as deoxidant; mixed N_2 and Cl_2 gases (N_2, 30 cm^3 min^{-1}; Cl_2, 5 cm^3 min^{-1}) was flowed as carrier; reaction time was 82 h.

distribution profiles for transported RCl_3, $CaCl_2$, $ThCl_4$, UCl_4, and phosphorous component (discussed later) along the temperature gradient. The employed temperature gradient has a smaller slope (5.4 °C cm^{-1}) above 800 °C, since lighter rare earth elements are the main constituent of monazite and their chlorides generally condensed at temperatures above 800 °C as mentioned in Chapters 1 and 2. For both the monazite concentrate and the oxide, rare earth chlorides were condensed in portions of FN = 1–5, over a temperature range 990–830 °C, while the other metal chlorides were mainly condensed in fractions at lower temperatures.

Extraction of Thorium and Uranium Chlorides. The monazite oxide contains thorium

and calcium in addition to the rare earths. For the monazite oxide, $ThCl_4$ was concentrated over the temperature range 800–550 °C (*FN* = 7–9; see Fig. 3.1(b)) without any contamination for the rare earth recoveries; this temperature range is in agreement with a result of the direct chlorination experiment of monazite concentrate which was studied by Hilal and El Gohary [29]. In contrast, $CaCl_2$ also condensed at *FN* = 1–5 with almost the same distribution profile as RCl_3. This is probably due to a low volatility of $CaCl_2$ [30] compared with that of $ThCl_4$. Figure 3.2 depicts the distribution profile of the complex former, KCl, which was widely distributed along the temperature gradient. Hence, RCl_3 was extracted not as a pure form but as the RCl_3-$CaCl_2$-KCl mixture, which can be used directly as a molten chloride bath for electrolytic reduction to produce rare earth metals; alternatively, if the metals are to be produced by metallothermic reduction, $CaCl_2$ and KCl will be removed as a slug.

The monazite concentrate contains uranium, aluminium, iron, and so on, in addition to the elements in the oxide. In this case, $ThCl_4$, $CaCl_2$, and KCl were condensed over almost the same temperature range (Figs. 3.1(c) and 3.2) as for the oxide. About 65% of total extracted uranium component was condensed in portions of *FN* = 5–8 (870–670 °C). Since the uranium component in the concentrate is expected to be converted to the volatile chloride UCl_4 under this Cl_2-rich atmosphere, this temperature range 870–670 °C seems too high for the condensation of UCl_4. In fact, the remaining 35% of the uranium component was condensed at *FN* = 13 (below 120 °C) and,

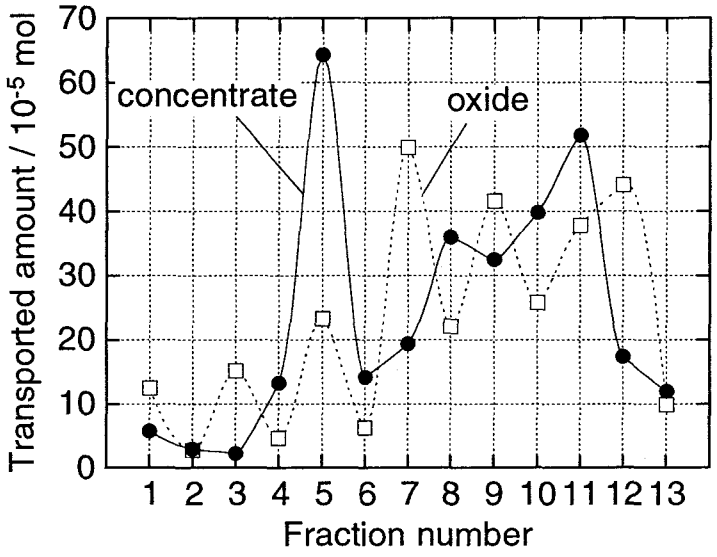

Figure 3.2. Distribution of KCl deposits. Raw materials were crude oxide and concentrate of monazite; each contains 9.4×10^{-3} mol of rare earths. Other reaction conditions were as in Fig. 3.1.

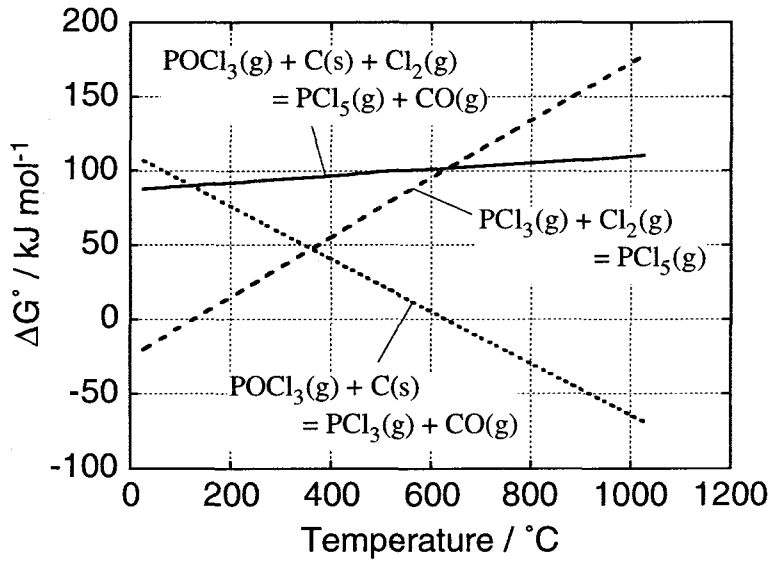

Figure 3.3. Standard free energy of equilibrium reactions between $POCl_3$, PCl_3, and PCl_5.

moreover, most of the uranium component was condensed at $FN = 13$ without using KCl. The condensation at 870–670 °C is probably due to the formation of a non-volatile double salt of UCl_4 with an alkali chloride, KCl [31]. The distribution profile of KCl (Fig. 3.2) which was analogous to that of uranium around $FN = 5$–8 also substantiated the double salt formation.

Consequently, the recovered $ThCl_4$ was contaminated by uranium condensed at $FN = 5$–8. The direct use of monazite concentrate as the starting material for the CVT process may not be suitable for the mutual separation of the thorium and uranium components. In this case, the direct chlorination of the concentrate should be performed first followed by the CVT reaction, accomplished by adding the complex former to the resulting crude RCl_3.

Condensation of Other Chlorides. Aluminium, iron, and zirconium, whose chloride are highly volatile, were transported to the portions below 550 °C ($FN = 10$–13). A phosphorous compound produced by the chlorination of PO_4^{3-} ion is condensed mainly at $FN = 13$. According to Hartley's work on direct chlorination of monazite on a thermodynamical aspect [32], the PO_4^{3-} is converted to $POCl_3$. However, the chlorination temperature employed for present work is 1000 °C, which is higher than that of Hartley's work. Calculations of free energy changes of reactions

$$POCl_3(g) + C(s) = PCl_3(g) + CO(g), \quad (3.3)$$

$$PCl_3(g) + Cl_2(g) = PCl_5(g), \quad (3.4)$$

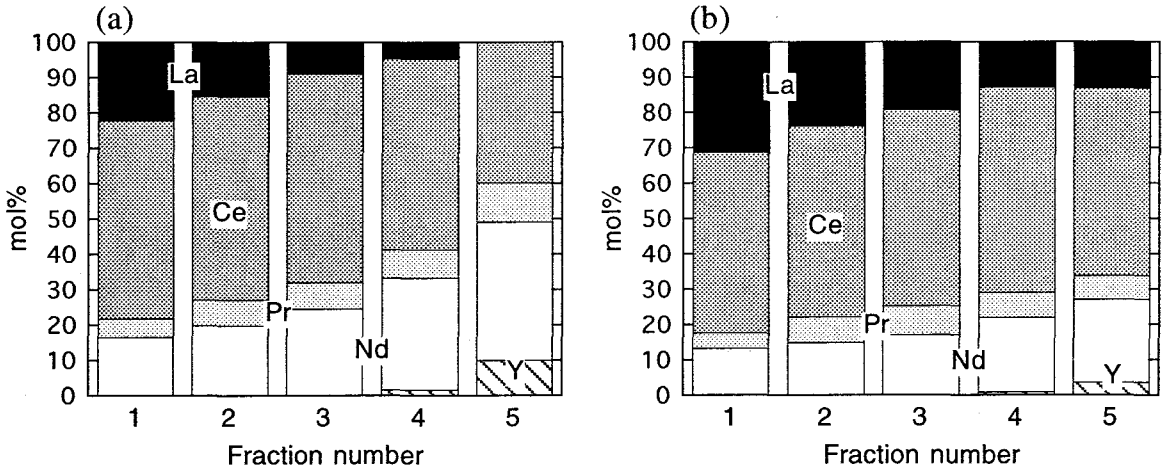

Figure 3.4. Composition of rare earth chlorides for the condensates at *FN*= 1–5. Raw materials were (a) crude oxide and (b) concentrate of monazite; each contains 9.4×10^{-3} mol of rare earths. Other reaction conditions were as in Fig. 3.1.

and

$$POCl_3(g) + C(s) + Cl_2(g) = PCl_5(g) + CO(g), \qquad (3.5)$$

using some existing thermodynamic functions [33] show that PCl_3 is more stable than $POCl_3$ above 630 °C due to a negative free energy change of reaction 3.3 (Fig. 3.3). Therefore, the phosphorous compound produced at 1000 °C is probably PCl_3. Moreover, PCl_5 is more stable than PCl_3 below 127 °C in the presence of Cl_2 gas. This suggests that the resulting PCl_3 reacts with Cl_2 in the carrier gas during transport and the condensed phosphorous compound at *FN*= 13 (below 120 °C) will be PCl_5. The condensate at *FN*= 13 was a yellow solid, probably a solid solution of co-deposited $AlCl_3$, $FeCl_3$, $ZrCl_4$, and UCl_4.

Composition of Extracted Rare Earth Chlorides. Figure 3.4 shows the compositions of RCl_3 at the fractions 1–5 where RCl_3 condensed. The chlorides of La, Ce, Pr, Nd, and Y were deposited in that order at the fractions shown from higher temperatures (*FN* = 1; 990–970 °C) to lower ones (*FN*= 5; 870–830 °C). This deposition tendency agrees with the order of ionic radius of rare earths, indicating that the vapor complexes, $KRCl_4(g)$, with smaller ionic radius of R^{3+} are more stable than those with larger ones and prefer to be concentrated at the fractions in the lower temperature region. This result coincides with the previous one in regard to $RAl_nCl_{3+3n}(g)$ vapor complexes whose stability also increased with the decrease of ionic radius of rare earth ions (see Section 1.3.2). For the use of both the concentrate and crude oxide, the majority of the YCl_3 was

condensed at $FN = 5$, and the mutual separation of yttrium and other rare earths was carried out satisfactorily.

Yields of Each Element. The yields of each element after the CVT reaction for 82 h are summarized in Table 3.2. The yields were calculated as

$$\text{yield} / \% = 100\, N_{\text{total}} / (N_{\text{total}} + N_{\text{boat}}) \qquad (3.6)$$

where N_{total} and N_{boat} are the molar quantity values of the total transported metal chloride and the residual metal chloride in the boat, respectively. Although the yields of the non-rare earth elements were almost 100%, except for the non-volatile $CaCl_2$, those of RCl_3 were generally lower. The yields of rare earth elements increased with decreasing ionic radius of the rare earths, also supporting the order in the stability of the vapor complexes.

In the absence of the complex former KCl (*i.e.* K_2CO_3), the yields of RCl_3, shown as (iii) and (iv) in Table 3.2, were reduced to about one-half of the value obtained in the presence of KCl ((i) and (ii)). This difference, (i) – (iii) and (ii) – (iv), corresponds to volatility enhancement of RCl_3 due to the formation of $KRCl_4(g)$ vapor complex. Moreover, the fact that the concentrate always provided higher yields than the oxide whether KCl was used or not, *i.e.* (i) > (ii) and (iii) > (iv), implies that the formation of some vapor species other than $KRCl_4(g)$ influences the transport of

Table 3.2. Yields of rare earth chlorides for the chemical vapor transport reaction using monazite concentrate or crude oxide

Raw material	Complex former	Yield of rare earths (%)						Yield of non-rare earths (%)						
		La	Ce	Pr	Nd	Y		Ca	Th	U	Al	Fe	Zr	P
conc.[a]	KCl	33	63	67	64	>99	(i)	76	>99	>99	>99	98	>99	>99
oxide	KCl	24	50	53	54	>99	(ii)	89	>99	–	–	–	–	–
conc.[a]	–[b]	17	38	38	36	>99	(iii)	60	>99	>99	>99	>99	>99	>99
oxide	–[b]	10	25	27	23	>99	(iv)	85	>99	–	–	–	–	–
		9	*13*	*14*	*10*	–	(i) – (ii)							
		7	*13*	*11*	*13*	–	(iii) – (iv)							
	average	*8*	*13*	*12.5*	*11.5*	–	(v)							
		16	*25*	*29*	*28*	–	(i) – (iii)							
		14	*25*	*26*	*31*	–	(ii) – (iv)							
	average	*15*	*25*	*27.5*	*29.5*	–	(vi)							

[a] Concentrate.

[b] Only chlorination was carried out.

RCl_3 in addition to $KRCl_4(g)$, since the total rare earth content in the starting material was 9.4×10^{-3} mol for both the concentrate and the oxide. If another vapor complex of RCl_3 is formed in addition to $KRCl_4$, the most plausible complex is that in the RCl_3-$POCl_3$ system, because $POCl_3$ is known to form highly stable oxygen-bridged 1:1 vapor complexes $MCl_x \cdot POCl_3$ [34] and, in this case, it seemed natural that it should form a similar complex $RCl_3 \cdot POCl_3(g)$ during the chlorination of RPO_4 as

$$RPO_4(s) + 3\ C(s) + 3\ Cl_2(g) \rightarrow RCl_3 \cdot POCl_3(g) + 3\ CO(g). \qquad (3.7)$$

However, a supplementary study (see Section 3.3.1(2)) could provide no positive evidence for the presence of the RCl_3-$POCl_3$ complex and also of the RCl_3-PCl_3 complex. Therefore, the additional vapor species are still vague. If the additional vapor species are practically formed, then the differences in the yields, (i) – (ii) and (iii) – (iv) listed in Table 3.2, correspond to the amount of the unknown vapor species. From the average values, (v), percentage of the generated unknown vapor species was calculated as 20%, when the concentrate was transported using KCl.

(2) Existence of Phosphoryl or Phosphorus(III) Chloride Complex

In order to investigate qualitatively the existence of the vapor complex(es) in the RCl_3-$POCl_3$ and the RCl_3-PCl_3 systems, the following experiments were carried out. Anhydrous $NdCl_3$ (1.0 g) was transferred into a pyrex tube in a nitrogen-filled glove box with water vapor content less than 1 ppm. The pyrex tube was cleaned, flamed and degassed under dynamic vacuum before use. The tube with $NdCl_3$ was then attached to a vacuum line where a glass tube with $POCl_3$ (0.148 cm^3) or PCl_3 (0.140 cm^3) was also attached. Under freezing the $POCl_3$ or the PCl_3 with methanol-liquid nitrogen, both the tubes were evacuated to about 0.5 Pa; the $POCl_3$ or the PCl_3 was, then, sublimed into the $NdCl_3$ tube which was immersed in the liquid nitrogen; the resulting tube, now containing both the $NdCl_3$ and $POCl_3$ or PCl_3 was then sealed off *in vacuo*.

The sealed tube (length, *ca* 35 cm) was placed in a tube furnace with slight slope so as to keep the mixed $POCl_3$ or PCl_3 and $NdCl_3$ at one end. The furnace was operated to heat the mixture at 327 °C while keeping the other end of the tube at 80 °C. Under these conditions no liquid $POCl_3$ or PCl_3 was observed at the hot end (327 °C) and part of $POCl_3$ or PCl_3 liquefied at the cool end, which then dripped toward the hot end.

After the reaction for 160 h, the tube was taken from the furnace and the cool end with the white condensate was cut and analyzed on an ICP-atomic emission spectrometer. However, the condensate contained only phosphorous, not neodymium.

As a result, it may be concluded that vapor complexes in the RCl_3-$POCl_3$ and the RCl_3-PCl_3 systems are not formed, or, if they are formed, higher temperatures are necessary to cause complexation. Since the MCl_x-$POCl_3$ complexes are more like adducts than complexes, the RCl_3-$POCl_3$ complex(es) might form in a temperature range where RCl_3(g) is present in a large relative abundance.

(3) Separation from Xenotime Concentrate

Xenotime concentrate contains rare earths as the orthophosphates, as does the monazite concentrate. The composition of the rare earths in the xenotime is different from those in the monazite, however, and yttrium and heavier rare earths have a large relative abundance. In the case of the

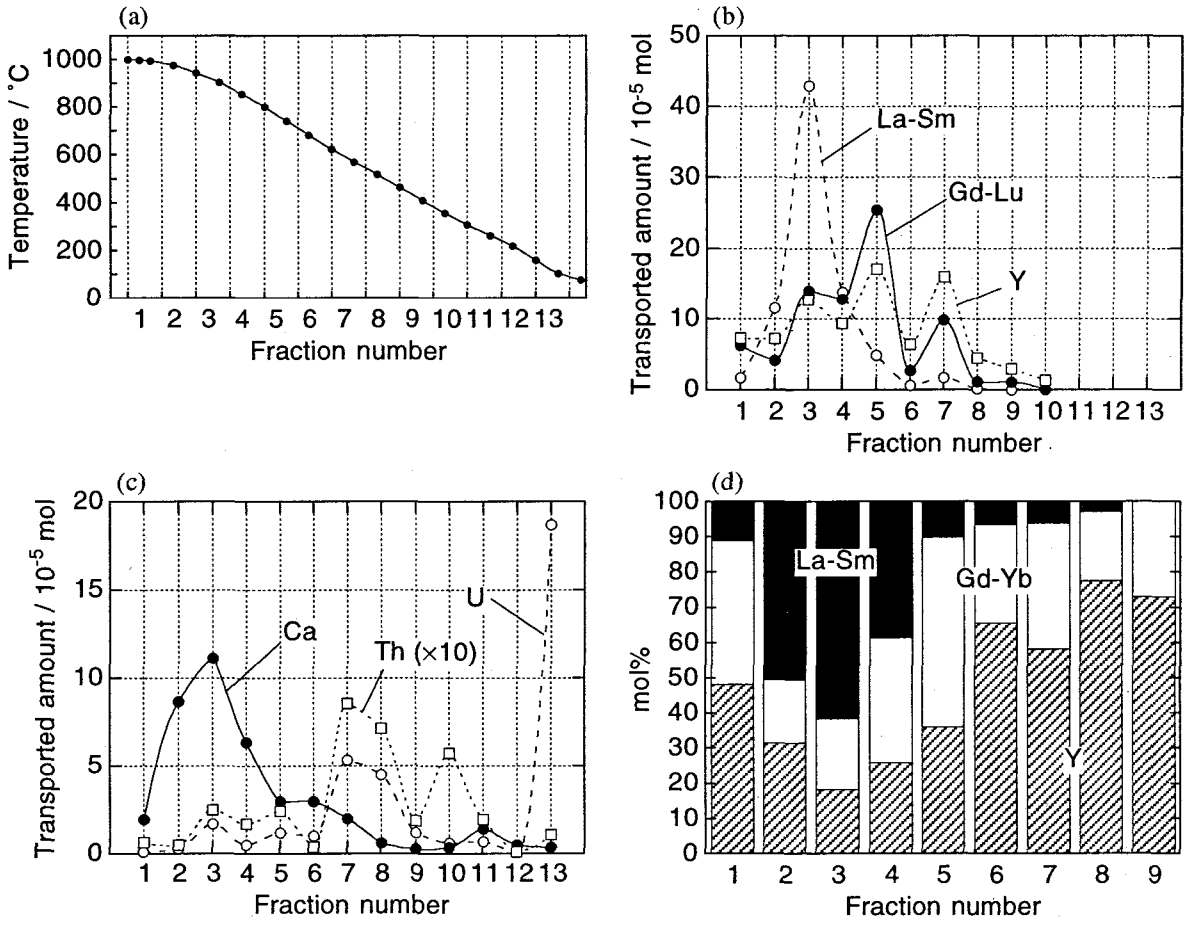

Figure 3.5. (a) Temperature gradient, (b, c) distribution of metal chloride deposits, and (d) composition of rare earth chlorides for the condensates at *FN*= 1–9. Raw material was xenotime concentrate containing 18.1×10^{-3} mol of rare earths; complex former was KCl which was mixed as precursor K_2CO_3 (9.1×10^{-3} mol); deoxidant, carrier gas, and reaction time were as in Fig. 3.1.

CVT reaction using the xenotime, therefore, RCl_3 also condensed in the lower temperature range (990–400 °C) rather than that observed for the monazite (990–830 °C), since the $KRCl_4(g)$ complexes of heavier rare earths are generally more volatile than those of lighter ones and have a tendency to decompose at lower temperatures. Thus, the temperature gradient operated for the CVT reaction using the xenotime is linear (27 °C cm^{-1}) and low temperature region, where heavier rare earth chlorides usually condense, is more widely ranged (Fig. 3.5(a)) than that for the monazite. Figure 3.5(b) and (c) show the distribution profiles of RCl_3 and other some metal chlorides, respectively. The RCl_3 recovered from high temperature fractions around $FN = 3$ (940–870 °C) was mixed with $CaCl_2$ and KCl, as also observed for the monazite. In these fractions light rare earth chlorides (La–Sm) were concentrated to *ca* 60 mol% of total rare earths as shown in Figure 3.5(d). In contrast, most of YCl_3 and the heavier rare earth chlorides condensed at $FN = 3$–7 (940–550 °C), and the YCl_3 at $FN = 7$ was concentrated to 60 mol% of total RCl_3. However, the distribution of the YCl_3 overlapped with those of $ThCl_4$, UCl_4, and $MnCl_2$. Since xenotime is important as a source of yttrium, the contamination of YCl_3 by those chlorides is not desirable.

As a result, the direct use of the xenotime concentrate as the raw material for the CVT reaction is not appropriate for a yttrium extraction. It is better that the direct chlorination of the xenotime is carried out first to remove volatile metal chlorides such as $ThCl_4$, UCl_4, $MnCl_2$, and $POCl_3$. The resulting crude RCl_3 should be used for the CVT reaction. This two-step process will render it possible to obtain a YCl_3 free from $ThCl_4$ and other contaminants.

Table 3.3. Yields (%) of rare earth chlorides for the chemical vapor transport reaction using rare earth concentrates or crude oxides[a]

Raw material	R/K ratio[b]	La	Ce	Pr	Nd	Sm	Gd	Tb	Dy	Er	Yb	Y
monazite concentrate	1/1	33	63	67	64	–	–	–	–	–	–	>99
	1/2	45	67	76	76	–	–	–	–	–	–	>99
	1/3	38	64	74	74	–	–	–	–	–	–	>99
xenotime concentrate	1/1	26	58	70	61	72	69	85	91	90	97	90
monazite oxide	1/1	24	50	53	54	–	–	–	–	–	–	>99
ionic ore[c]	1/1	24	57	59	57	78	89	81	94	–	97	84
bastnaesite oxide	1/1	7.5	15	28	25	–	–	–	–	–	–	–
	1/1.5	15	27	46	44	–	–	–	–	–	–	–
	1/2	28	48	67	67	–	–	–	–	–	–	–

[a] KCl was used as complex former.

[b] R/K mole ratio of initially loaded raw mixture.

[c] A crude oxide prepared from ionic ore in Xun-wu, China.

Yields of each rare earth are given in Table 3.3. Analogous to the case of monazite, the yield increased with decreasing ionic radius of R^{3+}, and the yields of non-rare earth elements (except for Ca) were almost 100%.

(4) Separation from Crude Oxides

Ionic Ore. Both KCl and $AlCl_3$ were employed as complex formers for the CVT reaction of the oxide prepared from ionic ore in Xun-wu, China. As shown in Table 3.1, the most abundant elements in the Xun-wu deposit are La, Nd, and Y. Figures 3.6 and 3.7 show the temperature gradient and the distribution profiles of RCl_3 and the complex formers, KCl and $AlCl_3$, respectively. The temperature gradient has a smaller slope (6.8 °C cm^{-1}) above 850 °C.

When KCl was the complex former, RCl_3 was condensed at 990–550 °C (*FN* = 1–10), which

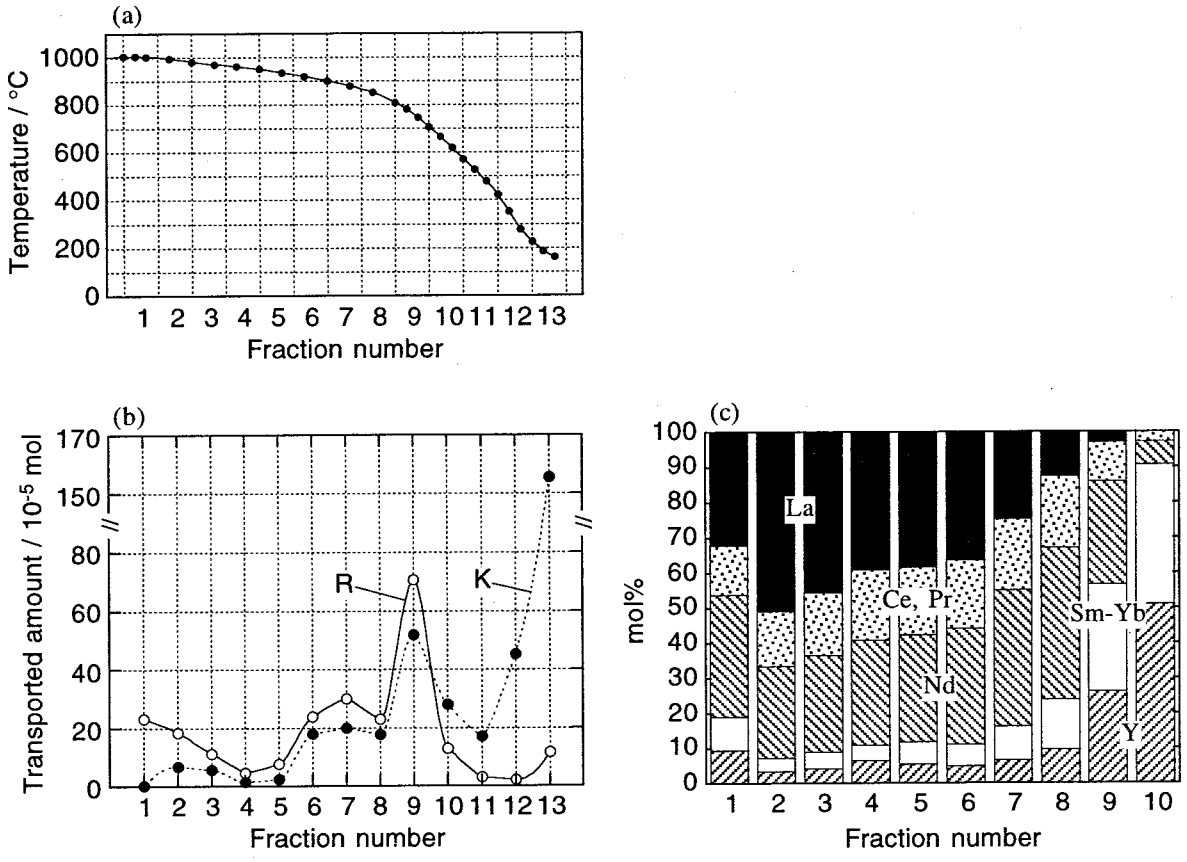

Figure 3.6. (a) Temperature gradient, (b) distribution of metal chloride deposits, and (c) composition of rare earth chlorides for the condensates at *FN* = 1–10. Raw material was oxide prepared from ionic ore in Xun-wu containing 10.0×10^{-3} mol of rare earths; complex former was KCl which was mixed as precursor K_2CO_3 (5.0×10^{-3} mol); deoxidant, carrier gas, and reaction time were as in Fig. 3.1.

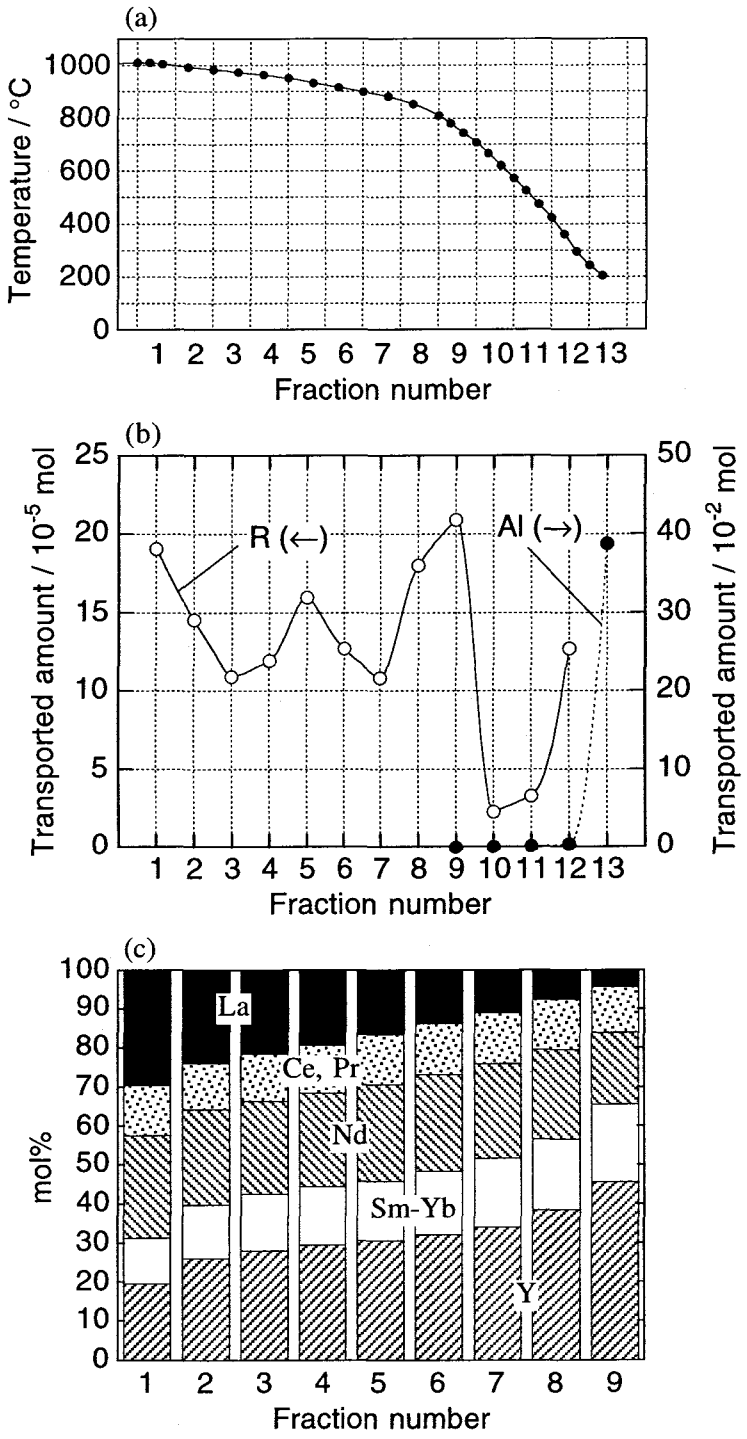

Figure 3.7. (a) Temperature gradient, (b) distribution of metal chloride deposits, and (c) composition of rare earth chlorides for the condensates at $FN = 1–9$. Raw material was oxide prepared from ionic ore in Xun-wu containing 50.0×10^{-3} mol of rare earths; complex former was $AlCl_3$ (3.7×10^{-1} mol); reaction time was 30 h; deoxidant and carrier gas were as in Fig. 3.1.

is the same temperature range observed for the CVT reaction of xenotime. The distribution profile of RCl_3 was similar to that of KCl, indicating qualitatively that the transport reaction of the RCl_3 is mediated by the RCl_3-KCl complex. Although the similarity in the distribution profile was also observed in the CVT of bastnaesite oxide described below, this was not the case for the monazite and xenotime concentrates, since KCl can form vapor complexes not only with RCl_3 but also with various other chlorides, by which process the distribution of KCl was affected.

By use of the CVT reaction with $AlCl_3$ as the complex former, RCl_3 was condensed at 990–250 °C (*FN* = 1–12), which is a wider range than with KCl, since the RCl_3-$AlCl_3$ vapor complex(es) is more stable than the RCl_3-KCl complex at the relatively low temperatures around 300–400 °C (see Section 2.3.1). The $AlCl_3$ was condensed only at *FN* = 12 and 13 (below 350 °C) and, therefore, the RCl_3 was obtained in the pure form.

Figures 3.6(c) and 3.7(c) show the compositions of RCl_3 where lighter rare earth chlorides prefer to be condensed at high temperatures and heavier ones at lower temperatures. The yields of each RCl_3 follow the same order for both monazite and xenotime.

Bastnaesite — Effect of the R/K Mole Ratio in the Raw Material. Since bastnaesite contains only lighter rare earth elements, *i.e.* La, Ce, Pr, and Nd, rare earth chlorides may be formed by the CVT reaction using bastnaesite oxide condensed at the same temperature region as in the case of monazite. The temperature gradient for bastnaesite has a smaller slope (12 °C cm^{-1}) above 800 °C.

Regarding the bastnaesite oxide, the effect of the R/K mole ratio of the initially introduced raw material on the yield and mutual separation efficiency of RCl_3 was investigated. The amount of bastnaesite was kept constant at 2.000 g for all runs and the amount of K_2CO_3 was altered from 0.748 g (R/K = 1/1) to 1.496 g (R/K = 1/2). The mutual separation efficiency was evaluated from the difference in the composition of RCl_3 between high (*FN* = 1–2) and low (*FN* = 7–8) temperature fractions. The CVT reaction using a pure anhydrous chloride RCl_3-NaCl (R = Pr, Nd; Pr/Nd = 1/1) mixture (see Section 2.3.1(3)) demonstrated that the equimolar raw mixture (R/Na = 1/1) gives the highest yield of RCl_3 and the best Nd/Pr separation factor, $\beta_{Nd/Pr}$. This is explained by the fact that the RCl_3-ACl (A = alkali metals) vapor complex is easy to form above R/A = 1/1 melt since the vapor complex also has 1/1 composition. For the bastnaesite, however, the yield increased with increasing KCl (*i.e.* K_2CO_3) content in the raw material (Table 3.3). At 1000 °C, as well as $KRCl_4$(g) and RCl_3(g), KCl(g) evaporated from the RCl_3-KCl melt in relatively large abundance (see Chapter 5 and also ref. [19a]). Therefore, the KCl content in the melt gradually decreases during the

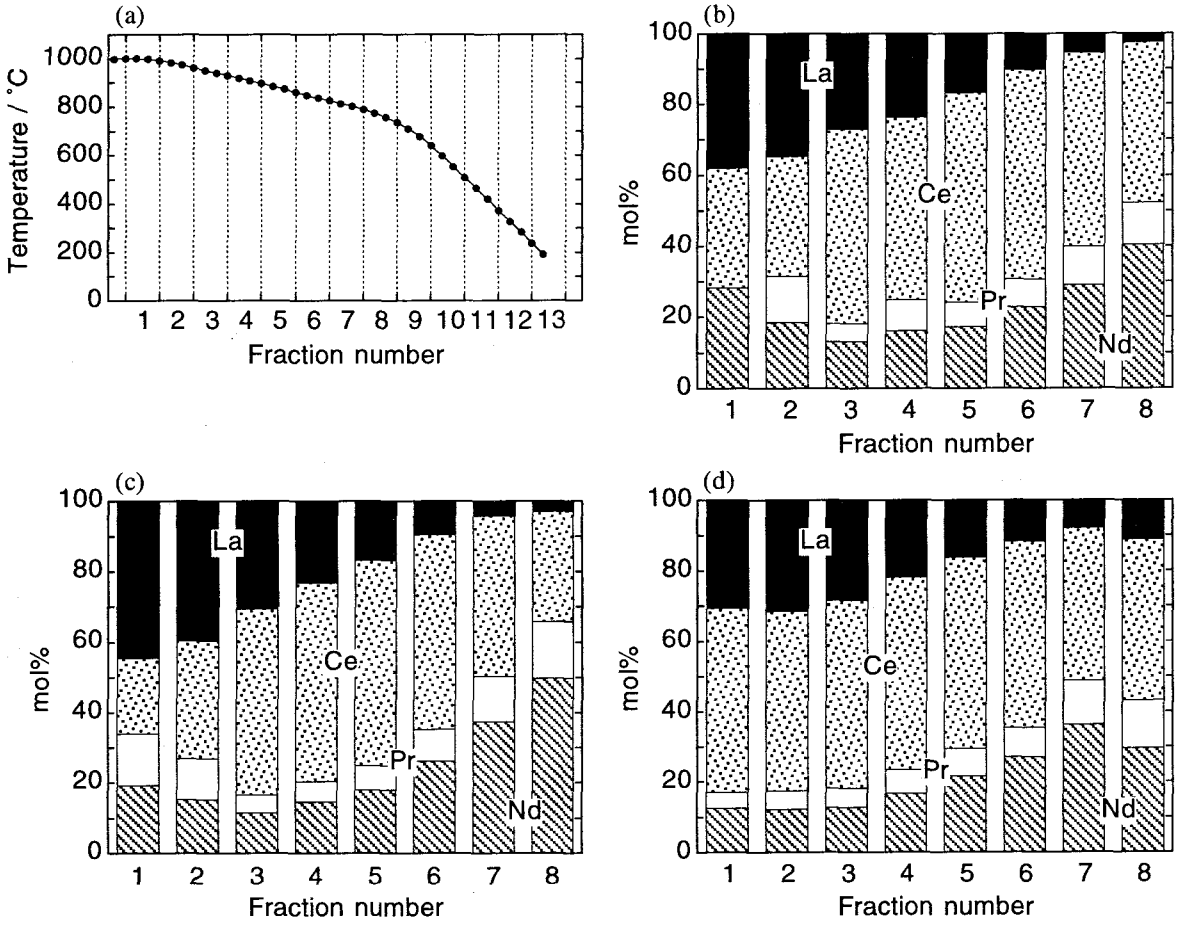

Figure 3.8. (a) Temperature gradient and (b–d) composition of rare earth chlorides for the condensates at $FN = 1$–8. Raw material was crude oxide of bastnaesite containing 10.8×10^{-3} mol of rare earths. Complex former was KCl which was mixed as precursor K_2CO_3: (b) 5.4×10^{-3} mol (R/K = 1/1); (c) 8.1×10^{-3} mol (R/K = 1/1.5); (d) 10.8×10^{-3} mol (R/K = 1/2). Deoxidant, carrier gas, and reaction time were as in Fig. 3.1.

reaction for 82 h. If the amount of initially loaded K_2CO_3 is small, *e.g.* R/K = 1/1, then KCl is exhausted during the course of the reaction and, hence, the yield is lowered. In contrast, for the CVT reaction using a pure RCl_3-NaCl mixture (Section 2.3.1), the reaction time was much shorter (6 h) and the loss of NaCl did not affect the yield and separation efficiency.

In contrast to the yield, the mutual separation efficiency was lowered with increasing KCl concentration (see Fig. 3.8). In the bastnaesite oxide La and Nd represent 32 and 15 mol% of total R_2O_3. When the R/K mole ratio was 1/1, La and Nd were concentrated up to 38 ($FN = 1$) and 41 mol% ($FN = 8$), respectively, while these were concentrated to only 33 mol% ($FN = 2$) and 35 mol% ($FN = 7$) when the mole ratio was 1/2. This is expressed quantitatively as follows. In this

CVT process, the mutual separation efficiency is governed by two factors: (i) selectivity in vaporization from the melt, and (ii) selectivity in condensation onto a temperature gradient. Since the CVT reaction is a batch-type reaction, if all of initially present RCl_3 were vaporized and transported completely, the effect of the former selectivity would be negligible. The CVT of a mixed praseodymium and neodymium oxides (see Section 2.3.2(2)) also suggests that the Nd/Pr separation factor, $\beta_{Nd/Pr}$, decreases with the advance of the reaction, that is, with increase of the yield (transported amount) of RCl_3 (see Fig. 2.7). In view of the separation efficiency, an appropriate R/K ratio for the case of CVT using the bastnaesite oxide will be of 1/1.5, which gives an similar separation efficiency to 1/1.

3.3.2. Chlorination and Chemical Vapor Transport Reaction Using Carbon Tetrachloride as a Chlorinating Agent

Chlorination Behavior of Monazite. The chlorination characteristics of CCl_4 were investigated without using the complex formers, KCl or $AlCl_3$. Though chlorination rate was accelerated with the rise of temperature, CCl_4 was remarkably deactivated by thermal decomposition at higher temperatures than 900 °C. Figure 3.9(a) shows the relationship between fraction of monazite chlorinated, x, and reaction time, t, under two CCl_4 pressures when chlorinated at 900 °C. In order to chlorinate 80% of initially loaded monazite, 82 and 48 h were necessary under the CCl_4 pressure of 4.0×10^3 and 10.0×10^3 Pa, respectively. Due to the low volatility of RCl_3, the resulting RCl_3 was remained in the raw material, whereas chlorides of Fe, Zr, and Th vaporized away immediately and did not remain. In this case, therefore, the sharp interface model [35], where unreacted inner core (*i.e.* monazite particle) is covered with ash layer of reaction product (RCl_3), is applicable to analyze the chlorination curves in Fig. 3.9(a). According to the model [35], the chlorination comprises three steps: (i) CCl_4 diffusion through a gas film on the RCl_3 ash layer, (ii) CCl_4 diffusion through the ash layer, and (iii) reaction of CCl_4 with the monazite core at interface between the ash layer and the core. A plot of $1-(1-x)^{1/3}$ against t was found to be linear (Fig. 3.9(b)), *i.e.* $1-(1-x)^{1/3} = kt$ (k = rate constant), suggesting that the third step determines the overall rate of the chlorination. The rate constants, k, were calculated as 5.4×10^{-3} ($p_{CCl_4} = 4.0 \times 10^3$ Pa) and 8.6×10^{-3} h^{-1} ($p_{CCl_4} = 10.0 \times 10^3$ Pa). The times required for complete chlorination, t^*, which were obtained from the reciprocal of the rate constants, were 186 and 116 h for the two CCl_4 pressures.

In general, the chlorination using CCl_4 proceeds at lower temperatures than carbochlorination using chlorine gas Cl_2 and carbon [26]. This means chlorination by CCl_4 is faster at the same reaction temperature. However, the carbochlorination of the monazite sand at 900 °C using Cl_2

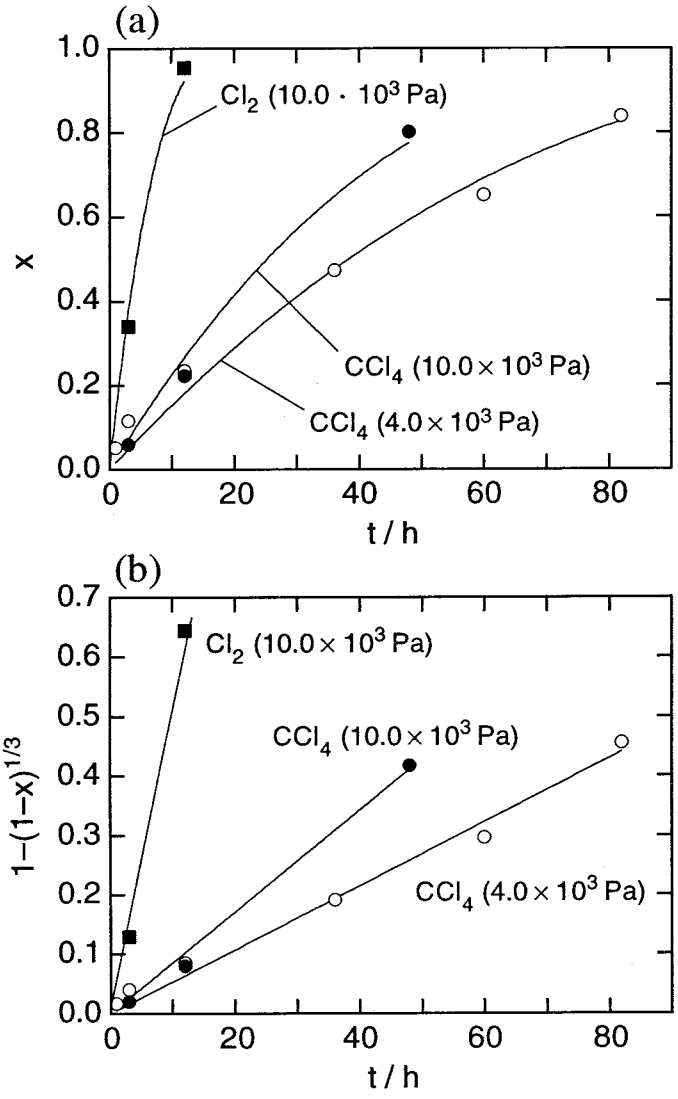

Figure 3.9. (a) Reaction rate, x, of monazite concentrate with time, t, during chlorination with CCl_4 and carbochlorination with Cl_2 at 1173 K and (b) plot of $1-(1-x)^{1/3}$ against reaction time.

(10.0×10^3 Pa) and active carbon powder (0.585 g) was completed within 6 h and, therefore, it turned out that the time required to complete the carbochlorination is much shorter. In a word, CCl_4 has lower efficiency than Cl_2 gas with respect to the chlorination of monazite. This is attributable to a high density of monazite sand compared to other many concentrates. If the monazite sand is ground to a powder, the time required for complete chlorination will be shortened. However, the process, using the monazite sand as it is, is favorable because to grind the monazite sand is difficult due to the hardness.

Since the chlorination using CCl_4 is probably expressed as

$$RPO_4(s) + 3\ CCl_4(g) \rightarrow RCl_3(s, l) + POCl_3(g) + 3\ COCl_2(g) \qquad (3.8)$$

and/or

$$RPO_4(s) + 3/2\ CCl_4(g) \rightarrow RCl_3(s, l) + POCl_3(g) + 3/2\ CO_2(g), \qquad (3.9)$$

the reaction is expected to have an order of 1.5–3.0. Contrary to the expect, a plot of k against $p_{CCl_4}{}^{1/2}$ (Fig. 3.10) shows that there is a correlation, $k = a\,(p_{CCl_4})^{1/2}$ (a = constant) and, hence, the reaction has the order of 1/2. This also indicate the unusual slow speed of the chlorination by CCl_4.

Extraction of Rare Earth Chlorides via Vapor Complexes. Figure 3.11 shows the distribution profile of metal chlorides along the temperature gradient after the reaction for 82 h. The pressure of CCl_4 was kept at 4.0×10^3 Pa. The chlorides of thorium and uranium were extracted even in the absence of complex former such as KCl and $AlCl_3$, while most of the rare earth chlorides were remained in the boat. Without the complex former, the thorium and uranium chlorides were condensed in the fractions of 7–9 at 580–340 °C (Fig. 3.11(b)). The yield of rare earths, thorium, and uranium after the chlorination for 82 h were 1.8, 99, and 54%, respectively; the yields were calculated according to eq. 3.6. When the complex former, $AlCl_3$, was used, the yield of RCl_3 was increased to 9.9% and the extracted RCl_3 was condensed in the fractions of 1–5 at 890–650 °C (Fig. 3.11(c)). The yield of RCl_3 was still lower than those of thorium and uranium. However, the

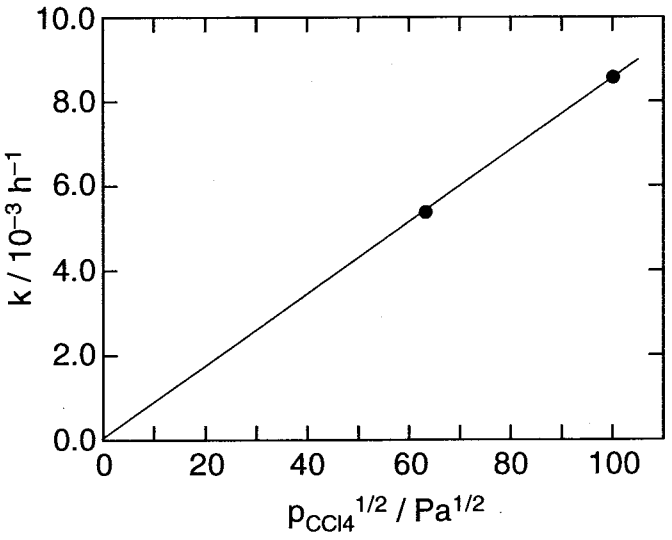

Figure 3.10. A plot of kinetic constant, k, and square root of CCl_4 pressure, p_{CCl_4}.

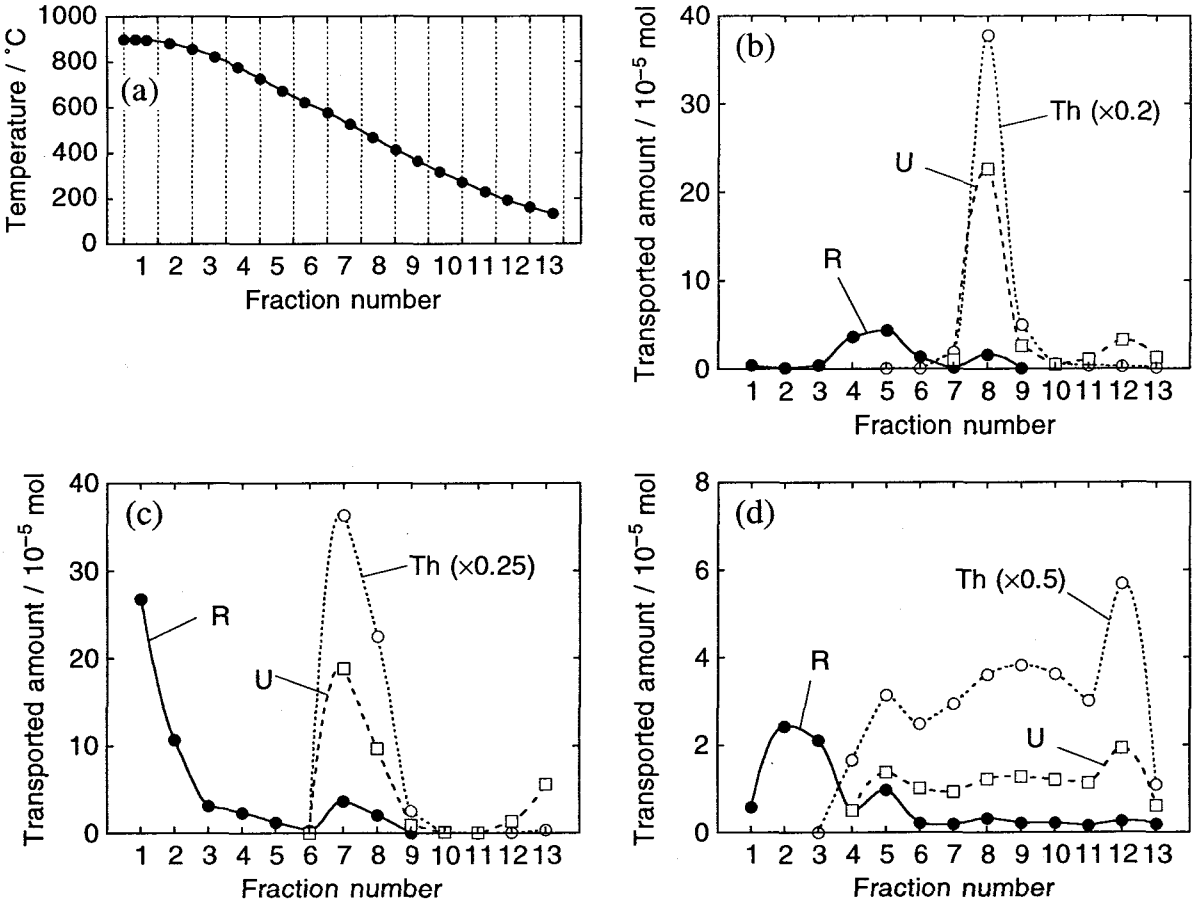

Figure 3.11. (a) Temperature gradient and (b–d) distribution of metal chloride deposits after the reaction for 82 h. Raw material was monazite concentrate (2.925 g) containing 9.4×10^{-3} mol of rare earths; complex formers were (b) not used, (c) $AlCl_3$ which was used as precursor Al_2O_3, and (d) KCl which was mixed as precursor K_2CO_3 (4.7×10^{-3} mol); mixed N_2 and CCl_4 gas ($p_{CCl4} = 4.0 \times 10^3$ Pa) was flowed.

yield can be improved if the reaction lasts for a longer time than 82 h. The thorium and uranium chlorides were condensed at the same temperature range as observed in the absence of complex former. Therefore, mutual separation of rare earth and thorium or uranium was conducted satisfactorily. Aluminium, iron and zirconium chlorides and a phosphorous compound, which is presumably $POCl_3$, produced by the chlorination of PO_4^{3-} ion were condensed mainly at the fraction number of 13 below 160 °C.

When the complex former was KCl, however, the yield of RCl_3 was 1.2%, which is the same level as obtained in the absence of the complex former. In this case, most of the KCl may have vaporized before the chlorination of the monazite to RCl_3, since the chlorination of the monazite using CCl_4 is much slower than that using Cl_2 gas as mentioned above. Moreover, thorium and

uranium chlorides were widely distributed along the gradient and were not clearly separated from extracted RCl_3. This probably is caused by the formation of non-volatile double salt of UCl_4 and $ThCl_4$ with an alkali chloride, KCl [31]. As a result, among the two complex formers tried, $AlCl_3$ has a positive effect on the extraction of RCl_3.

3.4. Conclusions

The CVT reaction can be conducted using rare earth concentrates or crude oxides as the raw materials and low-volatile RCl_3 is extracted as the vapor phase by forming $KRCl_4(g)$ or $RAl_nCl_{3+3n}(g)$ vapor complexes. However, the direct use of the concentrate as the raw material is not always appropriate, a two-step process of the direct chlorination followed by the CVT reaction being advantageous for the metal separation. Rare earth chlorides with smaller R^{3+} radii, *i.e.* heavier rare earth chlorides including YCl_3, are generally more readily transported and concentrated in the condensate at a lower temperature zone, with lighter ones condensing at higher temperature fractions. This tendency, suggesting that the smaller R^{3+} provides more stable vapor complexes, is underlined by the order in the yields of each RCl_3: the yields of heavier chlorides are generally higher than those of lighter ones. For the CVT reaction using bastnaesite, an R/K mole ratio less than 1/1 is appropriate if the reaction lasts for a long time, *e.g.* 82 h.

In addition to the process using Cl_2 gas as a chlorinating agent, the CVT reaction using CCl_4 was also examined for rare earths and thorium separation from monazite. The chlorination rate was unexpectedly slower than the carbochlorination under the same reaction conditions. The chlorination with CCl_4 was topochemical, and the amount of monazite reacted after different periods, t, followed the relationship, $1-(1-x)^{1/3} = kt$, suggesting that the kinetic control is the step of the reaction between CCl_4 and the monazite core at the interface. The kinetic order of the reaction was 1/2. By the use of complex former, $AlCl_3$, rare earth chlorides were extracted owing to the chemical vapor transport phenomenon mediated by volatile $RAl_nCl_{3+3n}(g)$ complexes.

Chapter 4

Recovery of Rare Metals from Industrial Wastes by Chemical Vapor Transport

4.1. Introduction

In recent years, a number of new materials, in which rare metal elements play an important role, have been rapidly advanced. However, the resources of rare metals are usually limited and unevenly distributed to some particular regions in the world and, hence, their cost and supply have strongly depended on political circumstances. Consequently, it becomes necessary to recover these rare metals from various kinds of industrial wastes by profitable methods and to recycle them for further production of the materials.

For sintered intermetallic compounds for the use of permanent magnet materials, for example, a large amount of their sludge is produced in shaping and grinding processes to commercially demanded forms, and the total volume of the sludge sometimes becomes greater than that of the commercial products. Fly ash produced by a combustion of fossil fuels, especially of fuel oil, is another type of waste which also contains rare metals such as vanadium and nickel. Hence, the recovery from those wastes is significant, and some wet processes are currently being developed [36]. However, a new simple and easy method is desired, since the wet processes always consist of a series of complicated treatments (see General Introduction).

On the other hand, the chemical vapor transport (CVT) technique described in the previous chapters seems to be a promising dry process not only for a separation of rare earths but also for many other metallurgical metal-extraction processes, including metal recycling. In the work presented in this chapter, the CVT process was applied to rare metal recycling precess from (i) scrap of rare earth–based intermetallic compounds, Sm_2Co_{17}, $Nd_2Fe_{14}B$, and $LaNi_5$ and (ii) a fly ash of a bitumen-in-water emulsion (Orimulsion^{TM}) which has been developed by British Petroleum Company p.l.c. and Petróleos de Venezuela S.A. in order to commercialize the extra-heavy bitumens from Venezuelan Orinoco region; the emulsion is of great significance for an alternative energy source for the future [37].

4.2. Experimental Details

Materials. The sludges of Sm_2Co_{17} and $Nd_2Fe_{14}B$ type intermetallic compounds were supplied by Shin-Etsu Chemical Co. Ltd. and used without any pretreatment except for drying overnight *in vacuo* at ambient temperature. The ground scrap of $LaNi_5$ alloy provided by Santoku Metal Industry was used without any pretreatment. Compositions of the metallic elements, including boron in the $Nd_2Fe_{14}B$, summarized in Table 4.1 were determined by means of X-ray fluorometry. The Sm_2Co_{17} sludge contains some additives (Fe, Cu, and Zr) and also the $Nd_2Fe_{14}B$ (Dy, Co, Al, Nb, and Mo) in order to improve magnetic properties. These scraps were oxidized to a certain degree since these contain metallic R, Fe, and Ni which are easily oxidized in the presence of oxygen or water. Abundances of the oxides in the scraps were 18% (Sm_2Co_{17} sludge), 35% ($Nd_2Fe_{14}B$ sludge), and 28% ($LaNi_5$ alloy). (In the case of Sm_2Co_{17} scrap, for example, 29.0 mg of the dried sludge was weighed and analyzed for the contents of five component metals, *i.e.* Sm, Co, Fe, Cu, and Zr. If these component metals had been fully oxidized with the most usual oxidation numbers, Sm_2O_3, Co_2O_3, Fe_2O_3, CuO, and ZrO_2, in the raw sludge, then the sum of the masses of these oxides corresponding to the determined molar quantities would be 36.7 mg. On the contrary, if all of the components had been wholly metallic, then the sum would be 27.3 mg. Therefore the abundance of the oxides in the Sm_2Co_{17} sludge was calculated as 18%, the ratio of 29.0 mg – 27.3 mg to 36.7 mg – 27.3 mg.)

The fly ash used for this work was produced during a combustion test by The Kansai Electric Power Co., Inc. The fly ash is ocherous powder, containing metal elements: V (3.5%), Ni (1.4%), Mg (7.2%), Al (1.6%), and Fe (0.73%). According to a powder diffraction analysis, the fly ash contains vanadium, nickel, and magnesium as $VOSO_4 \cdot 3H_2O$, $(NH_4)_2Ni(SO_4)_2 \cdot 6H_2O$, and $(NH_4)_2Mg(SO_4)_2 \cdot 4H_2O$, respectively [38].

Table 4.1. Composition (wt%) of scrap of rare earth intermetallic compounds used for raw materials for the chemical vapor transport reaction

Raw material	La	Nd	Sm	Dy	Fe	Co	Ni	Cu	Zr	Al	B	Nb, Mo
Sm_2Co_{17} sludge	–	–	22	–	15	51	–	5.2	1.8	–	–	–
$Nd_2Fe_{14}B$ sludge	–	26	–	2.2	56	3.3	–	–	–	1.0	1.0	trace
mixture[a]	–	13	11	1.1	36	27	–	2.6	0.9	0.5	0.5	trace
$LaNi_5$ powder	30	–	–	–	–	–	64	–	–	–	–	–

[a] Mixture of Sm_2Co_{17} sludge and $Nd_2Fe_{14}B$ sludge.

Operation. Details of the apparatus employed for the CVT reaction have been reported in Chapter 1.

Aluminium chloride (10.0 g), the complex former, was sealed in a Pyrex glass ampule (inner diameter, 14 mm; length, 10 cm) and loaded into furnace A. The ampule has a small orifice (diameter, 0.3–0.5 mm) in order to generate gaseous aluminium chloride slowly when furnace A is heated. The scrap or the fly ash was weighed, put on a small carbon or alumina boat (length, *ca* 8 cm), and placed at the summit of the temperature gradient in furnace B; the temperature was *ca* 1050 °C for the scraps and 300–600 °C for the fly ash. A mixed N_2 and Cl_2 gases (N_2, 30 cm^3 min^{-1}; Cl_2, 5 cm^3 min^{-1}) was flowed through the reactor as a carrier gas and a chlorinating agent, respectively. After the desired temperature gradient was attained by operating furnace B, furnace A was heated over the temperature range 80–200 °C in order to generate the gaseous aluminium chloride, $Al_2Cl_6(g)$, the complex former.

The scrap or the fly ash on the boat was heated and directly chlorinated by Cl_2 gas. The resulting metal chloride mixture vaporizes according to a simple sublimation,

$$n\,MCl_x(s, l) = M_nCl_{nx}(g), \qquad (4.1)$$

or vapor complexation with the $Al_2Cl_6(g)$ introduced from furnace A to B by the carrier gas,

$$MCl_x(s, l) + m/2\,Al_2Cl_6(g) = MAl_mCl_{x+3m}(g). \qquad (4.2)$$

(In practice, although a part of the $Al_2Cl_6(g)$ is decomposed into monomeric $AlCl_3(g)$ at high temperatures [39], the gaseous aluminium chloride in the present thesis is described as $Al_2Cl_6(g)$ for the sake of convenience.) The resulting gas phase species were driven with the carrier gas along the temperature gradient and the metal chlorides (MCl_x) were deposited at different places in the reactor tube corresponding to the sublimation and decomposition temperatures of the reverse reaction of eqs. 4.1 and 4.2, respectively.

After the CVT reaction had lasted for 6 h (the scraps) or for 1.5–12 h (the fly ash), the deposits were collected by removing the 13 pieces of inner tubing. The deposits were then dissolved individually into deionized water to determine the compositions of metal chlorides for every portion (*FN*, fraction number) with a wavelength dispersive type of X-ray fluorescent spectrometer (Rigaku System 3270A) using Zn^{2+} as an internal standard substance. When the sludge of $Nd_2Fe_{14}B$ was used as raw material, the boron content of every fraction was determined with an atomic absorption spectrometer (Nippon Jarrel-Ash AA-8500 mark II) using the absolute calibration method.

4.3. Results and Discussion

4.3.1. Recovery from Sm_2Co_{17} Sludge

Transport Conditions. Among the five metal chlorides produced by chlorination of the Sm_2Co_{17} sludge, $SmCl_3$ is most difficult to transport chemically owing to the low volatility of rare earth chlorides. The CVT reactions under various conditions were tested using the Sm_2Co_{17} sludge (1.0 g) as a raw material. Six conditions attempted are listed in Table 4.2. The transported amounts of $SmCl_3$ under these conditions were compared in terms of boat materials, a chlorinating agent, and a complex former. Reaction time was kept at 6 h for all runs.

First, an alumina boat was utilized to load the sludge. Under condition (i), without using any complex former, the total amount of transported $SmCl_3$ portion was quite small, while most other metal chlorides were effectively extracted. On the contrary, under condition (iii), using $AlCl_3$ as the complex former, the amount of transported $SmCl_3$ was increased by a factor of 30 (4.0×10^{-4} mol). This demonstrates the effectiveness of using $AlCl_3$ as the complex former for the CVT of non-volatile $SmCl_3$.

The CVT reaction under condition (i) produced white residue on the alumina boat, which was analyzed by means of powder X-ray diffraction. The obtained diffraction pattern coincided with the diffraction pattern for SmOCl [40]. This suggests either that samarium species (Sm and Sm_2O_3) in the sludge are not fully chlorinated into $SmCl_3$ but into SmOCl in the presence of Cl_2 gas, *i.e.*

Table 4.2. Amount of transported $SmCl_3$ under various reaction conditions

Transport condition	Boat material	Chlorinating agent	Complex former	Transported amount (10^{-4} mol)
(i)	alumina	Cl_2	–	0.13
(ii)	alumina	–	$AlCl_3$[a]	1.8
(iii)	alumina	Cl_2	$AlCl_3$	4.0
(iv)	carbon	Cl_2	–	2.0
(v)	carbon	Cl_2	$AlCl_3$	5.6
(vi)	alumina[b]	Cl_2	$AlCl_3$	4.2

[a] Aluminium chloride also acts as chlorinating agent; see text.

[b] Active carbon powder (0.20 g) was added to the raw material.

$$2\ Sm_2O_3(s) + 2\ Sm(s) + 3\ Cl_2(g) \rightarrow 6\ SmOCl(s) \qquad (4.3)$$

or that, even if chlorinated into $SmCl_3$, the $SmCl_3$ immediately reacts with Al_2O_3, the boat material, and forms SmOCl:

$$SmCl_3(s, l) + Al_2O_3(s) \rightarrow SmOCl(s) + 2\ AlOCl(s) \qquad (4.4)$$

although X-ray diffraction pattern did not show the existence of AlOCl. On the contrary, SmOCl can react with $Al_2Cl_6(g)$ to directly form the vapor complex without the formation of $SmCl_3$ as an intermediate, *i.e.*

$$2\ SmOCl(s) + (n+1)\ Al_2Cl_6(g) \rightarrow 2\ SmAl_nCl_{3+3n}(g) + 2\ AlOCl(s) \qquad (4.5)$$

and, hence, the transported reaction took place under condition (iii). In this case, therefore, the $Al_2Cl_6(g)$ functions also as chlorinating agent. This is supported by the fact that the transport reaction more or less takes place under condition (ii), in the absence of Cl_2 gas flow.

In conclusion, the increase in the amount of transported $SmCl_3$ portion was attributed not only to a volatility enhancement due to the vapor complexation with $Al_2Cl_6(g)$ but also to effective chlorination of SmOCl by the $Al_2Cl_6(g)$. Halogenation by gaseous aluminium halides is applied to the preparation of anhydrous metal halides from corresponding oxides on a laboratory scale [8, 9]. For example, the chlorination of R_2O_3 is expressed as

$$2\ R_2O_3(s) + 3\ Al_2Cl_6(g) \rightarrow 4\ RCl_3(s) + 6\ AlOCl(s) \qquad (4.6)$$

and

$$R_2O_3(s) + Al_2Cl_6(g) \rightarrow 2\ RCl_3(s) + Al_2O_3(s). \qquad (4.7)$$

According to eqs. 4.5–4.7 the $Al_2Cl_6(g)$ which acts as a chlorinating agent is converted to AlOCl or Al_2O_3. The formation of these inert substances against vapor complexation reduces the effective amount of $Al_2Cl_6(g)$ as a complex former. In order to depress the formation of SmOCl and the consumption of $Al_2Cl_6(g)$ as chlorinating agent, a carbon boat was used instead of that of alumina. The carbon boat which itself acts as a deoxidant *via* the reactions

$$Sm_2O_3(s) + 3\ C(s) + 3\ Cl_2(g) \rightarrow 2\ SmCl_3(s, l) + 3\ CO(g) \qquad (4.8)$$

and

$$SmOCl(s) + C(s) + Cl_2(g) \rightarrow SmCl_3(s, l) + CO(g) \qquad (4.9)$$

promotes the chlorination of Sm_2O_3 (or SmOCl) by Cl_2. In this case, carbon monoxide (CO),

carbon tetrachloride (CCl_4), or thionyl chloride ($SOCl_2$) indeed seem to be effective deoxidizing agents in attacking oxide and oxychloride, but these are not suitable in view of economy. The carbon boat is gradually corroded away according to eqs. 4.8 and 4.9 with the progress of the CVT reaction. From the industrial aspect, however, the use of an exchangeable reactor made of carbon is economically advantageous rather than the use of expensive materials such as alumina and mullite.

With the carbon boat (condition (v)) the amount of transported $SmCl_3$ portion increased 45 times over the amount transported in condition (i). Furthermore, about 2.0×10^{-4} mol of $SmCl_3$, 15 times as large as that under condition (i), was transported even in the absence of complex former $AlCl_3$ (condition (iv)). On the contrary, addition of active carbon (0.2 g) in the alumina boat instead of using the carbon boat (condition (vi)) is also effective in chlorinating the sludge. These results suggest that the use of the alumina boat reduces the transported amount of $SmCl_3$, owing presumably to the reaction of $SmCl_3$ with Al_2O_3 as eq. 4.4. Based on the results, condition (v) was adopted as the transport condition for further investigation of the recovery characteristics unless otherwise indicated.

Recovery of Samarium and Cobalt. Figure 4.1 shows deposition profiles for transported $SmCl_3$ and $CoCl_2$ portions against the fraction number (*FN*), together with the operated temperature gradient. The amount of $SmCl_3$ deposit peaked at $FN = 3$ (approximate temperature range, 960–1000 °C), while $CoCl_2$ peaked at $FN = 11$ (520–700 °C). The $CoCl_2$ was obtained as anhydrous blue plates.

The CVT reaction lasted for 6 h and the yield of $CoCl_2$ calculated as eq. 3.6 was more than 99.9% whereas that of $SmCl_3$ was 59%. This is attributed to the fact that the formation reaction of vapor complexes RAl_nCl_{3+3n} is generally slow to equilibrate [14]. Figure 4.1(c) shows the profiles of purities of $SmCl_3$ and $CoCl_2$ represented in mole percent against the sum of the molar quantities of deposited elements, *i.e.* Sm, Co, Fe, Cu, and Zr. The chlorides $SmCl_3$ and $CoCl_2$ were concentrated up to 99.5 mol% and 99.1 mol% at $FN = 3$ and $FN = 11$, respectively.

Since the sublimation temperature of $CoCl_2$ is relatively low at about 500 °C, the $CoCl_2$ formed by the chlorination of the sludge was transported and condensed at $FN = 11$ even without the complex former, $AlCl_3$ (condition (iv)). Under this condition, however, a contamination with $CuCl_2$ (or CuCl) was significant for $FN = 11$; the purity of $CoCl_2$ ($FN = 11$) was lowered at 98.4 mol%. Consequently, the transport condition (v) is also suitable for the recovery of $CoCl_2$ as well as the case of $SmCl_3$.

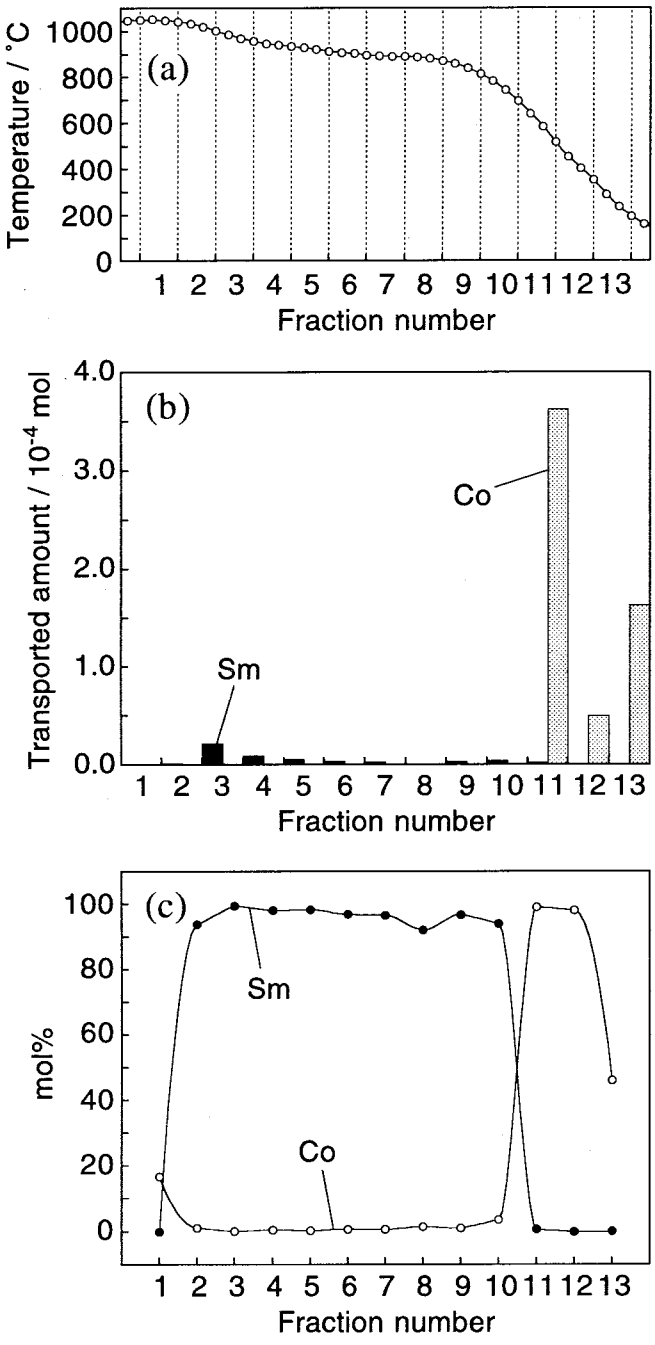

Figure 4.1. (a) Temperature gradient and distribution of $SmCl_3$ and $CoCl_2$ deposits represented (b) in moles and (c) in mole percent. Raw material was dried Sm_2Co_{17} sludge (1.0 g) containing Fe, Cu, and Zr as additives; complex former was $AlCl_3$ (10.0 g); mixed N_2 and Cl_2 gases (N_2, 30 cm^3 min^{-1}; Cl_2, 5 cm^3 min^{-1}) was flowed as carrier; reaction time was 6 h.

Deposition of Other Metal Chlorides. The vapor pressure of iron chloride or its complex with $AlCl_3$ is high below 350 °C. Therefore, 99.4% of transported iron chloride ($FeCl_3$ or $FeCl_2$) was condensed at $FN = 13$ as well as $AlCl_3$, and was not contaminated with recovered $SmCl_3$ and $CoCl_2$. Copper chloride ($CuCl_2$ or CuCl) was also condensed at $FN = 13$ under condition (v). However, as mentioned above, copper chloride was most concentrated at $FN = 10$ (700–815 °C) owing to the low volatility of copper chloride itself under condition (iv). Zirconium chloride ($ZrCl_4$) was condensed at $FN = 13$ under any transport condition at the sublimation temperature of 331 °C.

4.3.2. Recovery from $Nd_2Fe_{14}B$ Sludge

Recovery of Neodymium and Dysprosium. Figure 4.2 shows deposition profiles for an RCl_3 mixture (R = Nd, Dy) and $FeCl_3$ (or $FeCl_2$). The temperature gradient operated was the same as in Fig. 4.1(a). The recovered amounts of rare earths were maximized at $FN = 3$. The purity of rare earth chloride mixture in this fraction was 98.4 mol%. Although $NdCl_3$ and $DyCl_3$ were recovered as the mixture, the mole ratio of Nd/Dy at each fraction increased with increase in its temperature range (see Fig. 4.2(b)). In other words, $NdCl_3$ is more concentrated in the fractions of higher temperatures. This is because the volatility of RAl_nCl_{3+3n} complexes with smaller rare earth ions was generally larger than those with larger rare earth ions (see Chapter 1) and, hence, the heavier rare earth chlorides, $DyCl_3$ in this case, tend to deposit at low temperature fractions. Application of a multiple CVT reaction employed for mutual separation of the $PrCl_3$-$SmCl_3$ binary system (Section 1.3.3) may make it possible to improve the purity of recovered $NdCl_3$. Alternatively, if the recovered rare earths are used for the processing of the same material ($Nd_2Fe_{14}B$ in this case), the mutual separation of $NdCl_3$ and $DyCl_3$ may not be required.

Under transport condition (v) the yields of $NdCl_3$ and $DyCl_3$ were 39% and 68%, respectively, while under condition (iv) they were 34% and 59%. It is worth noting that the difference in the amount between the two conditions was smaller than the difference for transported $SmCl_3$ when Sm_2Co_{17} sludge was used as raw material: 28% under condition (iv) and 59% under condition (v). This means that the $FeCl_3$ formed by chlorination of $Nd_2Fe_{14}B$ sludge also acts as a complex former and that the rare earth chlorides are effectively transported in the absence of $AlCl_3$. However, purity of recovered rare earths was not so good, 91.1 mol% ($FN = 1$) at the most, without $AlCl_3$.

Deposition of Other Metal Chlorides. More than 99.9% of $FeCl_3$ (or $FeCl_2$) and $AlCl_3$ were deposited at $FN = 13$. Further, $CoCl_2$ was also condensed at $FN = 13$ for the most part (98.9%)

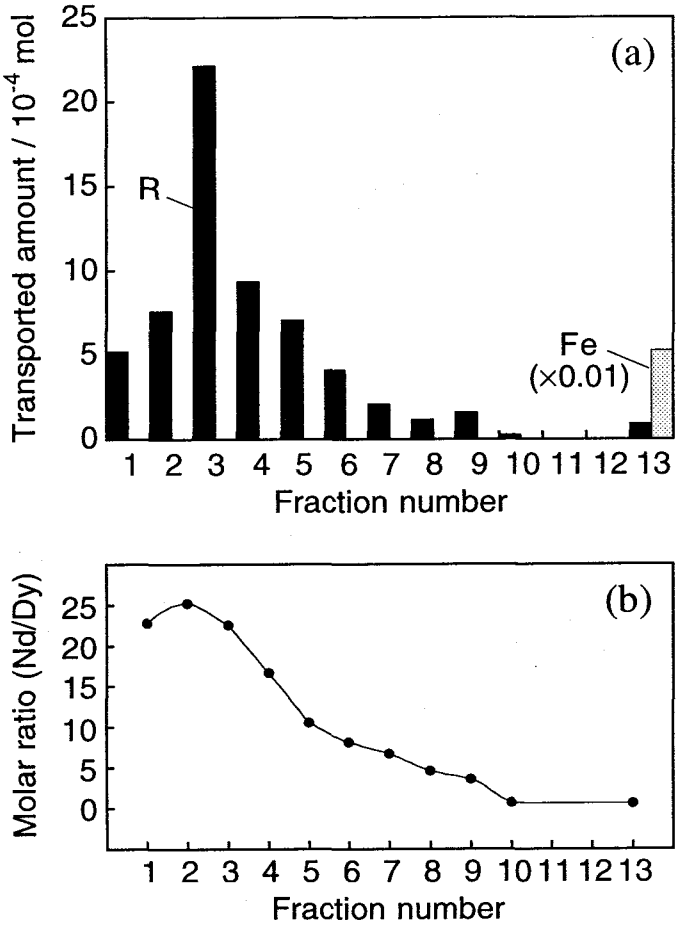

Figure 4.2. (a) Distribution of RCl_3 mixture (R = Nd and Dy) and $FeCl_3$ deposits and (b) relationship between molar ratio Nd/Dy and fraction number. Raw material was dried $Nd_2Fe_{14}B$ sludge (1.0 g) containing Co, Al, Nb, and Mo as additives; complex former, carrier gas, and reaction time were as in Fig. 4.1.

while $CoCl_2$ was recovered in high purity at $FN = 11$ when Sm_2Co_{17} sludge was used as raw material. This difference is attributed to the "recrystallization effect" mentioned below.

The chlorides of boron and niobium were selectively deposited at $FN = 13$. Molybdenum was not detected from any fractions because the content in the sludge was quite small. However, the molybdenum should also deposit at $FN = 13$ as chloride considering the fact that the gaseous complexation between $MoCl_5$ and $AlCl_3$ does not occur [3a, 41] and that the boiling point of $MoCl_5$ is low at 268 °C.

4.3.3. Recovery of Rare Earths from a Mixed Sludge

Sludge is not always in a "pure" state, which is produced in the shaping process of a single

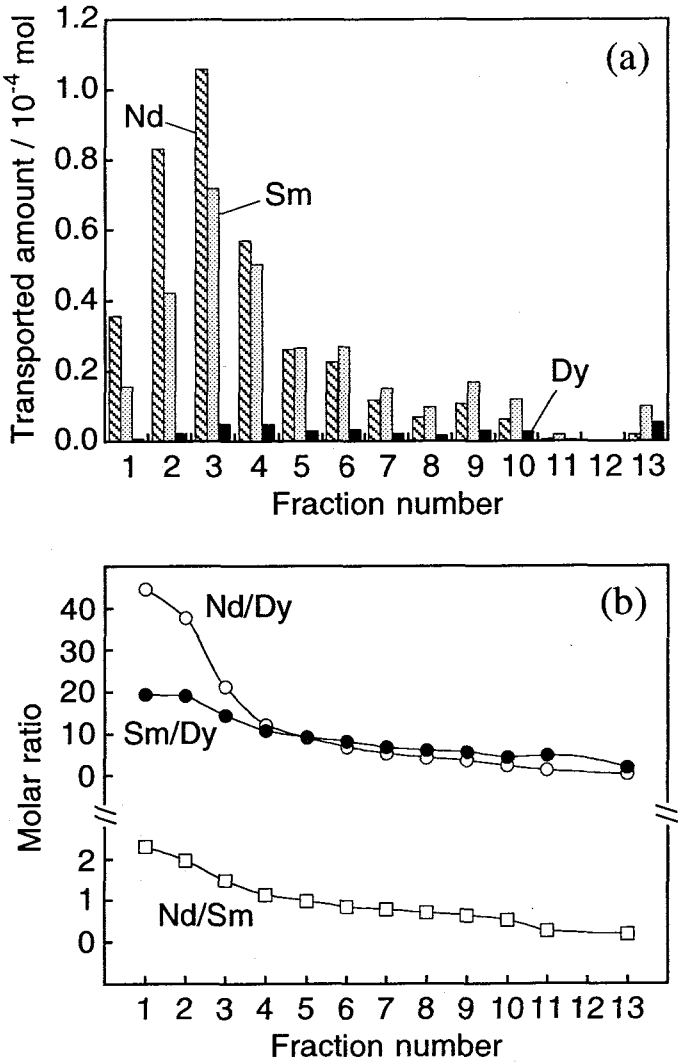

Figure 4.3. (a) Distribution of $NdCl_3$, $SmCl_3$, and $DyCl_3$ deposits and (b) relationship between mole ratios Nd/Dy, Sm/Dy, and Nd/Sm and fraction number. Raw material was mixture of dried Sm_2Co_{17} sludge (0.50 g) and $Nd_2Fe_{14}B$ sludge (0.50 g) containing some additives as in Table 4.1; complex former, carrier gas, and reaction time were as in Fig. 4.1.

material. It is probable that many kinds of sludge produced from various materials are mixed together. In order to demonstrate the recovery from sludge in an "impure" state, the CVT reaction of a 1/1 mixed sludge of Sm_2Co_{17} (0.50 g) and $Nd_2Fe_{14}B$ (0.50 g) was demonstrated.

Figure 4.3 shows the deposition profiles of $NdCl_3$, $SmCl_3$, and $DyCl_3$ along the temperature gradient together with mole ratios of Nd/Sm, Sm/Dy, and Nd/Dy, that is the ratios of lighter and heavier rare earth element. Although the rare earth chlorides were recovered as a mixture by only one CVT operation, lighter elements of each pair were always concentrated in the fractions of the

high temperature zone just as observed in the recovery from $Nd_2Fe_{14}B$ sludge. The slope of the molar ratio curves decreased in the order Nd/Dy > Sm/Dy > Nd/Sm. This indicates that the rare earth pairs for which atomic numbers are close to each other are difficult to separate mutually.

Deposition profiles of other metal chlorides were similar to the case of Sm_2Co_{17} or $Nd_2Fe_{14}B$ sludge treated independently as the raw material.

4.3.4. Deposition Temperature of $CoCl_2$ — a "Recrystallization Effect"

When Sm_2Co_{17} sludge was transported under condition (v), 63% of total transported $CoCl_2$ was recovered from $FN = 11$ (520–700 °C) in high purity. However, when $Nd_2Fe_{14}B$ sludge, which contains a small amount of cobalt as an additive (see Table 4.1), was transported under the same condition, 98% of the $CoCl_2$ was selectively deposited at $FN = 13$ (below 350 °C). This difference in deposition temperature of $CoCl_2$ is interpreted as follows. The $CoCl_2$, whose volatility is higher than those of RCl_3, is vaporized according to a simple sublimation process expressed as eq. 4.1. On the contrary, $CoCl_2$ is known to form more volatile vapor complexes with $Al_2Cl_6(g)$ [3a] as

$$CoCl_2(s, l, g) + n/2\ Al_2Cl_6(g) = CoAl_nCl_{2+3n}(g). \quad (n = 1\text{–}3) \qquad (4.10)$$

At the temperatures around $FN = 11$, partial pressure of $CoAl_nCl_{2+3n}(g)$ complexes is larger than that of free $Co_nCl_{2n}(g)$ in the presence of excess amount of complex forming $Al_2Cl_6(g)$. When the Sm_2Co_{17} sludge was used as the raw material of the CVT reaction, cobalt species in the boat are in excess against the complex former. Therefore, a large portion of cobalt species is transported *via* $Co_nCl_{2n}(g)$ and $CoCl_2(s)$ deposits at $FN = 11$ corresponding to the sublimation temperature of $CoCl_2$, *ca* 500 °C. However, when $Nd_2Fe_{14}B$ is the raw material, the situation is reversed and the complex

Table 4.3. Amount of deposit of $CoCl_2$ at $FN = 11$ (700–520 °C) and 13 (below 350 °C)

Raw material (1.0 g)	Chlorinating agent	Complex former	Condensed amounts (10^{-5} mol)	
			$FN = 11$	$FN = 13$
Sm_2Co_{17} sludge	Cl_2	–	479	5.42
Sm_2Co_{17} sludge	Cl_2	$AlCl_3$	362	163
mixture[a]	Cl_2	–	19.2	186
$Nd_2Fe_{14}B$ sludge	Cl_2	$AlCl_3$	2.44	9.05
$Nd_2Fe_{14}B$ sludge	Cl_2	$AlCl_3$	0.02	28.1

[a] Mixture of Sm_2Co_{17} sludge and $Nd_2Fe_{14}B$ sludge.

former is in excess, since the content of cobalt as one of the additives in the sludge is small (3.3 wt%; see Table 4.1). Hence, the majority of cobalt vapor species, $Co_nCl_{2n}(g)$, which volatilize from the raw material, react with $Al_2Cl_6(g)$ vapor during the transportation by the carrier gas to form the stable vapor complex $CoAl_nCl_{2+3n}(g)$ and, finally, deposit at $FN = 13$. In this case in particular the proportion of the condensed amount of $CoCl_2$ at $FN = 13$ to the total transported amount was quite high (98%) since $FeCl_3$ also acts as a complex former as mentioned above.

Table 4.3 summarizes amounts of $CoCl_2(s)$ deposited at $FN = 11$ and 13 under various CVT reactions for 6 h. Total amount of complex former ($AlCl_3$ and $FeCl_3$) increases with the order (up to down) in Table 4.3. The proportion of $CoCl_2$ deposited at $FN = 13$ is increased in the same order. When Sm_2Co_{17} sludge was transported under condition (iv), for example, which is the reaction where there are scarcely any compounds acting as a complex former, the deposition at $FN = 13$ hardly took place.

We can compare this operation of removing the impurity, cobalt in this case, from rare earth by the vapor complexation with a complex former with a purification technique by means of recrystallization. The former technique is based on a gas-solid equilibrium, the latter on a liquid-solid equilibrium. If one looks on the gaseous $AlCl_3$ (or $FeCl_3$) as a "solvent" for the recrystallization technique, the formation of vapor complexes and the transportation along a temperature gradient correspond to the dissolution of a solute in a heated solvent and cooling the solution, respectively, because both techniques take advantage of difference in affinity between plural chemical species: the former is between metal chlorides and a complex former and the latter solutes and a solvent.

4.3.5. Recovery of Lanthanum and Nickel from $LaNi_5$ Scrap

When a powder of $LaNi_5$ alloy (0.50 g) was used as a raw material for the CVT reaction under condition (v), recovery of the two rare elements, La and Ni, was also effectively performed. As shown in Fig. 4.4, they were obtained as anhydrous chlorides and provided deposition profiles with peaks at $FN = 3$ and $FN = 11$. Purities of the chlorides were more than 99.9 mol% in these fractions.

However, the yield of $LaCl_3$ (27%) after reaction for 6 h is lower than that for $NdCl_3$ (39%), $SmCl_3$ (59%) and $DyCl_3$ (68%) when Sm_2Co_{17} or $Nd_2Fe_{14}B$ were used as raw because the vapor complex $LaAl_nCl_{3+3n}(g)$ containing the largest ionic radius element, lanthanum, among rare earths is the most difficult to form (see Section 1.3.2).

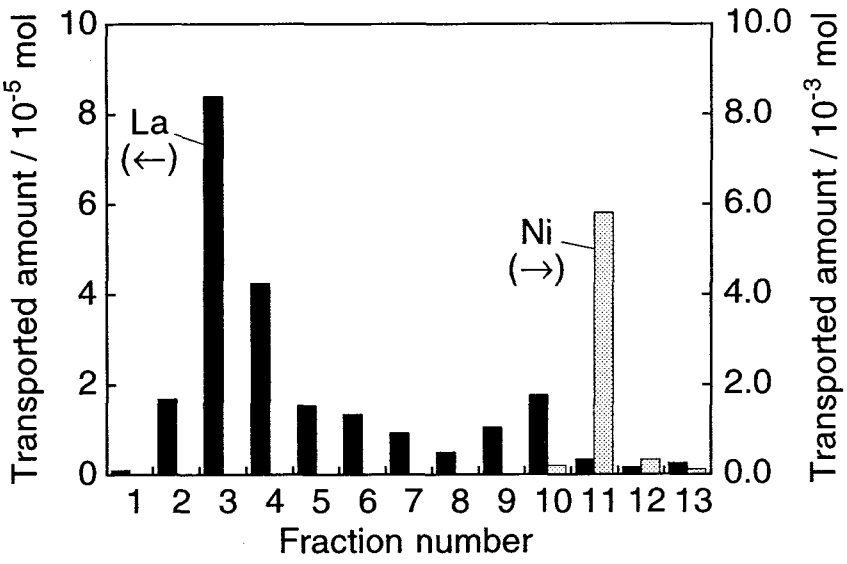

Figure 4.4. Distribution of $LaCl_3$ and $NiCl_2$ deposits. Raw material was ground $LaNi_5$ alloy (0.50 g); complex former, carrier gas, and reaction time were as in Fig. 4.1.

4.3.6. Recovery of Rare Metals from a Fly Ash of Bitumen-in-Water Emulsion

Recovery of Vanadium by Chlorination. On chlorination the fly ash above 500 °C, the vanadium component was extracted thoroughly and condensed in $FN = 13$ (*ca* 80 °C) without using the complex former, $Al_2Cl_6(g)$. The chlorination of vanadium in the ash presumably gives low boiling compounds, VCl_4 (b.p. 149 °C) and/or VCl_3O (b.p. 127 °C), since other vanadium chlorides or oxychlorides are non-volatile or not stable in the temperature range of < 600 °C. Table 4.4 shows the yield of vanadium under several reaction conditions. The vanadium was extracted almost completely above 500 °C within 6 h. However, the chlorination at 600 °C brought the vanadium contaminated by iron chloride ($FeCl_3$) which also deposited around $FN = 13$. On the other

Table 4.4. Yield (%) of vanadium when fly ash of bitumen-in-water emulsion was treated with Cl_2 gas

Reaction temperature (°C)	Yield after reaction for			
	1.5 h	3 h	6 h	12 h
600	94	~100	~100	~100
500	–	92	~100	~100
400	–	–	78	~100
300	–	–	–	12

hand, high purity vanadium chloride (or oxychloride) was obtained when chlorinated at 500 °C, since $FeCl_3$ did not evaporate in this temperature.

Recovery of Nickel and Magnesium via Vapor Complexes. Though nickel and magnesium in the ash were chlorinated, the yields of these metal chlorides were low without using the $Al_2Cl_6(g)$, because the chlorides of nickel and magnesium are less volatile than vanadium chloride (or oxychloride). Only 27% and < 0.1% of $NiCl_2$ and $MgCl_2$ were extracted, respectively, when the ash was treated with Cl_2 gas at 600 °C for 12 h. In this case, however, the use of $Al_2Cl_6(g)$ improved the yield of these chlorides, since the $Al_2Cl_6(g)$ reacts with the chlorides providing the volatile complexes, $NiAl_2Cl_8(g)$ [42] and $MgAl_2Cl_8(g)$ [43]. The yield of nickel and magnesium increases with the increase of reaction temperature and time as summarized in Table 4.5. It is noteworthy that the yield of $MgCl_2$ becomes larger than that of $NiCl_2$ when the $Al_2Cl_6(g)$ is used, suggesting that the effect of vapor complexation on transport reaction is more pronounced for $MgCl_2$ than that for $NiCl_2$. This is in accordance with the Dewing's results on the volatility of divalent chlorides in the presence of $AlCl_3$ [43], where $MgAl_2Cl_8(g)$ is more volatile than $NiAl_2Cl_8(g)$ at the same temperature and the pressure of $Al_2Cl_6(g)$.

Figure 4.5 shows the deposition profile of nickel, magnesium, and vanadium chlorides together with the temperature gradient in Furnace B. When a linear (16 °C cm^{-1}) temperature gradient (see Fig. 4.5(a)) was used, the deposition profile of the $NiCl_2$ (*FN* = 6–9, 400–210 °C) was overlapped with that of $MgCl_2$ (*FN* = 6–11, 400–170 °C). Consequently, the purity of recovered $NiCl_2$ was 6.5% even by the treatment at 600 °C for 12 h. However, a slight difference between the temperatures of two deposition maxima, *i.e. ca* 400 °C for $NiCl_2$ and *ca* 360 °C for $MgCl_2$, suggests

Table 4.5. Yield of extracted metal elements when fly ash of bitumen-in-water emulsion was treated with Cl_2 and $AlCl_3$

Reaction temperature (°C)	Reaction time (h)	Yield (%)		
		V	Ni	Mg
600	12	~100	67	91
600[a]	12	~100	27	< 0.1
600	6	~100	42	61
500	12	~100	50	79
400	12	97	< 0.1	11

[a] Without using complex former $AlCl_3$.

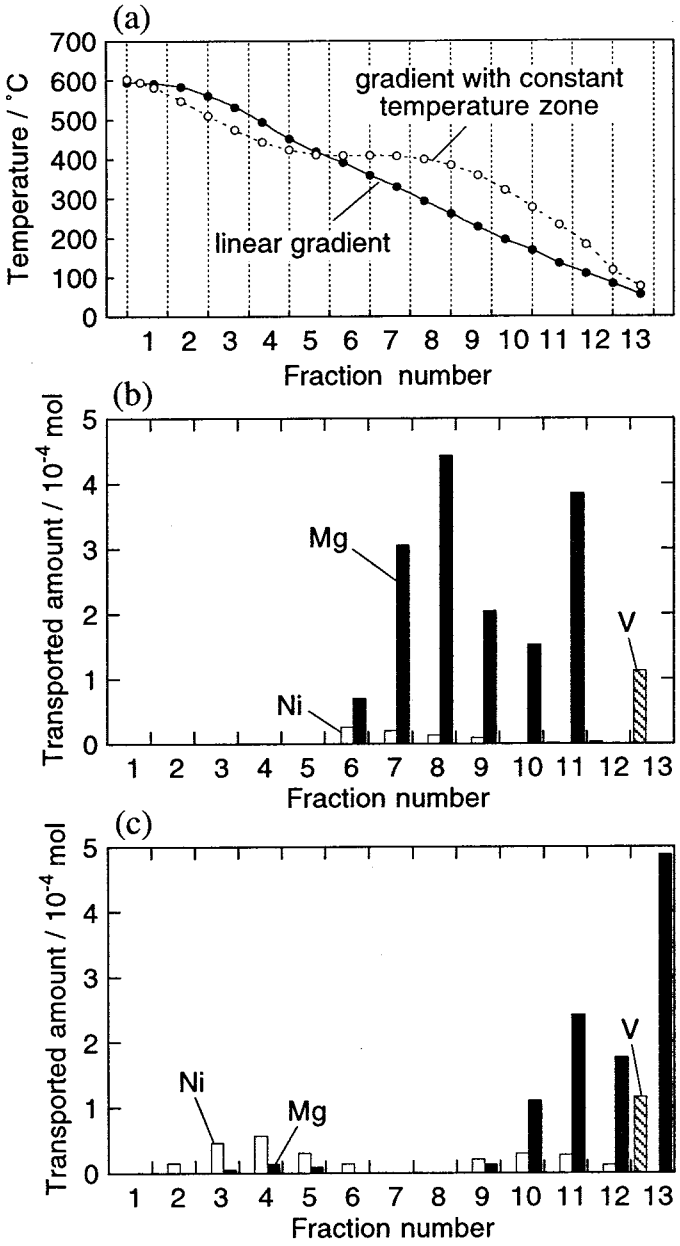

Figure 4.5. (a) Two types of temperature gradient and distribution of nickel, magnesium, and vanadium chlorides (oxichlorides) when transported along (b) linear and (c) stepwise temperature gradients. Raw material was fly ash of bitumen-in-water emulsion (0.50 g); complex former was $AlCl_3$ (10.0 g); mixed N_2 and Cl_2 gases (N_2, 30 cm^3 min^{-1}; Cl_2, 5 cm^3 min^{-1}) was flowed as carrier; reaction time was 12 h.

that the mutual separation of the $NiCl_2$ and $MgCl_2$ is possible by employing a temperature gradient with a constant temperature zone around these temperatures. The deposition profile along the temperature gradient with the constant temperature zone of 410 °C (see Fig. 4.5(a)) is shown in Fig.

4.5(c). Under this reaction condition no deposition of the chlorides was observed around the constant temperature zone (*FN* = 7, 8) and, hence, the whole deposits can be divided into two parts: Ni-rich portion (*FN* = 2–6) and Mg-rich portion (*FN* = 9–13). Although the yield of $NiCl_2$ was lowered (46%), the purity of $NiCl_2$ in the Ni-rich portion was nevertheless improved to 78%.

When the Al_2Cl_6(g) was used, $MgCl_2$, $FeCl_3$, and $AlCl_3$ (the complex former) also deposited at *FN* = 13 and, therefore, the recovered vanadium has a low purity. Consequently, the simple chlorination by Cl_2 seems to be appropriate as for the vanadium recovery from the ash. To conclude above, the most appropriate flowsheet for recovering the vanadium, nickel, and magnesium from the fly ash is: (i) chlorination of the fly ash by Cl_2 gas at 500 °C to obtain vanadium from the fraction at *ca* 80 °C; (ii) heating the residual mixture at 600 °C to remove the $FeCl_3$; (iii) introduction of the Al_2Cl_6 gas to transport the $NiCl_2$ and $MgCl_2$ by the CVT reaction along the temperature gradient with the constant temperature region at 410 °C. The reaction time of each reaction (i)–(iii) depends on the quantity of the fly ash treated.

4.4. Conclusions

The recovery of rare metals was conducted effectively using the CVT process mediated by vapor complexes in metal halide systems. Rare earths, cobalt and nickel of almost 100% purity, were obtained from Sm_2Co_{17}, $Nd_2Fe_{14}B$, and $LaNi_5$ scraps through only one process. The obtained anhydrous rare earth chlorides can be converted directly to corresponding rare earth metals again, which are recycled to use for further processing of rare earth intermetallic compounds.

On the other hand, the recovery of nickel and vanadium in a fly ash of bitumen-in-water emulsion, as a new fuel, was also successfully carried out. Vanadium component in the fly ash was thoroughly recovered by chlorination at 500 °C within 6 h, whereas nickel and magnesium were extracted *via* vapor complexes with $AlCl_3$ at 600 °C.

Chapter 5

Vapor Pressure and Structure of the RCl_3-KCl Vapor Complex

— a High Temperature Mass Spectroscopic Study of the Vapor over the RCl_3-KCl Equimolar Melt (R = Nd, Er) —

5.1. Introduction

Various kinds of metal halides form halogen-bridged vapor complexes with other volatile halides such as aluminium, iron, and alkali halides [1–7]. The vapor complexes of the rare earth halides with alkali halides have been well investigated for the iodide systems, because the iodide systems are important for high intensity metal halide lamps; some lamps using the ScI_3-NaI and DyI_3-NdI_3-CsI mixtures have already been manufactured commercially. Recently, the iodide systems have been systematically investigated by means of Knudsen effusion mass spectrometry [1, 44]. On the other hand, though volatile chloride complexes, $ARCl_4(g)$ (R = rare earths, A = alkali metals), are also known to form [7], study of the chloride complexes using the mass spectroscopy is rather limited [5b, 45]. Vapor complexes of the RCl_3-ACl system have been applied for a high temperature extraction and separation process for rare earths using a chemical vapor transport reaction (see Chapters 1–4).

In the work presented in this chapter, the vapor species over the $NdCl_3$-KCl quasi-binary melt were investigated at high temperatures up to 1273 K, which is a usual operating temperature for the chemical vapor transport of rare earths, by means of the Knudsen effusion mass spectroscopy, and the vapor pressures of the gaseous species were estimated. Furthermore, a qualitative observation of the vapor over the $ErCl_3$-KCl quasi-binary and the $NdCl_3$-$ErCl_3$-KCl quasi-ternary melts was carried out using the method.

5.2. Experimental Details

High purity anhydrous $NdCl_3$ and $ErCl_3$ (Shin-Etsu Chemical Co. Ltd.) were used without any pretreatment. Potassium chloride (Wako Chemical, 99.9%) was dried by heating at 773 K *in vacuo* for 12 h. All chemicals were handled in an argon filled glove box. These chlorides were weighed, well mixed with an agate mortar and a pestle, and loaded in a cylindrical molybdenum

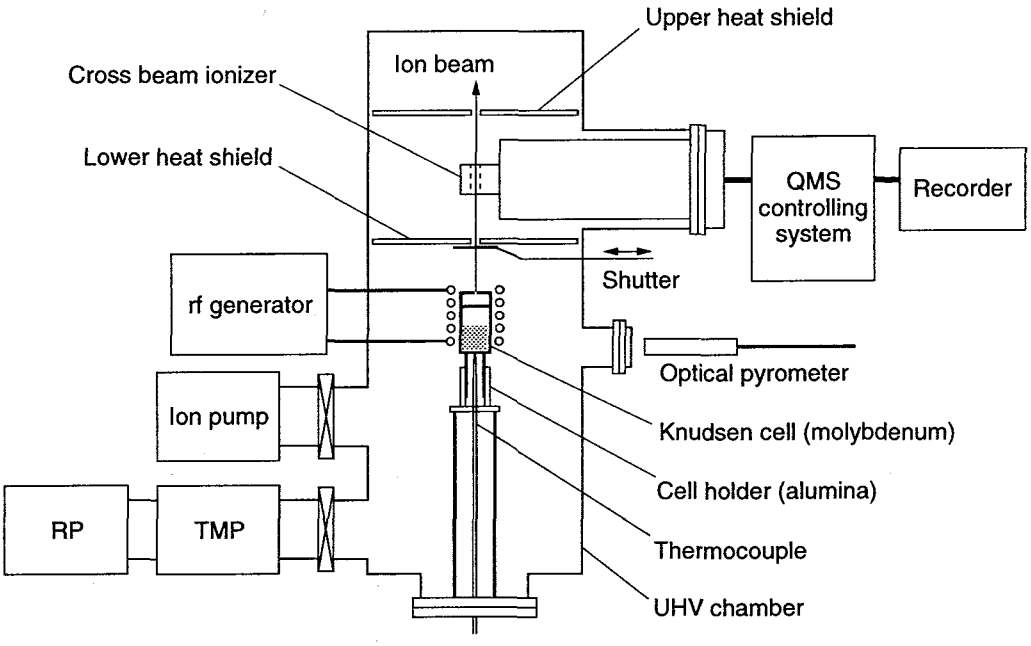

Figure 5.1. Layout of mass spectrometer equipped with Knudsen cell.

Knudsen cell (inner diameter, 10 mm; length, 19 mm) which has an orifice of 0.5 mm diameter.

The apparatus for recording the mass spectra consists of a quadrupole mass spectrometer with a cross-beam ion source and the molybdenum Knudsen cell (see Fig. 5.1). The cell was placed in an ultrahigh vacuum chamber (*ca* 10^{-9}–10^{-10} Torr). The chamber was evacuated by a turbo molecular pump with a rotary pump and baked for two days. An ion pump was then operated to evacuate the chamber; then the cell was heated by an rf generator up to 673 K in order to degas the sample. The temperature of the cell was measured with both a thermocouple and an optical pyrometer.

Gaseous species effusing from the cell were ionized by electron impact at an electron energy of about 15 eV; the energy was calibrated by a known ionization potential of neutral species. A shutter installed between the cell and the ion-source was used to distinguish the effused gas from residual gases. The partial pressure, $p(i)$, of species i at the temperature, T, was determined in a usual manner, based on a relation,

$$p(i) = \sum_j k \frac{I_j(i)T}{\sigma(i)\gamma_j \Delta E_j}, \tag{5.1}$$

where k is the proportionality constant, $I_j(i)$ the intensity of the ions j which were generated from the species i, $\sigma(i)$ the relative ionization cross section, γ_j the multiplier gain of the detector for the

ions j, and ΔE_j the difference between the appearance potential for ions j and the energy of an impacted electron. The ionization cross sections for monomeric species, KCl and $NdCl_3$, were computed by taking the sum of Mann's atomic cross section [46] of the component atoms, while those for complexes, K_2Cl_2 and $KNdCl_4$, were calculated as 0.75 times the sum of those for monomers [47]. The multiplier gain of the detector was obtained from a calibration curve.

The proportionality constant, k, was obtained from the comparison of the $p(KCl)^2/p(K_2Cl_2)$ ratio over pure KCl solid with equilibrium constant for the $K_2Cl_2(g) = 2\ KCl(g)$ reaction obtained from the thermodynamic data [33]:

$$K_p / \text{atm} = p(KCl)^2/p(K_2Cl_2) = 1115708 \exp(-21991T^{-1}). \qquad (5.2)$$

On ionizing at an electron energy of 15.0 eV, the ions K^+, KCl^+, and K_2Cl^+ were observed, whereas $K_2Cl_2^+$ ion was not found. This is explained on the basis of a general rule that $M_mX_{n-1}^+$ ions are formed preferentially with large relative abundances on ionizing metal halides $M_mX_n(g)$ by electron impact [1]. The fact that the appearance potentials obtained by means of extrapolated voltage difference method [48] were 9.0, 8.4, and 9.4 eV for K^+, KCl^+, and K_2Cl^+, suggested that the ion K^+ does not originate from metallic K(g). Both the K^+ and KCl^+ ions were assigned to KCl(g), while K_2Cl^+ was assigned to the $K_2Cl_2(g)$ dimer in analogy with other mass spectrometric studies on the vapor over alkali halide-containing melts [1b]. A mean value of the k from measurements at various temperatures was $(1.72 \pm 0.15) \times 10^{-12}$ atm K^{-1}.

5.3. Results and Discussion

5.3.1. The $NdCl_3$-KCl Binary System

Vapor Species over the $NdCl_3$-KCl Melt. On ionizing at an electron energy of 13.8 eV, five ions: K^+, KCl^+, K_2Cl^+, $NdCl_2^+$, and $KNdCl_3^+$, were observed over the $NdCl_3$-KCl equimolar melt. Table 5.1 lists the intensity of each ion. In this case, molecular ions such as $K_2Cl_2^+$, $NdCl_3^+$, and $KNdCl_4^+$ were not found. The appearance potentials were as follows: 9.0 eV (K^+); 8.4 eV (KCl^+); 9.4 eV (K_2Cl^+); 10.8 eV ($NdCl_2^+$); 10.1 eV ($KNdCl_3^+$). The appearance potential of $KNdCl_3^+$ was almost the same as that of a similar complex ion $NaGdCl_3^+$ (10.1 ± 0.5 eV) reported by Ciach *et al* [25]. Ionization efficiency curves of the five ions did not exhibit any irregular threshold.

Consequently, the KCl^+ ion was considered to originate from KCl(g), while the K_2Cl^+, $NdCl_2^+$, and $KNdCl_3^+$ ions were assigned to K_2Cl_2, $NdCl_3$, and $KNdCl_4$ species, respectively, according to the general rule mentioned above. Based on the rule and the result for pure KCl, it seemed natural

Table 5.1. Ion intensities determined upon investigating the vapor over the $NdCl_3$-KCl equimolar melt

T(K)	I_{K^+}	I_{KCl^+}	I_{K^+}/I_{KCl^+}	$I_{K_2Cl^+}$	$I_{NdCl_2^+}$	$I_{KNdCl_3^+}$
1018	6.0×10^2	2.8×10	22	2.0		
1037	1.0×10^3	4.2×10	25	4.0		
1063	2.0×10^3	7.4×10	26	4.7		
1063	2.1×10^3	7.6×10	27	4.7		
1093	4.0×10^3	1.3×10^2	30	8.6	9.9	
1113	6.7×10^3	2.0×10^2	33	1.4×10	1.2×10	
1143	1.0×10^4	2.8×10^2	35	1.9×10	1.8×10	5.5
1169	1.6×10^4	3.6×10^2	44	2.7×10	2.6×10	1.1×10
1198	2.3×10^4	4.8×10^2	47	3.8×10	3.2×10	1.2×10
1223	3.2×10^4	6.5×10^2	49	5.2×10	3.9×10	1.9×10
1256	4.8×10^4	9.2×10^2	53	7.8×10	5.9×10	2.3×10
1273	5.8×10^4	1.1×10^3	55	8.3×10	8.6×10	2.9×10

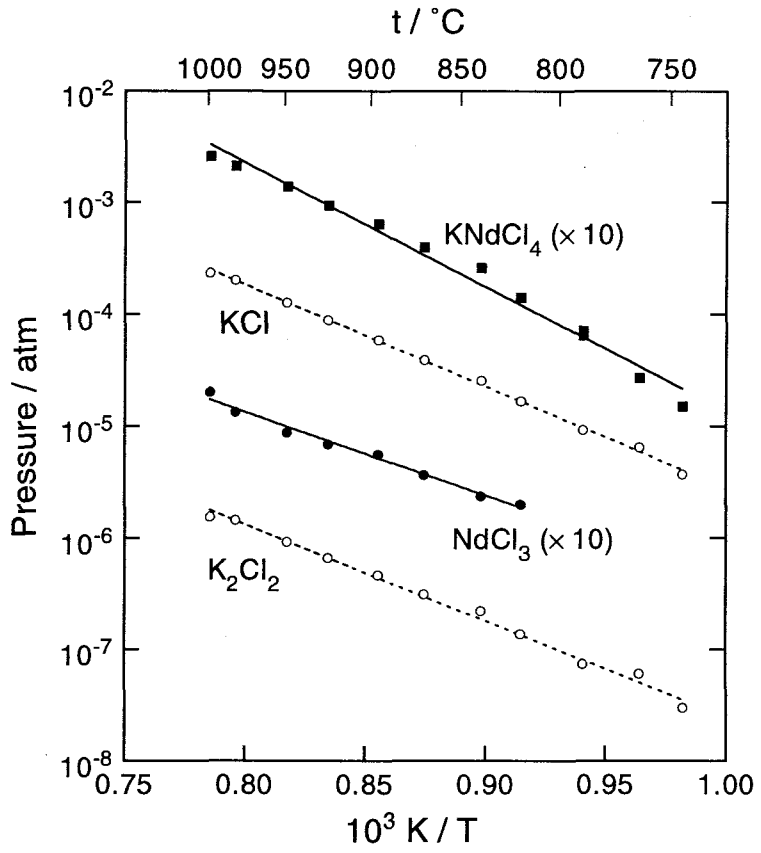

Figure 5.2. Partial pressures of gaseous species over the $NdCl_3$-KCl equimolar melt as a function of the reciprocal temperature.

that the K^+ ion was assigned to KCl. However, the intensity ratio I_{K+}/I_{KCl+} largely increases with the increase of the temperature (see Table 5.1), suggesting K^+ was generated not only from KCl, since the ions originating from the same neutral molecule generally show the same temperature dependencies [1]. Therefore, the K^+ ion was considered to originate also from another K-containing species, $KNdCl_4$.

The intensity of K^+ ion, I_{K+}, in Table 5.1 was divided into that from KCl, $I_{K+}(KCl)$, and that from $KNdCl_4$ complex, $I_{K+}(KNdCl_4)$, in the following manner. First, the $I_{K+}(KCl)$ values were calculated from the intensities of KCl^+ and K_2Cl^+ ions, $I_{KCl+}(KCl)$ and $I_{K_2Cl+}(K_2Cl_2)$, by using eqs. 5.1 and 5.2, assuming that the proportionality constant, k, and the equilibrium constant, K_p, of the reaction $K_2Cl_2(g) = 2\ KCl(g)$ are the same as those obtained for the measurement of pure KCl. Then, resulting $I_{K+}(KCl)$ values were subtracted from I_{K+} values to obtain $I_{K+}(KNdCl_4)$ values: $I_{K+}(KNdCl_4) = I_{K+} - I_{K+}(KCl)$.

The equilibrium partial pressures of KCl(g), $K_2Cl_2(g)$, $NdCl_3(g)$, and $KNdCl_4(g)$ are shown in Fig. 5.2 as a function of reciprocal temperature. The pressures are represented in eqs. 5.3–5.6 for the temperature range between 1018 and 1273 K:

$$\log[p(KCl)/atm] = -(9.09 \pm 0.11) \times 10^3 T^{-1} + (3.53 \pm 0.03), \quad (5.3)$$

$$\log[p(K_2Cl_2)/atm] = -(8.62 \pm 0.23) \times 10^3 T^{-1} + (1.02 \pm 0.05), \quad (5.4)$$

$$\log[p(NdCl_3)/atm] = -(7.45 \pm 0.35) \times 10^3 T^{-1} + (0.09 \pm 0.04), \quad (5.5)$$

$$\log[p(KNdCl_4)/atm] = -(11.1 \pm 0.4) \times 10^3 T^{-1} + (5.21 \pm 0.10). \quad (5.6)$$

The pressures of KCl(g), $NdCl_3(g)$, and $KNdCl_4(g)$ at 1273 K, which is a usual reaction temperature for the rare earth separation process using vapor complex formation (see Chapters 1–4), were 2.5×10^{-4}, 1.7×10^{-6}, and 3.1×10^{-4} atm. This means that the rate of vaporization of K-containing species is almost twice as fast as that of Nd-containing ones, since the pressures of KCl(g) and $KNdCl_4(g)$ are nearly equal to each other. Therefore, composition of the KCl-$NdCl_3$ melt gradually shifts to a $NdCl_3$-rich side during keeping at high temperatures. This phenomenon was observed also during the rare earth separation process using the RCl_3-KCl (R = Pr and Nd; Pr/Nd = 1/1) equimolar mixture as a raw material; here the change of the composition lowered the transport efficiency of RCl_3 (see Section 2.3.2(3)). In other words, the deviation of the melt to a $NdCl_3$-rich side lowers the vapor pressure of $KNdCl_4(g)$.

Since the $NdCl_3$-KCl mixture is expected to be molten completely above *ca* 820 K [49], the $\log p(i)$ *vs* $1/T$ plot should be linear for all vapor species. However, the vapor pressure curve of $KNdCl_4(g)$ displayed slight upward curvature. One reason for such curvature is that the vapor

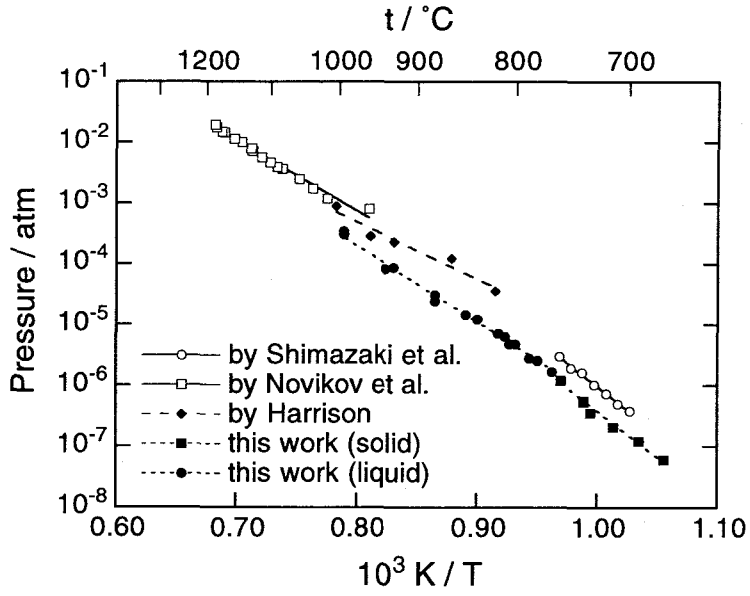

Figure 5.3. Vapor pressure of $NdCl_3(g)$ over pure $NdCl_3$ solid and liquid as a function of the reciprocal temperature.

species in the cell might not be completely equilibrated. In order to attain equilibrium, however, the cell temperature was monitored by both thermocouple and pyrometer and kept constant for about 10 minutes before each measurement. The author did not try to keep the cell temperature for a longer time, because, as mentioned above, the composition of the sample is changing every moment at high temperatures.

Volatility Enhancement of $NdCl_3$ by Forming $KNdCl_4(g)$ Complex. Vapor pressure of $NdCl_3(g)$ over a pure $NdCl_3$ is also measured by the same operations. The pressures over pure $NdCl_3$ solid (947–1030 K) and liquid (1039–1268 K) are represented as follows:

$$\log[p(NdCl_3 \text{ over solid})/\text{atm}] = -(15.2\pm0.6)\times10^3 T^{-1} + (8.79\pm0.05), \qquad (5.7)$$

$$\log[p(NdCl_3 \text{ over liquid})/\text{atm}] = -(12.5\pm0.2)\times10^3 T^{-1} + (6.30\pm0.06). \qquad (5.8)$$

These vapor pressures are the same level as those measured by means of other techniques [23, 50, 51] (see Fig. 5.3).

The overall concentration of the neodymium in the vapor phase over the $NdCl_3$-KCl equimolar melt, that is the sum of the $p(KNdCl_4)$ (eq. 5.6) and $p(NdCl_3)$ (eq. 5.5), was compared with the

vapor pressure of $NdCl_3(g)$ over pure $NdCl_3$ (eqs. 5.7 and 5.8), as shown in Fig. 5.4. Around 1273 K, the concentration of the neodymium over the $NdCl_3$-KCl melt is almost equal to $NdCl_3(g)$ pressure over the pure $NdCl_3$ liquid. Therefore, volatility enhancement of the $NdCl_3$ by the formation of the vapor complex was not so large. On the contrary, the volatility enhancement becomes remarkable at lower temperatures, below the melting point of $NdCl_3$ (*ca* 1030 K). According to the extrapolation of the log $p(i)$ *vs* $1/T$ plots, the volatility enhancement is estimated to be 31 at 823 K, above which the $NdCl_3$-KCl equimolar mixture is completely molten [49]. The phenomenon of the volatility enhancement can be expressed qualitatively as follows. Coordination of Cl^- ion around Nd^{3+} ion in pure $NdCl_3$ solid and liquid are nine [52] and six [53], respectively, while Nd^{3+} in $NdCl_3(g)$ has a 3-fold coordination. Therefore, the vaporization of pure $NdCl_3$ needs to overcome three to six Nd–Cl bonds. On the other hand, the Nd^{3+} ion in the $NdCl_3$-KCl equimolar melt has 6-fold coordination [53], while $KNdCl_4(g)$ complex contains Nd^{3+} coordinated by four Cl^- ions (see below). Hence, on vaporization of the $KNdCl_4(g)$ from the melt, fewer Nd–Cl bonds, *i.e.* two Nd–

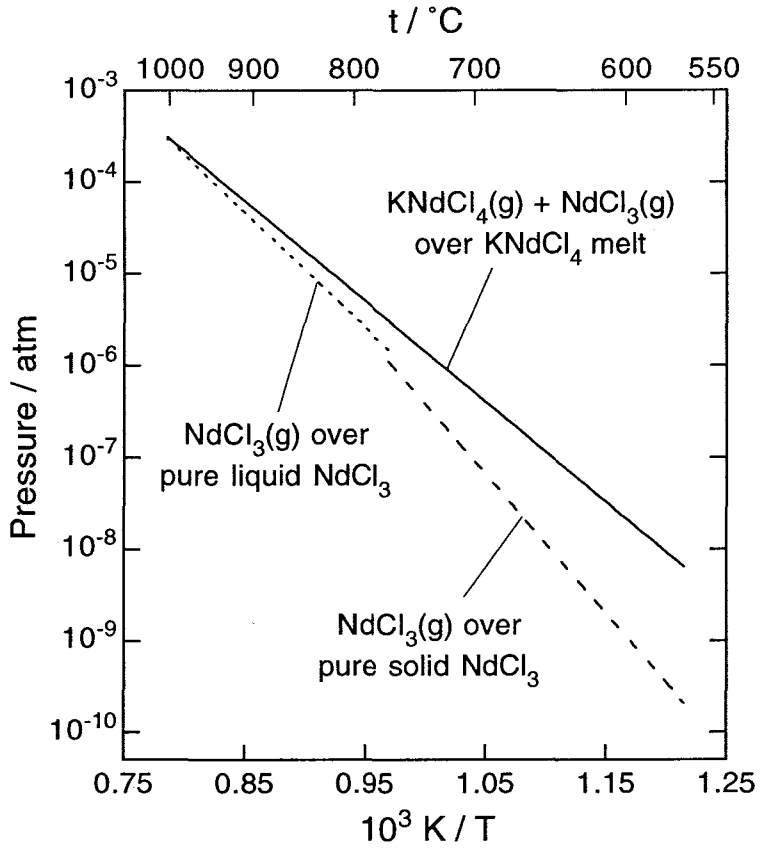

Figure 5.4. Comparison of vapor pressures of Nd-containing species over the $NdCl_3$-KCl equimolar melt, pure $NdCl_3$ liquid, and pure $NdCl_3$ solid.

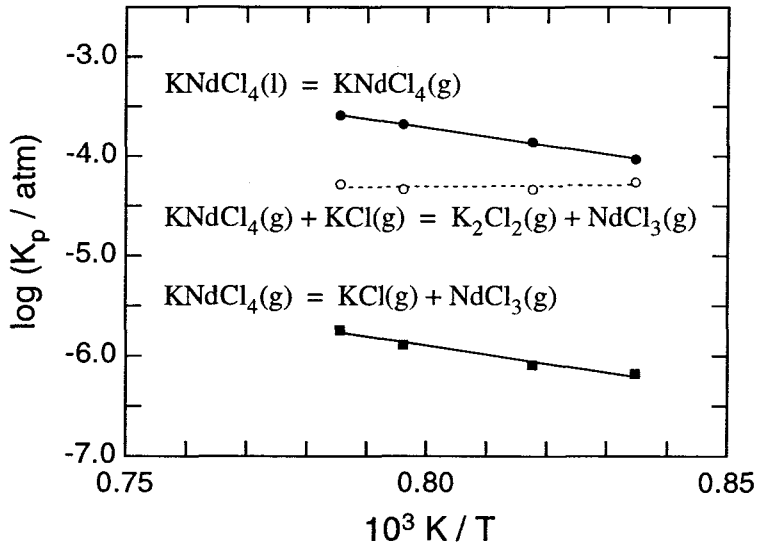

Figure 5.5. Relationship between equilibrium constant of some reactions and the reciprocal temperature in the $NdCl_3$-KCl quasi-binary system.

Cl interactions, need to be broken. At higher temperatures around 1200 K, it becomes easy even for pure $NdCl_3$ to obtain enough energy to overcome Nd–Cl bonds; thus, the volatility enhancement is decreased. The enhancement increases with decrease in temperature are generally observed for many complex forming halide systems.

Evaluation of Thermodynamic Functions. Second-law enthalpy changes, ΔH°_T, of the reactions,

$$KNdCl_4(l) = KNdCl_4(g), \quad (5.9)$$

$$KNdCl_4(g) + KCl(g) = NdCl_3(g) + K_2Cl_2(g), \quad (5.10)$$

and

$$KNdCl_4(g) = KCl(g) + NdCl_3(g), \quad (5.11)$$

were evaluated from the slope of log K_p *vs* $1/T$ plot (Fig. 5.5) for each reaction. The mean enthalpy changes of the reactions 5.9–5.11 at 1198–1273 K were calculated as 168 ± 4 kJ mol^{-1}, -10 ± 21 kJ mol^{-1}, and 173 ± 21 kJ mol^{-1}, respectively. Novikov *et al* obtained a rather bigger enthalpy change of reaction 5.11, $\Delta H^\circ_{1350K} = 247 \pm 17$ kJ mol^{-1}, by a calculation from overall composition and pressure [19a]. However, the reason of the difference cannot be explained, since these authors did not give detailed calculations.

It is noteworthy that the enthalpy change of isomolecular exchange reaction 5.10 is near zero, suggesting that no drastic structure change takes place through the reaction. According to electron diffraction measurements, the $K_2Cl_2(g)$ and $NdCl_3(g)$ molecules are known to have D_{2h}-type square and C_{3v}-type pyramidal structures, respectively [54]. Therefore, the most plausible structure of $KNdCl_4(g)$ is C_{2v}-type structure as shown in Fig. 5.6, since only a $NdCl_3$ unit with C_{3v} symmetry is "replaced" by a linear KCl unit from left- to right-hand side of the reaction 5.10.

This C_{2v}-type structure of $KNdCl_4(g)$ is supported by an enthalpy change of reactions 5.10 and 5.11 deduced from Hastie's empirical rule [5a] for dissociation energy. According to the rule, dissociation energy of $M–Cl^b$ bond, $D(M–Cl^b)$, is 0.6 ± 0.04 times that of $M–Cl^t$ bond, $D(M–Cl^t)$, where Cl^b and Cl^t represent bridging and terminal chlorine atoms, respectively. Then, the enthalpy changes of reactions 5.10 and 5.11 were expressed as

$$\begin{aligned}
&\Delta H^\circ(\text{eq. 5.10}) \\
&\quad = [2\,D(\text{Nd–Cl}^t) + 2\,D(\text{Nd–Cl}^b) + D(\text{K–Cl}^t) + 2\,D(\text{K–Cl}^b)] \\
&\qquad\qquad - [3\,D(\text{Nd–Cl}^t) + 4\,D(\text{K–Cl}^b)] \\
&\quad = [2\,D(\text{Nd–Cl}^t) + 2\times 0.6\,D(\text{Nd–Cl}^t) + D(\text{K–Cl}^t) + 2\times 0.6\,D(\text{K–Cl}^t)] \\
&\qquad\qquad - [3\,D(\text{Nd–Cl}^t) + 4\times 0.6\,D(\text{K–Cl}^t)] \\
&\quad = 0.2\,D(\text{Nd–Cl}^t) - 0.2\,D(\text{K–Cl}^t), \qquad (5.12)
\end{aligned}$$

and

$$\begin{aligned}
&\Delta H^\circ(\text{eq. 5.11}) \\
&\quad = [2\,D(\text{Nd–Cl}^t) + 2\,D(\text{Nd–Cl}^b) + 2\,D(\text{K–Cl}^b)] \\
&\qquad\qquad - [3\,D(\text{Nd–Cl}^t) + D(\text{K–Cl}^t)] \\
&\quad = [2\,D(\text{Nd–Cl}^t) + 2\times 0.6\,D(\text{Nd–Cl}^t) + 2\times 0.6\,D(\text{K–Cl}^t)] \\
&\qquad\qquad - [3\,D(\text{Nd–Cl}^t) + D(\text{K–Cl}^t)] \\
&\quad = 0.2\,D(\text{Nd–Cl}^t) + 0.2\,D(\text{K–Cl}^t). \qquad (5.13)
\end{aligned}$$

C_{2v} C_{3v} D_{2h}

Figure 5.6. Structure model for $KNdCl_4(g)$ complex deduced from structures of $K_2Cl_2(g)$ and $NdCl_3(g)$ together with a relatively small enthalpy change of an isomolecular exchange $KNdCl_4(g) + KCl(g) = NdCl_3(g) + K_2Cl_2(g)$.

From the dissociation energies of K–Cl^t and Nd–Cl^t, *i.e.* D(K–Cl^t) = 425 kJ mol^{-1} and D(Nd–Cl^t) = 464 kJ mol^{-1} [33, 55], the $\Delta H°$(eq. 5.10) and $\Delta H°$(eq. 5.11) are calculated as 8 and 178 kJ mol^{-1}, which almost agree with the above experimental values, – 10 ± 24 and 173 ± 21 kJ mol^{-1}.

5.3.2. The $ErCl_3$-KCl Binary and the $NdCl_3$-$ErCl_3$-KCl Ternary Systems

On ionizing at an electron energy of *ca* 15 eV, six ions, K^+, KCl^+, K_2Cl^+, $ErCl_2^+$, $ErCl_3^+$, and $KErCl_3^+$, were observed over the $ErCl_3$-KCl equimolar melt. However, the sample in the Knudsen cell was exhausted much faster than the case of the $NdCl_3$-KCl mixture, and quantitative measurements up to 1273 K were impossible. This phenomenon agrees with the fact that vapor complexes containing rare earth with larger atomic number, or with smaller ionic radius, have higher volatility (see Chapters 1 and 3).

Vapor over the $NdCl_3$-$ErCl_3$-KCl (Nd/Er/K = 1/1/2) ternary melt was also investigated. These ions: K^+, KCl^+, K_2Cl^+, RCl_2^+, RCl_3^+, and $KRCl_3^+$ (R = Nd, Er), were observed. In this case, intensities of Er-containing ions diminished much faster than those of Nd-containing ones, also indicating the larger volatility of the $KErCl_4$(g) complex.

5.4. Conclusions

Vapor over the $NdCl_3$-KCl equimolar molten mixture was investigated at 1018–1273 K by means of Knudsen effusion mass spectrometry. The vapor species KCl, K_2Cl_2, $NdCl_3$, and $KNdCl_4$ were present in the vapor over the melt and their vapor pressures were evaluated. Volatility enhancement of Nd-containing species by the formation of the vapor complex $KNdCl_4$ decreases with the increase of temperature. Enthalpy change of the isomolecular exchange $KNdCl_4$(g) + KCl(g) = $NdCl_3$(g) + K_2Cl_2(g) was relatively small, – 10 ± 21 kJ mol^{-1}, suggesting that the structural change of the reaction is not drastic and the $KNdCl_4$(g) complex has a C_{2v}-type configuration. Qualitative observation of the vapor over the $ErCl_3$-KCl and $NdCl_3$-$ErCl_3$-KCl mixtures where R/K = 1/1 suggested that Er-containing species vaporize much faster than Nd-containing ones.

Chapter 6

Structure of the (R = Nd, Gd) RCl_3-$AlCl_3$ Vapor Complex, Liquid, and Solid — a High Temperature Raman Spectroscopic Study —

6.1. Introduction

It has been established [1–6] that the volatility of rare earth chlorides apparently increases in the presence of aluminum chloride by several orders of magnitude due to gas-solid reactions leading to the formation of vapor complexes. These reactions are of importance for developing industrial separation and extraction processes as described in Chapters 1–4. At relatively "high" pressures (1–5 atm) of aluminum chloride and at temperatures less than 600 K, a non-volatile liquid mixture has been observed in the systems involving samarium chloride [8] which diminishes the partial pressures of the complexes and thus inhibits vapor transport. The study described in this chapter concerns the formation of such liquid mixtures in binary $NdCl_3$-$AlCl_3$ and $GdCl_3$-$AlCl_3$. In simple visual experiments, the author established the formation of stable liquids and glasses and examined their structural properties by means of vibrational Raman spectroscopy. Based on the obtained structure of the liquids, structures of the RCl_3-$AlCl_3$ (R = Nd, Gd) vapor complexes were deduced.

6.2. Experimental Details

High purity $AlCl_3$ was prepared by repeated slow sublimations using a temperature gradient in a pyrex tube sealed *in vacuo*. Anhydrous $NdCl_3$ and $GdCl_3$ were purified by dynamic sublimation in high vacuum (10^{-5}–10^{-8} Pa) at 800 °C. All handling of chemicals took place in a nitrogen-filled glove box with a water vapor content less than 5 ppm. The Raman (optical) cells were made of fused silica tubing (outer diameter, 4 ± 0.1 mm; inner diameter, 2 ± 0.1 mm, length, *ca* 3 cm). Before use, the cells were carefully cleaned, rinsed with hydrofluoric acid and water, flamed and degassed. Preweighed amounts of $AlCl_3$ and RCl_3 were transferred into each cell, which was then sealed *in vacuo*.

Raman spectra were excited with several lines of a 4 W Spectra Physics Ar^+ ion laser or Spectra Physics Kr^+ ion laser. The scattered light was corrected at an angle of 90° and analyzed

with a Spex 1402 double monochromator, an RCA-C31034 photomultiplier tube and EG&G photon counting (Model 9315), and rate mater (Model 9344) electronics. An optical furnace for obtaining high temperature Raman spectra is shown in Fig. 6.1 .

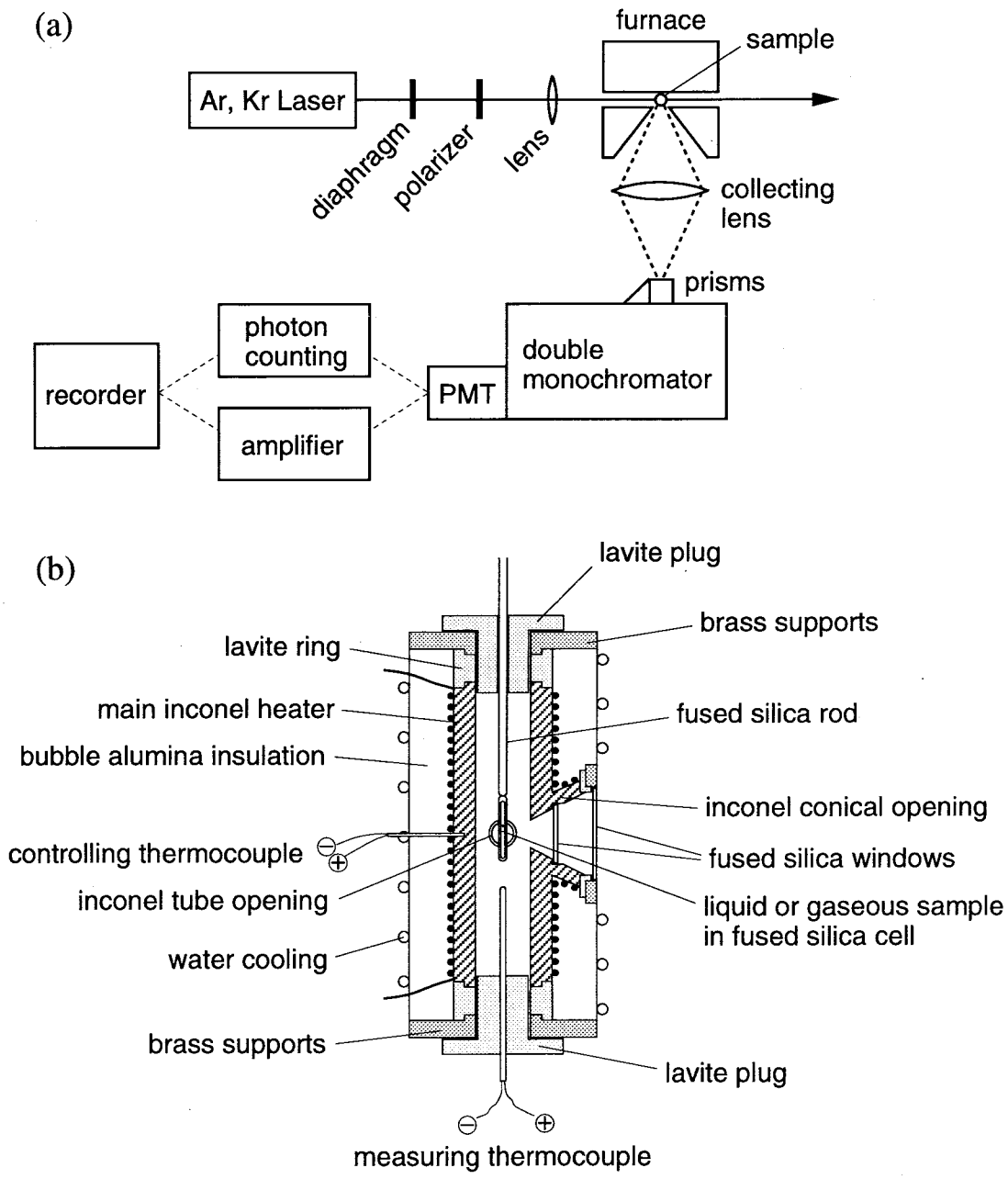

Figure 6.1. (a) Instrumentation for high temperature Raman spectroscopy and (b) optical furnace for obtaining high temperatures (ref. [4d])

6.3. Results and Discussion

6.3.1. The $GdCl_3$-$AlCl_3$ System

Several cells were made for studying the $GdCl_3$-$AlCl_3$ system at different compositions. On heating the samples in the temperature range 250–300 °C for a few hours and subsequently at 350 °C, $GdCl_3$ was slowly (overnight) dissolved in liquid Al_2Cl_6 and a colorless and clear solution was obtained. However, for $GdCl_3$ mole fractions $x_{GdCl_3} > 0.25$, solid $GdCl_3$ remained undissolved even at 425 °C. The pressure of aluminum chloride (as Al_2Cl_6) over the liquid with $x_{GdCl_3} = 0.25$ was less than 2 atm. Upon rapid cooling of Gd/Al = 1/3 liquid, a glassy solid was formed which remained stable for several days/months. Slow cooling of the liquid and/or devitrification of the glassy solid gave a crystalline compound which presumably was $GdAl_3Cl_{12}$ as reported before [56, 57].

The Raman spectra of the 1/3 mixture as crystalline and glassy solids and liquid are shown in Fig. 6.2. The spectrum of the crystalline solid is similar to those reported for $TbAl_3Cl_{12}$ [57]. The doublet around 350 cm^{-1} is attributed to Al–Cl vibrations within the "$AlCl_4$" tetrahedra which according to the crystal structure have two types of chloride, one of which is "bridged" to Gd (*i.e.*, Al–Cl–Gd, $\nu \approx 350$ cm^{-1}) and the other "terminal" ($\nu \approx 360$ cm^{-1}). Based on the trends observed in the vibrational frequencies of many rare earth chloride compounds [58], the $\nu = 249$ cm^{-1} band was assigned to a Gd–Cl stretching mode. The doublet of the crystal at *ca* 350 cm^{-1} gives one band in the glass which remains unresolved even at liquid nitrogen temperature indicating that the preferential orientation of "$AlCl_4$" in the crystal is lost in the glass state and also in the liquid. Finally, another characteristic of the liquid-glass spectra is the appearance of a very weak shoulder band at *ca* 315 cm^{-1} which, by comparison with other aluminum chloride-metal chloride mixtures [4a], is assigned to "Al_2Cl_7".

6.3.2. The $NdCl_3$-$AlCl_3$ System

The dissolution of $NdCl_3$ in molten aluminum chloride was achieved in similar manner as in the $GdCl_3$-$AlCl_3$. The solutions were transparent purple (in the sunlight) and the solubility of $NdCl_3$ reached its maximum at $x_{NdCl_3} \approx 0.2$. Rapid cooling of the liquid gave a glass which was stable for several hours/days.

The Raman spectra of the Nd/Al = 1/4 mixture as liquid and glass are also shown in Fig. 6.2. The spectra exhibit a strong fluorescence background which increases with decreasing temperature. The detailed features of the spectra are similar to those in the gadolinium system showing the

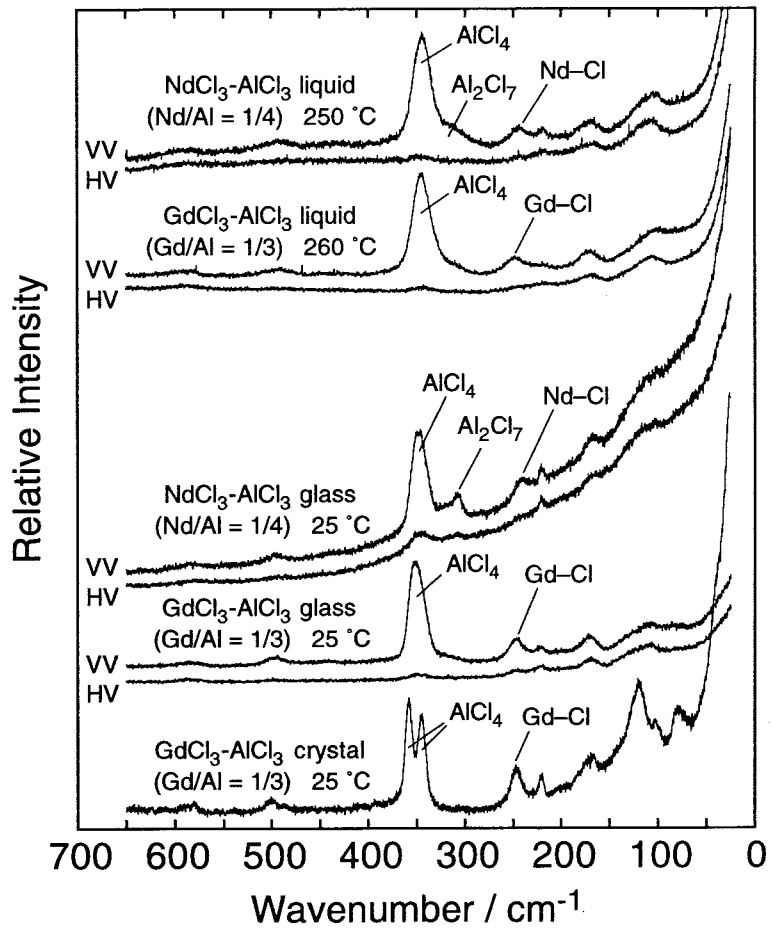

Figure 6.2. Raman spectra of the RCl_3-$AlCl_3$ systems. Spectral slit width, *ca* 6 cm^{-1}; time constant, $\tau = 0.1$ s; scan rate, 2 cm^{-1} s^{-1}; laser line, $\lambda_0 = 488.0$ nm; laser power, *ca* 60 mW (for molten mixtures and crystalline solids) and *ca* 30 mW (for glasses).

Nd–Cl stretching at *ca* 240 cm^{-1} and the main "$AlCl_4$" modes at 347 (ν_1), 496 (ν_3) and 116 cm^{-1} (ν_2). The "Al_2Cl_7" band is more pronounced in the neodymium spectra appearing as a shoulder in the liquid ($\nu = 311$ cm^{-1}) and as a well defined band in the glass ($\nu = 308$ cm^{-1}).

6.3.3. Coordination Number of R in the RCl_3-$AlCl_3$ Liquids

In crystalline $GdAl_3Cl_{12}$, the coordination of Gd is eight-fold [56, 57]. Since there are no drastic changes in the Gd–Cl frequency on going from the crystal ($\nu = 247$ cm^{-1}) to the glass and liquid ($\nu = 249$ cm^{-1}), it may be concluded that the eight-fold coordination is preserved in the glass and liquid phases. It should be noted, however, that all the isostructural and network-like RAl_3Cl_{12} (R = Gd, Th, Dy) compounds show [57] practically identical Raman spectra having the same R–Cl frequency. Thus, if the local environments around Gd and Nd in the RCl_3-$AlCl_3$ systems were

(a) $NdCl_3$-$AlCl_3$ (x_{NdCl3} = 20 mol%)

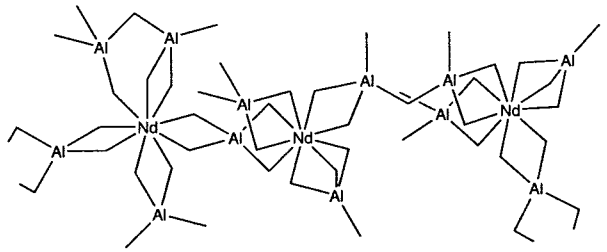

(b) $GdCl_3$-$AlCl_3$ (x_{GdCl3} = 25 mol%)

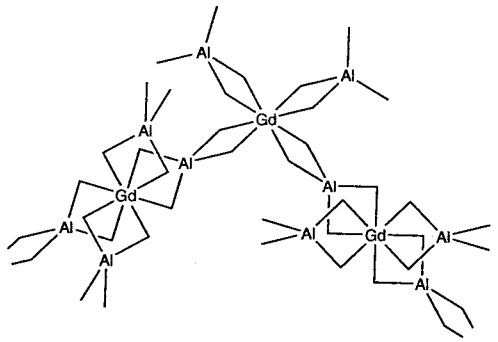

Figure 6.3. Model structure of liquids and glasses formed in the (a) $NdCl_3$-$AlCl_3$ and (b) $GdCl_3$-$AlCl_3$ systems.

similar, then we would expect both the Gd–Cl and Nd–Cl frequencies to be around 250 cm^{-1}. The observed difference in the spectra (Fig. 6.2) of *ca* 10 cm^{-1} between the Gd (ν = 249 cm^{-1}) and Nd (ν = 240 cm^{-1}) indicates that it is more likely that the coordination of Nd is higher than that of Gd. As in the case of crystalline $NdCl_3$ [52], a nine-fold coordination is preferred and presumably is conserved in the liquid/glass.

It follows from the above that in the RCl_3-$AlCl_3$ liquids and glasses the main participating "units" are "$AlCl_4$" and in part "Al_2Cl_7" with the rare earth having coordination eight or nine. The bonding between these "units" and their ease of coordination around R determine their tendency for formation of glass state. In order to satisfy the preferential coordination of R, the "$AlCl_4$" tetrahedra may offer a vertex, an edge, or a face [4b] and can be linked in the same manner to another R or form "Al_2Cl_7" chlorine single bridges. Figures 6.3(a) and (b) give schematic possible structures of these glasses and liquids where the R atom is coordinated with "$AlCl_4$" and "Al_2Cl_7" units which link the neighboring rare earths. The model does not exclude or imply the presence of $AlCl_4^-$- and $Al_2Cl_7^-$-like ions. It is possible that the schematic structures shown are either network-like as in $ZnCl_2$ glasses or ionic-like as in nitrate glasses [59]. In the latter case, the predomi-

nant $AlCl_4^-$ ions should be positioned in fixed orientations towards the R^{3+} ion.

6.3.4. Coordination Number of R in RAl_3Cl_{12} Vapor Complex

Though in many cases high temperature Raman spectroscopy is the most effective means to determine the structure of vapor complexes [4], the Raman spectra of vapor phase in the RCl_3-$AlCl_3$ (R = Nd, Gd, Lu, Sc) systems show only the fundamentals of $Al_2Cl_6(g)$ [60] due to relatively low vapor pressure (< 0.01 atm) of the complexes. In the spectra of the $NdCl_3$-$AlCl_3$ vapor, however, strong fluorescence was observed by changing the frequency of the incident laser line. Figure 6.4 shows the fluorescence spectra excited with 19436.3 cm^{-1} (514.5 nm) laser line. The fluorescence bands can be assigned to $^4G_{5/2}$ (or $^2G_{7/2}$) $\rightarrow$ $^4I_{9/2}$, $^4G_{7/2} \rightarrow {}^4I_{9/2}$, and $^2G_{9/2} \rightarrow {}^4I_{9/2}$ transitions of a Nd^{3+} ion [61] and, therefore, give an evidence that $NdAl_nCl_{3+3n}$ complex(es) really exist in the vapor phase. Increasing temperature from 250 °C to 425 °C increased the overall intensity; this is attributed to the increase of the amount of the $NdAl_nCl_{3+3n}$. Further changing of laser line, 476.5 nm (20986.4 cm^{-1}; blue), 501.7 nm (19932.2 cm^{-1}; blue green), and 647.1 nm (15453.6 cm^{-1}; red), provided other fluorescence due to $^4G_{9/2}$ (or $^2D_{3/2}$) $\rightarrow$ $^4I_{9/2}$, $^2H_{11/2} \rightarrow {}^4I_{9/2}$, $^4F_{9/2} \rightarrow {}^4I_{9/2}$, $^4F_{7/2}$ (or $^4S_{3/2}$) $\rightarrow$ $^4I_{9/2}$, $^4F_{5/2}$ (or $^2H_{9/2}$) $\rightarrow$ $^4I_{9/2}$, and $^4F_{3/2} \rightarrow {}^4I_{9/2}$ transitions as shown in Fig. 6.5.

Anyway, we could not obtain any structural information from the Raman measurement of RCl_3-$AlCl_3$ vapor complexes. On the other hand, the structure of the RAl_3Cl_{12} vapor complex can be postulated from structure of corresponding melt (liquid), since the coordination number of cen-

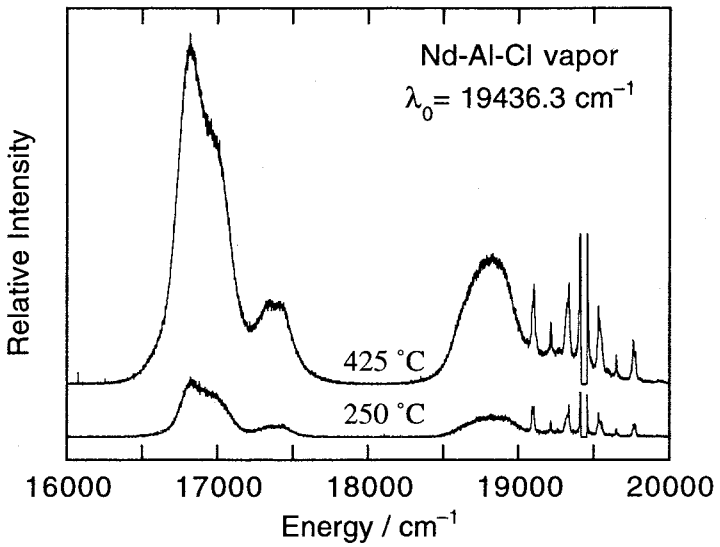

Figure 6.4. Fluorescence spectra of the $NdCl_3$-$AlCl_3$ vapor at 250 and 425 °C excited with 514.5 nm (blue) laser line.

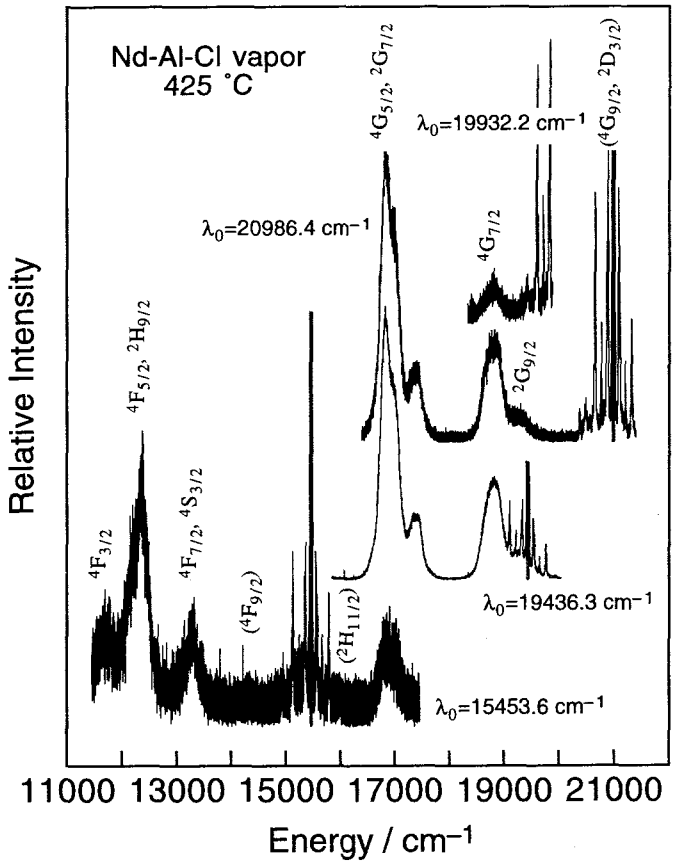

Figure 6.5. Fluorescence spectra of the $NdCl_3$-$AlCl_3$ vapor at 425 °C excited with 476.5 (20986.4 cm^{-1}; blue), 501.7 (19932.2 cm^{-1}; green), 514.5 (19436.3 cm^{-1}; green), and 647.1 nm (15453.6 cm^{-1}; red) laser lines.

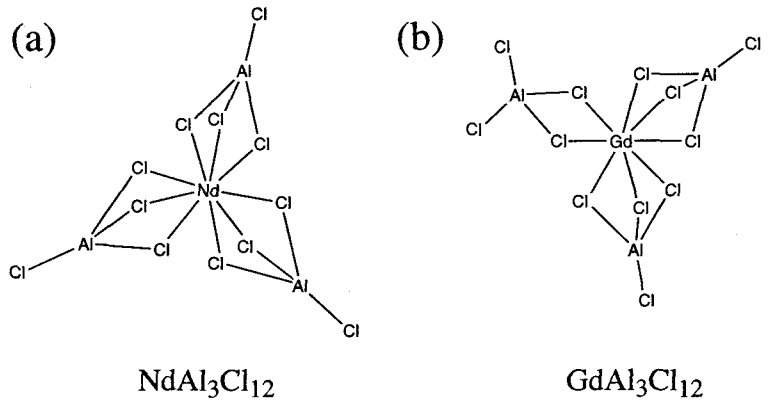

Figure 6.6. Model structures of RAl_3Cl_{12} (R = Nd and Gd) vapor complexes.

tered metal ion in vapor complexes is mostly the same as that of corresponding condensed phase (for example, see ref. [3a, 62, 63]). If coordination numbers of a R^{3+} ion of RCl_3-$AlCl_3$ melt and of RAl_3Cl_{12} vapor are the same, the $NdAl_3Cl_{12}$ and $GdAl_3Cl_{12}$ vapor complexes also have 9- and 8-coordinate structures (Fig. 6.6).

6.4. Conclusions

The existence of liquid mixtures (melts) in the RCl_3-$AlCl_3$ (R = Nd, Gd) binary systems which form stable glasses is established. Based on Raman spectroscopic measurements, a structural model is proposed for these glasses and liquids where the main participating units are "$AlCl_4$" and in part "Al_2Cl_7". The coordination number of the rare earth is nine-fold for neodymium and eight-fold for gadolinium. Though the Raman spectra of the RCl_3-$AlCl_3$ (R = Nd, Gd, Lu, Sc) vapor complexes could not be measured due to relatively low vapor pressure of the complexes, fluorescence bands of the $NdCl_3$-$AlCl_3$ vapor shows the presence of the complex containing Nd^{3+} ion. The structures of $NdAl_3Cl_{12}$ and $GdAl_3Cl_{12}$ vapor complexes were deduced from the structures of corresponding melts.

Summary

In the work of this thesis, a new all-dry method for separation or recovery of rare metals, especially of rare earths, has been investigated using chemical vapor transport reaction mediated by metal chloride vapor complexes, and some fundamental properties of rare earth chloride vapor complexes were also examined. The results obtained through this work are summarized as follows:

Chapter 1. The chemical vapor transport reactions of hydrous and anhydrous rare earth chlorides, RCl_3 were carried out using gaseous aluminium chloride as complex former. Transport efficiency for each RCl_3 was increased with increase in the atomic number of R or, in other words, with decrease in ionic radius of R^{3+}, except for the transport of europium chloride, whose stable valence is Eu^{2+} at high temperatures around 1000 °C. Hydrous chlorides were also transported in the presence of active carbon, and mutual separations of hydrous rare earth chloride mixtures, $PrCl_3$-$ErCl_3$, $PrCl_3$-$SmCl_3$, and $PrCl_3$-$GdCl_3$-$ErCl_3$, were performed *via* the vapor complex, $RAl_nCl_{3+3n}(g)$. Heavier rare earth chlorides were more readily transported and concentrated in the deposits in lower temperature zones of a temperature gradient while lighter ones were selectively condensed in higher temperature zones. By optimization of the temperature gradient, separation characteristics (efficiency and purity) were improved, and $PrCl_3$ of almost 100% purity was obtained for the separation of the $PrCl_3$-$ErCl_3$ mixture. From the transport reaction of the $PrCl_3$-$SmCl_3$ mixture with various compositions, it turned out that a multiple (repeated) transport reaction renders it possible to obtain $PrCl_3$ with high purity.

Chapter 2. Mutual separations of mixed praseodymium and neodymium chlorides or oxides was preformed using the chemical vapor transport reactions. For the transport of the $PrCl_3$-$NdCl_3$ mixture, a series of alkali metal chlorides (ACl) was tried as a complex former as well as aluminium chloride. Separation factor show a tendency to increase in the order, $AlCl_3 < NaCl <$ KCl, RbCl, CsCl, as well as the yields. For the transport reaction using both $AlCl_3$ and KCl (or NaCl) as the complex formers, the co-deposition of KCl with RCl_3, which took place when KCl was singly used, was depressed and RCl_3 was obtained in a form free from the used complex formers, since the co-deposited KCl residue is removed by the regeneration of much volatile complexes, $KAlCl_4(g)$. The influence of RCl_3/ACl mixing ratio was also examined, and equimolar

mixture gave the highest separation factor and yield.

Upon investigating the transport reactions using the mixed oxide directly, some potassium salts, K_2CO_3, K_2SO_4, KNO_3, KF, and $KAl(SO_4)_2$, were tried as a precursor of a complex former, KCl, in order to avoid the deviation of composition from R/K = 1/1. The yields of transported RCl_3 were 55, 37, 32, 18, and 26%, respectively, while the yield when the KCl was directly used as the complex former was 25%. The transport reactions using K_2CO_3 were carried out under various kinds of temperature gradients with a constant-temperature plateau zone, and the decrease of the temperature for such a plateau zone gave a high purity $NdCl_3$ whose yield is, however, very low and *vice versa*. This alternative feature was simulated by employing empirical vapor pressures of $KPrCl_4(g)$ and $KNdCl_4(g)$ which were evaluated from transported amounts of $PrCl_3$ and $NdCl_3$ by altering the plateau temperature. Finally, a heat necessary for the transport reaction of Nd_2O_3 using K_2CO_3 was calculated as 191.2 kJ mol^{-1} of Nd.

Chapter 3. The chemical vapor transport reactions using rare earth concentrates, monazite and xenotime, or some crude oxides were investigated. The raw materials were chlorinated by Cl_2 gas at 1000 °C and the resulting RCl_3 was transported *via* $KRCl_4(g)$ or $RAl_nCl_{3+3n}(g)$ vapor complex. As mentioned in Chapter 1, chlorides of heavier rare earths including YCl_3 were generally more readily transported and concentrated in the deposit at a relatively low temperature portions, and yields of individual rare earth after the transport for 82 h were increased with decrease of ionic radius of R^{3+} ion: 20–30% for La; 50–60% for Ce; 60–70% for Pr and Nd; > 80% for Gd–Lu and Y. The direct use of the concentrates for the transport reaction is, however, not always an appropriate process, since condensation of chlorides of non-rare earth elements such as Th and U sometimes overlapped with each other or with that of RCl_3.

Chlorination behavior using carbon tetrachloride as a chlorinating agent were additionally investigated with respect to the monazite concentrate. The chlorination with CCl_4 was topochemical, and the amount of monazite reacted after different periods, t, followed the relationship, $1-(1-x)^{1/3} = kt$, where x represents fraction of monazite reacted and k is the rate constant. Between the k and partial pressure of CCl_4, p_{CCl4}, there was a correlation, $k = a\,(p_{CCl_4})^{1/2}$ (a, constant), suggesting the reaction has an order of 1/2.

Chapter 4. The chemical vapor transport process was applied to recovery of rare metals from various industrial wastes. Recovery of rare earths, Co, and Ni, from sludges of Sm_2Co_{17} and $Nd_2Fe_{14}B$ type magnets and $LaNi_5$ intermetallic compound was carried out by a high temperature

chlorination at 1000 °C followed by the transport using $AlCl_3$ as a complex former. Rare earth chlorides were concentrated in the deposit in the relatively high-temperature zone, 800–900 °C, while $CoCl_2$ and $NiCl_2$ were in the low-temperature zone, 500–700 °C. Purity of each recovered chloride was more than 99%, since chlorides of other metals, such as Fe, Cu, Zr, and Al, were condensed at the outlet of the reactor (below 350 °C) without any contamination for the recoveries. After the transport reaction for 6 h, yields of Ni and Co were more than 99%, whereas those of La, Nd, Sm, Dy were lower, *i.e.* 27%, 39%, 59%, 68%.

Recovery of V, Ni, and Mg from a fly ash of bitumen-in-water emulsion, as a new fuel, was also conducted. Vanadium components were recovered thoroughly at 500 °C even in the absence of a complex former, $AlCl_3$, while $NiCl_2$ and $MgCl_2$ were extracted *via* vapor complexes, $NiAl_2Cl_8(g)$ and $MgAl_2Cl_8(g)$ at 600 °C. The most appropriate flowsheet for recovering the V, Ni, Mg is: (i) chlorination at 500 °C to extract vanadium; (ii) heating the residual mixed chloride at 600 °C to remove $FeCl_3$; (iii) introduction of gaseous $AlCl_3$ to transport $NiCl_2$ and $MgCl_2$ along temperature gradient with a constant-temperature plateau zone at 410 °C.

Chapter 5. Vaporization of the RCl_3-KCl (R = Nd and/or Er) equimolar molten mixture was investigated at 1018–1273 K by means of Knudsen effusion mass spectrometry. The vapor species KCl, K_2Cl_2, RCl_3, and $KRCl_4$ were found in the vapor over the melt, and their vapor pressures were evaluated for the $NdCl_3$-KCl system: 2.5×10^{-4}, 1.8×10^{-6}, 1.7×10^{-6}, 3.1×10^{-4} atm, respectively. Volatility enhancement of $NdCl_3$ by the formation of the vapor complex $KNdCl_4$ decreases with increase in temperature, and the enhancement factor at 823 K is estimated to be 31. Second-law enthalpy change of the reactions

$$KNdCl_4(l) = KNdCl_4(g), \quad (1)$$

$$KNdCl_4(g) + KCl(g) = NdCl_3(g) + K_2Cl_2(g), \quad (2)$$

and

$$KNdCl_4(g) = KCl(g) + NdCl_3(g), \quad (3)$$

were evaluated at mean temperature, 1235 K, as 168 ± 4, -10 ± 21, and 173 ± 21 kJ mol^{-1}, respectively. A relatively small enthalpy change of the isomolecular exchange suggests that the structural change of the reaction is not drastic and that the $KNdCl_4(g)$ complex has two bridging and two terminal chlorine atoms, presumably a C_{2v}-type configuration. The structure of $KNdCl_4(g)$ was also supported by an agreement of calculated enthalpy change of eqs. 2 and 3, *i.e.* 8 and 173 kJ

mol^{-1}, based on an empirical rule.

Chapter 6. The existence of liquid mixtures (melts) in the RCl_3-$AlCl_3$ (R = Nd, Gd) binary systems which form stable glasses is established. Based on Raman spectroscopic measurements, a structural model is proposed for these liquid mixtures where the main participating units are "$AlCl_4$" tetrahedra and in part "Al_2Cl_7". The coordination of the rare earth is 9-fold for neodymium and 8-fold for gadolinium. Taking into account a similarity in coordination number of centered metal ion between vapor complex and corresponding condensed phase, $NdAl_3Cl_{12}$ and $GdAl_3Cl_{12}$ complexes may have 9- and 8-coordinate structures, respectively. Though Raman spectra of the $NdCl_3$-$AlCl_3$ vapor complex did not obtained at < 425 °C due to relatively low pressure of the complex, strong laser-induced fluorescence of the vapor was observed and the fluorescence bands were assigned to f–f transitions of Nd^{3+} ion. This indicates the presence of large quantity of Nd^{3+} ion in the vapor phase such a low temperature.

References

[1] a) K. Hilpert, Chemistry of Inorganic Vapors, in M. J. Clarke, J. B. Goodenough, J. A. Ibers, C. K. Jørgensen, D. M. P. Mingos, J. B. Neilands, G. A. Palmer, D. Reinen, P. J. Sadler, R. Weiss, and R. J. P. Williams (eds.), *Structure and Bonding*, Vol. 73, Springer, Berlin, 1990, pp. 97; b) K. Hilpert, *J. Electrochem. Soc.*, **136**, 2099 (1989).

[2] D. S. McPhail, M. G. Hocking, and J. H. E. Jeffes, *J. Mater. Sci.*, **20**, 449 (1983).

[3] a) H. Schäfer, *Adv. Inorg. Chem. Radiochem.*, **26**, 201 (1983); b) H. Schäfer, *Angew. Chem., Int. Ed. Engl.*, **15**, 713 (1976).

[4] a) M. H. Brooker and G. N. Papatheodorou, Vibrational Spectroscopy of Molten Salts and Related Glasses and Vapors, in G. Mamantov (ed.), *Advance in Molten Salt Chemistry*, Vol. 5, Elsevier, New York, 1983, pp. 26; b) G. N. Papatheodorou, Spectroscopy, Structure and Bondings of High-Temperature Metal Halide Vapor Complexes, in E. Kaldis (ed.), *Current Topics in Materials Science*, Vol. 10, North Holland, New York, 1982, pp. 249; c) G. N. Papatheodorou, Vibrational Spectroscopy of High Temperature Metal-Halide Vapor Complexes, in J. L. Gole and W. C. Stwalley (eds.), *Metal Bonding and Interactions in High Temperature Systems* (ACS Symposium Series, Vol. 179), American Chemical Society, 1982, pp. 309; d) G. N. Papatheodorou, Resonance Raman Spectra of Metal Halide Vapor Complexes, in J. W. Hastie (ed.), *Proc. 10th Mater. Res. Symp. on Characterization of High Temp. Vapors and Gases* (NBS Special Publication, Vol. 561), National Bureau of Standards, Washington DC, 1979, pp. 647.

[5] a) J. W. Hastie, *High Temperature Vapors*, Academic Press, New York, 1975; b) J. W. Hastie, Thermodynamic Studies, by Mass Spectrometry, of Molten Mixed Halide Systems, in J. Braunstein, G. Mamantov, and G. P. Smith (eds.), *Advance in Molten Salt Chemistry*, Vol. 1, Plenum. Press, New York, 1972, pp. 225.

[6] F. P. Emmenegger, *J. Cryst. Growth*, **17**, 31 (1972).

[7] G. I. Novikov and F. G. Gavryuchenkov, *Russ. Chem. Rev.*, **36**, 156 (1967).

[8] G. N. Papatheodorou and G. H. Kucera, *Inorg. Chem.*, **18**, 385 (1979).

[9] H. Gunsilius, W. Urland, and R. Kremer, *Z. Anorg. Allg. Chem.*, **550**, 35 (1987).

[10] T. S. Zvarova and I. Zvara, *J. Chromatogr.*, **44**, 604 (1969).

[11] G. Adachi, K. Shinozaki, Y. Hirashima, and K. Machida, *J. Less-Common Met.*, **169**, L1 (1991).

[12] a) C. Steidl, F. Dienstbach, and K. Bächmann, *Polyhedron*, **2**, 727 (1983); b) C. Steidl, K. Bächmann, and F. Dienstbach, *J. Phys. Chem.*, **87**, 5010 (1983).

[13] D. M. Gruen and H. A. Øye, *Inorg. Nucl. Chem. Lett.*, **3**, 453 (1967).

[14] H. A. Øye and D. M. Gruen, *J. Am. Chem. Soc.*, **91**, 2229 (1969).

[15] J. W. Hastie, P. Ficalora, and J. L. Margrave, *J. Less-Common Met.*, **14**, 83 (1968).

[16] M. Sørlie and H. A. Øye, *J. Inorg. Nucl. Chem.*, **40**, 493 (1978).

[17] H. R. Hoekstra, J. P. Hessler, C. W. Williams, and W. T. Carnall, in D. L. Hildebrand, and D. D. Cubicioti (eds.), *Proc. Symp. on Characterization of High Temperature Vapors and Gases*, NBS, Washington DC, 1979, pp. 123.

[18] *X-ray Powder Diffraction Standards*, ASTM, Philadelphia, PA, Cards 12-787 ($PrCl_3$); 12-785 ($NdCl_3$).

[19] a) G. I. Novikov and A. K. Baev, *Russ. J. Inorg. Chem.*, **9**, 905 (1964); b) F. G. Gavryuchenkov and G. I. Novikov, *Russ. J. Inorg. Chem.*, **11**, 810 (1966).

[20] a) T. B. Pierce and P. F. Peck, *Analyst*, **88**, 217 (1963); b) C. G. Brown and L. G. Sherrington. *J. Chem. Tech. Biotechnol.*, **29**, 193 (1979).

[21] S. Millman and P. Kusch, *Phys. Rev.*, **56**, 303 (1939).

[22] I. Barin and O. Kanacke, *Thermodynamical Properties of Inorganic Substances*; Splinger-Verlag, Berlin, 1973.

[23] G. I. Novikov and A. K. Baev, *Russ. J. Inorg. Chem.*, **7**, 694 (1962).

[24] B. H. Zimm and J. E. Mayer. *J. Chem. Phys.*, **12**, 362 (1944).

[25] S. Ciach, A. J. C. Nicholson, D. L. Swingler, and P. J. Thistlethwaite, *Inorg. Chem.*, **12**, 2072 (1973).

[26] B. Jezowska-Trzebiatowska, S. Kopacz, and T. Mikulski, *The Rare Elements — Occurrence and Technology* —, Elsevier, Amsterdam, 1990, pp. 97.

[27] C. K. Gupta and N. Krishnamurthy, *Int. Mater. Rev.*, **37**, 197 (1992).

[28] a) R. Lavecchia, L. Piga, F. Pochetti, and L. Chacon, *Trans. Instn Min. Metall. (Sect. C: Mineral Process. Extr. Metall.)*, **102**, 174 (1993); b) P. K. Jena, D. H. Gameiro, and E. A. Brocchi, *Trans. Instn Min. Metall. (Sect. C: Mineral Process. Extr. Metall.)*, **100**, 65 (1991).

[29] O. M. Hilal and F. A. El Gohary, *Ind. Eng. Chem.*, **53**, 997 (1961).

[30] H. Bloom and B. J. Welch, *J. Phys. Chem.*, **62**, 1595 (1958).

[31] A. W. Henderson and K. B. Higbie, *Ind. Eng. Chem.*, **50**, 611 (1958).

[32] F. R. Hartley, *J. Appl. Chem.*, **2**, 24 (1952).

[33] M. W. Chaser Jr., C. A. Davies, J. R. Downey Jr., D. J. Fruip, R. A. McDonald, and A. N.

Syverund, *JANAF Thermochemical Tables, 3rd ed.*, American Chemical Society, New York, 1985, (*J. Phys. Chem. Ref. Data*, **14** (1985)).

[34] V. L. Shubaev, A. V. Suvorov, and G. A. Semenov, *Russ. J. Inorg. Chem.*, **15**, 479 (1970); S. Boghosian, D. A. Karydis, and G. A. Voyiatzis, *Polyhedron*, **12**, 771 (1993); S. Boghosian and G. N. Papatheodorou, *Polyhedron*, **9**, 1393 (1986).

[35] L. K. Doraiswamy and B. D. Kulkarni, Gas-Solid Noncatalytic Reactions, in J. J. Carberry and A. Varma (eds.), *Chemical Reactors and Reaction Engineering*, Marcel Dekker, New York, 1987, pp. 293.

[36] a) H. Koshimura and S. Yamamoto, in *Proc. Symp. on Solvent extraction*, Japanese Association of Solvent Extraction, Tokyo, 1983, pp. 155; 1984, pp. 115; 1987, pp. 227; b) J. W. Lyman and G. R. Palmer, *High Temp. Mater. Process*, **11**, 175 (1993); c) J. W. Lyman and G. R. Palmer, *JOM: J. Miner. Met. Mater.*, **45** (May), 32 (1993); d) C. E. Davila Armas and A. J. Monhemius, *Proc. Symp. High Temp. Mat. Chem.*, **4**, 521 (1987); e) K. Sato, *Kogyo Rare Metal*, **106**, 30 (1993).

[37] C. Birkby and R. H. Tombs, *VGB Tech. Ver. Grosskraftwerksbetr., [Tech. Ber.] VGB-TB*, VGB-TB **017**, Kraftwerke **1991**, 170 (1991); A. Williams, *Energy World*, **1990** (June), 11.

[38] *X-ray Powder Diffraction Standards*, ASTM, Philadelphia, PA, Cards 19-1416 ($VOSO_4 \cdot 3H_2O$), 31-62 ($(NH_4)_2Ni(SO_4)_2 \cdot 6H_2O$), and 18-111 ($(NH_4)_2Mg(SO_4)_2 \cdot 4H_2O$).

[39] G. E. Vrieland and D. R. Stull, *J. Chem. Eng. Data*, **12**, 532 (1967).

[40] *X-ray Powder Diffraction Standards*, ASTM, Philadelphia, PA, Card 12-790 (SmOCl).

[41] H. Schäfer and U. Flörke, *Z. Anorg. Allg. Chem.*, **479**, 89 (1981).

[42] G. N. Papatheodorou, *J. Phys. Chem.*, **77**, 472 (1973).

[43] E. W. Dewing, *Metall. Trans.*, **1**, 2169 (1970).

[44] S. Boghosian and O. Herstad, *Polyhedron*, **13**, 1639 (1994), and references cited therein.

[45] For example, see: G. A. Semenov and F. G. Gavryuchenkov, *Russ. J. Inorg. Chem.*, **9**, 123 (1964); D. S. McPhail, M. G. Hocking, and J. H. E. Jeffes, *Int. J. Mass Spectrom. Ion Processes*, **59**, 261 (1984).

[46] J. B. Mann, Ionization Cross Sections of the Elements, in K. Ogata and T. Hayakawa (eds.), *Recent Developments in Mass Spectroscopy (Proc. Int. Conf. Mass Spectroscopy)*, University of Tokyo Press, Tokyo, 1970, pp. 814.

[47] M. Miller, U. Niemann, and K. Hilpert, *J. Electrochem. Soc.*, **141**, 2724 (1994).

[48] D. L. Hildenbrand, *Int. J. Mass Spectrom. Ion Phys.*, **4**, 75 (1970).

[49] H. -J. Sheifert, *J. Thermal Analysis*, **33**, 625 (1988).

[50] E. Shimazaki and K. Niwa, *Z. Anorg. Allg. Chem.*, **314**, 21 (1962).

[51] E. R. Harrison, *J. Appl. Chem.*, **2**, 601 (1952).

[52] W. H. Zachariasen, *Acta Cryst.*, **1**, 265 (1948).

[53] G. M. Photiadis, G. A. Voyiatzis, and G. N. Papatheodorou, *Molten Salt Forum*, **1–2**, 183 (1993-1994).

[54] M. Hargittai, *Coord. Chem. Rev.*, **91**, 35 (1988).

[55] G. P. Dudchik, O. G. Polyachenok, and G. I. Novikov, *Russ. J. Phys. Chem*, **45**, 409 (1971).

[56] D. Hake and W. Urland, *Z. Anorg. Allg. Chem.*, **586**, 99 (1990).

[57] J. Shamir, D. Hake, and W. Urland, *J. Raman Spectrosc.*, **23**, 137 (1992).

[58] G. Schaack and J.A. Koningstein, *J. Phys. Chem. Solids*, **31**, 2417 (1970).

[59] C.A. Angell, *J. Non-Cryst. Solids*, **102**, 205 (1988).

[60] G. N. Papatheodorou and R. W. Berg, *Chem. Phys. Lett.*, **75**, 483 (1980).

[61] G. H. Dieke, *Spectra and Energy Levels of Rare Earth Ions in Crystals*, Interscience Publishers, New York, 1968.

[62] S. Boghosian and G. A. Voyiatzis, *Polyhedron*, **12**, 2965 (1993).

[63] D. R. Taylor and E. M. Larsen, *J. Inorg. Nucl. Chem.*, **41**, 481 (1979).

Acknowledgments

The author would like to express his heartfelt gratitude to Professor Dr. Gin-ya Adachi, Department of Applied Chemistry, Faculty of Engineering, Osaka University, for his continuous guidance, many invaluable suggestions, and his sincere encouragement throughout the work. The author would also like to thank Professor Dr. Hiroshi Yoneyama, Department of Applied Chemistry, Faculty of Engineering, Osaka University for his helpful comments and suggestions.

The author is deeply grateful to Associate Professor Dr. Ken-ichi Machida for his constant guidance and stimulating discussions, and to Dr. Nobuhito Imanaka and Dr. Hiroki Sakaguchi for their helpful suggestions and heartfelt advice.

The author desires to express his sincere thanks to Professor Dr. George N. Papatheodorou, Dr. Soghomon Boghosian, and Ms. Georgia D. Zissi, Department of Chemical Engineering, University of Patras and Institute of Chemical Engineering and High Temperature Chemical Processes (ICE/HT), and all other members of the research group of Professor G. N. Papatheodorou for their kind guidance, helpful comments, and discussions on Raman spectroscopic measurements of the RCl_3-$AlCl_3$ melts and solids.

Furthermore, the author is much obliged to Professor Dr. Hiroshi Kudo, Department of Chemistry, Graduate School of Science, Tohoku University, and Mr. Masashi Hashimoto, Advanced Science Research Center, Japan Atomic Energy Research Institute, for kind measurements and helpful discussions on Knudsen effusion mass spectra of vapor over the RCl_3-KCl melt.

Special thanks should be given to the author's co-workers, Mr. Kiyoshi Shinozaki, Mr. Teruaki Fukami, Mr. Ken-ichi Nishikawa, Mr. Tetsuya Ozaki, and Mr. Toshiki Miyazawa for their helpful assistance and support in the course of this work, and all other members of the research group under direction of Professor G. Adachi, Osaka University.

The Japan Society for the Promotion of Science is also acknowledged for a research fellowship.

Finally the author is particularly grateful to his parents Kazuo Murase and Chieko Murase, his grandparents the late Kenji Tanaka and Suiko Tanaka, and his brother Akifumi Murase for perpetual support and continuous encouragement.